DISTILLATION SYNTHESIS TOOLBOX FOR PRE–FLOWSHEET DESIGN

Cameron Joseph Wilson

A dissertation submitted to the Faculty of Engineering and the Built Environment, University of the Witwatersrand, Johannesburg, in fulfillment of the requirements for the degree of Master of Science in Engineering.

Johannesburg, 2005

DECLARATION

I hereby declare this dissertation as my own unaided work. It is being submitted for the Degree of Master of Science in Engineering in the University of the Witwatersrand, Johannesburg. It has not been submitted before for any degree or examination in any other University.

_____

Cameron Joseph Wilson

_____day of_____ (year) _____

ABSTRACT

Preliminary evaluations during flowsheet synthesis require simple effective tools for comparison and elimination of process alternatives. This work investigates three areas of interest in distillation.

Column profile map theory has simplified complex column investigations. The predictions of the difference point equation at finite reflux were experimentally verified for the acetone, methanol and ethanol system in a continuous column apparatus.

Residue curve analysis is usually limited to systems with four components for distillation system analysis. An alternative representation, based on combinatorial topology and temperature sequencing, is introduced for use in high level synthesis decisions for higher component order systems.

Attainable region (AR) theory is applied to an ideal binary distillation system for a geometrically based method of cost analysis. A constrained attainable region is constructed from a series of equilibrium step compositions with varying reflux and corresponding cost associations. The AR is shown to be useful for costing and optimization.

ACKNOWLEDGEMENTS

This work would not have been possible without the guidance and supervision of Prof. D. Glasser and Prof. D. Hildebrandt. Their unending enthusiasm was a constant source of motivation and purpose. The additional insightful assistance of Dr. S. Kauchali was always well received a special thanks is noted.

I am forever in gratitude to fellow peers including M. Peters, A. Moodley, K. Leeuw, S. Holland, M. Vrey and many others.

Financial assistance by the National Research Foundation, COMPS and the University of the Witwatersrand was much appreciated.

TABLE OF CONTENTS

LIST OF FIGURES

LIST OF TABLES

LIST OF SYMBOLS

SYMBOLS

A	:	Area *[units^2]*
d	:	Distributed reflux addition stream [*mol/s*]
$\dot{D}$	:	Feed flowrate [*mol/s*]
$\dot{F}$	:	Feed flowrate [*mol/s*]
k	:	Response factor
$\dot{L}$	:	Liquid flowrate [*mol/s*]
n	:	Stage number
P	:	Pressure [*KPa*]
P_{tot}	:	Total Pressure [bar]
P_{vapi}	:	Vapour Pressure of component i [bar]
r	:	Reflux ratio
R_{Δ}	:	Column section reflux ratio
T	:	Temperature [*K*]
$\dot{V}$	:	Vapour flowrate *[mol/s]*
x	:	Liquid composition vector
x_{Δ}	:	Difference point
y	:	Vapour composition vector
z	:	Distance *[m]*

GREEK LETTERS

α_i	:	Volatility of component *i* relative to a chosen reference component
δ	:	Difference vector
γ	:	Activity Coefficient
κ	:	Capacity variable
τ	:	Dimensionless time

SUBSCRIPTS

A	:	Referring to Acetone
B	:	Referring to bottoms
D	:	Referring to distillate
E	:	Referring to Ethanol
F, f	:	Referring to feed

i	:	Referring to component *i*
L	:	Referring to liquid
M	:	Referring to Methanol
n	:	Referring to stage
T	:	Referring to Tops
V	:	Referring to vapour
z	:	Referring to particular length

ABBREVIATIONS

AR	:	Attainable region
CFSTR	:	Continuous-flow stirred-tank reactor
CPM	:	Column Profile Map
CSTR	:	Continuous stirred-tank reactor
DE	:	Differential Equation
DPE	:	Difference Point Equation
DSR	:	Differential side-stream reactor
GC	:	Gas Chromatograph
LLE	:	Liquid-Liquid Equilibrium
NRTL	:	Non Random Two Liquid
RCM	:	Residue Curve Map
TCD	:	Thermal Conductivity Detection
VLE	:	Vapour Liquid Equilibrium

CHAPTER 1: INTRODUCTORY OVERVIEW

This dissertation consists of three different topics that are not mutually exclusive but are unique enough to warrant their separation. As such, three chapters are presented. The chapters are to be submitted for publication and are thus in the form of papers, each with their own titles, abstracts, introduction and conclusions. With exception are the nomenclature in the form of a list of symbols and the references at the end of the main dissertation body. Below is an integrated introduction outlining the work presented in the three chapters.

----------§----------

The thermodynamic and topological analysis of distillation systems is based on the classic works of Schreinemakers (1902) and Ostwald (1902), where the relationship between the behaviour of open evaporation residue curves of ternary mixtures and vapour liquid equilibrium (VLE) was established.

Residue curves are composed of the successive remaining liquid compositions in a simple distillation process. This provided one of the first graphical representations useful for understanding the volatility and compositional changes of three component batch evaporative systems. Hausen (1952) and Rische (1955) later extended their function and showed their equivalence to the compositional profile of a packed column at infinite reflux.

Doherty (1978) introduced the use of ordinary differential equations (ODE's) as a differential approximation to the liquid composition profiles in the rectifying and stripping sections of a distillation column. Existing methods of distillation separation synthesis were limited to simple distillation processes prior to the introduction of column profile map theory (Tapp et al., 2003).

Column profiles maps as introduced by Tapp et al. (2003) are linear transforms of residue curves at finite reflux described by the difference point equation. The profiles are unique in that they may be constructed from a composition point other than the product composition. This fixed composition point for a particular map is termed the difference point. Newly defined column sections extend distillation system analysis to multiple feed addition, side-stream withdrawal and column coupling.

An apparatus has been built to investigate the transformed profiles for the acetone, methanol and ethanol system at finite reflux by replicating a column section. The experimental profiles are found to compare well with those predicted by the difference point equation. The deviation of profiles from infinite reflux is highlighted by achieving inverse temperature profiles experimentally. It should be noted that this is the first successful attempt at accurately measuring experimental column profiles in a continuous column.

----------§----------

Residue curve analysis is not only limited to simple distillation systems. The usefulness of residue curve maps in interpreting multi-component systems is usually limited to four components. However, the important information in residue curves is in the topology of the maps or rather the structure of the map. The curvature of the composition profiles in the visual map is only important for column sizing.

Work by Doherty and Perkins (1978, 1979) showed that only a finite number of singular points may exist for a particular distillation system. Stable and unstable points are local maxima and minima in temperature respectively. As a consequence of the simultaneously existing temperature function a natural partial ordering appears amongst the singular points. This partial ordering has been used to formulate temperature sequences as a complete method of categorizing the feasible distillation

boundary maps for ternary systems which commonly have unique binary and ternary azeotropes (Peterson and Partin, 1997).

The use of combinatorial topology has been suggested for exploration of multi-component mixtures with more than four components (Rev, 1994). Further combinatorial work has been extended into process synthesis systems by the use of bipartite graphs, termed P-graphs (Friedler, 1992; Feng, 2000; Feng 2003). Another method for higher dimension mixtures has been investigated by Thong and Jobson (2001a, b, c) using a modified form of the rectification body method developed by Bausa (1998).

This work proposes a unique graphical combinatorial approach adapted from Henley and Williams (1973) for developing a representation for higher dimension mixtures. The work derives from a likening between residue curve map binary component boundaries and simple distillation column component splits. A number of heuristic rules are introduced to obtain a maximal chain structure to represent a distillation system having only known the component boiling temperatures and those of any azeotropes.

The method is initially developed for four component mixtures for ease of comparison and verification of the resulting representation with existing methods. A six component example is then completed to show the robustness of the method in its application to assist in the necessary steps for the rectification body and column feasibility design approach (Thong and Jobson 2001a, b, c); and as a precursor to P-graph methods (Friedler, 1992). A highlight of the method is its prediction of component sequences in Petlyuk columns.

----------§----------

In process synthesis, preliminary evaluation and comparison of process alternatives is essential. Process alternatives may be evaluated as a set of paths in an indirect optimization exercise. Graphical methods provide an effective means for conveying complex relationships in an easily interpretable manner.

A relatively new optimization tool called attainable region (AR) analysis has been pioneered by Hildebrandt and Glasser (Godorr, Hildebrandt & Glasser, 1994; Hildebrandt & Bieglar, 1995; Jobson, Hildebrandt & Glasser, 1996; Glasser & Hildebrandt, 1997; McGregor, 1998).

AR methods are primarily used to view process alternatives at the conceptual design of flowsheet development but costing may be included to extend the feasibility analysis to become an optimisation tool. Jobson et al. (1996) introduce the concept of capacity variables as cost indicators for separation processes involving vaporisation and condensation. Kauchali et al. (1999) introduce a modified form of the capacity variables formulated by Jobson et al. (1996) for use in a complex countercurrent distillation column developed by McGregor (1998).

This work introduces a modified or rather manipulated version of the original capacity variable by Jobson et al. (1996). The new method is applied to the rectifying section of a binary distillation column by a further modification to allow for the number of stages in successive column sections (Kauchali et al. 1999). An AR is constructed from the composition vector and the capacity difference vector for an ideal binary mixture.

The work is not limited to binary systems and a ternary equivalent is offered. This work shows that a costing function included in an AR analysis can prove to be a valuable optimization tool.

CHAPTER 2: EXPERIMENTAL COLUMN PROFILE MAPS WITH VARYING DELTA POINTS IN A CONTINUOUS COLUMN FOR THE ACETONE METHANOL ETHANOL SYSTEM

ABSTRACT

Traditionally, residue curves have been divided into rectifying and stripping sections, where the profiles are described by the liquid composition along the length of the column. However, the equations used do not fully describe the transition from the rectifying to the stripping section. Use of the Difference Point Equation in column profile map theory allows the selection of composition profiles in newly defined columns sections. Manipulation of the column sections allows the designer to dictate the separation sequence within certain constraints.

An experimental investigation has been undertaken for the acetone, methanol and ethanol system. Controlling the vapour and liquid feed compositions, temperatures, and flow rates, a number of column profiles at finite reflux were obtained. The results are compared with column profile maps predicted by the Difference Point Equation. An internal check of constant molar overflow and adiabatic operation of the column is performed via the Difference point.

A highlight of the experiment is two experimentally obtained inverse temperature profiles.

2.1 INTRODUCTION

The thermodynamic and topological analysis of distillation systems is based on the classic works of Schreinemakers (1902) and Ostwald (1902), where the relationship between the behaviour of open evaporation residue curves of ternary mixtures and vapour liquid equilibrium (VLE) was established.

Residue curves are composed of the successive remaining liquid compositions in a simple distillation process. Different starting compositions result in a set of residue curves in the mass balance constraint space. Shreinemakers (1902) established that the interior of the composition space could be entirely populated with residue curves. The populated composition space is termed the residue curve map (RCM).

Residue curves were one of the first graphical representations useful for understanding the volatility and compositional changes of three component batch evaporative systems. Hausen (1952) and Rische (1955) later extended their function and showed their equivalence to the compositional profile of a packed column at infinite reflux. Serafimov (1968) suggested predicting feasible separations from the use of structural information in VLE diagrams. In this way, RCM's are useful for split feasibility and thermodynamic understanding of VLE behaviour. Their application in finite reflux systems is however only qualitative and they were thus essentially limited to infinite reflux investigations.

Finite reflux split feasibilities were investigated by the introduction of operating leaves (Castillo et al., 1998 and Tapp et al., 2003). For a specific product composition, the operation leaf is the total attainable composition region in a column section. This method proved to be useful for split feasibility tests and for determining the minimum reflux ratio, but is limited to simple one feed, two product columns.

Doherty (1978) had introduced the use of ordinary differential equations (ODE's) as a differential approximation to the liquid composition profiles in the rectifying and stripping sections of a distillation column. It was later shown that the differential model results were very similar to those for stage by stage calculations (Van Dongen & Doherty 1985). Feasible column profiles were indicated by an intersection of the approximated rectifying and stripping profiles but the differential equations were not valid near the feed stage. Optimal placement of the feed stage was based on heuristics (Fenske 1932) or rigorous calculation methods (Yeomanns 1998).

The limitation of simple distillation analysis was addressed by Tapp et al (2003) with use of the difference point equation (DPE) adapted from Doherty's (1978) original rectifying and stripping differential equations (DE's). Use of the difference point in the design of non-reactive and extractive cascades had been made by Hoffman (1964) and later Hauan et al. (2003). The difference point was defined by Tapp et al. (2003) as a pseudo net molar flow composition within a column section.

A column section was redefined as a length of column between points of addition or removal of material or heat (Tapp et al. 2003). The use of a net flux allowed a degree of freedom within mass balance constraints of a column section whereby mass balances could be achieved by simple addition (or subtraction) of the net fluxes within the column section (Tapp et al 2004). The inclusion of other distillation processes such as multiple feed addition, side-stream withdrawal and column coupling was now possible.

The work by Tapp et al. (2004) is an extension of the work by Franklin (1986) where the idea of producing composition profiles from a point other than product composition point was proposed. This point termed the difference point may be used in the difference point equation to populate the composition space with column profiles. This set of trajectories is defined as a column profile map (CPM) by Tapp et al. (2004). The difference point equation is a linear transform of the residue curve

map equation and thus column profile map are simply transformed residue curve map.

An important result of this linear relationship is the shifting of composition profiles that lie outside mass balance constraints in residue curve maps, to become realizable in column profile maps.

This work aims to investigate and verify these transformations experimentally at finite reflux for a real system. The acetone, methanol and ethanol system will be investigated in a continuous column apparatus. The apparatus replicates a general column section without reflux or reboil. There is a single vapour and a single liquid feed with two product streams. The temperature, composition and flow rate of the feed streams are controlled for the single pass stream interaction. Liquid flowrates were more than the vapour flowrates resulting in a negative reflux ratio newly defined for column sections.

Experimental runs were selected according to theoretically predicted column profiles at finite refluxes in regions of extreme deviation from total reflux behaviour highlighting the infinite reflux transformation. The theoretical profiles were then compared to the liquid profiles sampled for the experimental runs. Agreement of delta points predicted from experimental data for the top and bottom of the column gave a measure of degree to which constant molar overflow was observed. The reproducibility of the experiments was shown by repeating two variations of inverse temperature profiles.

This method is thus an accurate measure of column profile maps regardless of whether one has vapour-liquid equilibrium (VLE) models or not. The method may be extended to ‘n’ component mixtures.

2.2 DERIVATION AND INTERPRETATION

2.2.1 THE DIFFERENCE POINT EQUATION

Consider the rectifying column section shown in Figure 2.1. Constant molar over flow has been assumed for the analysis. Analogous to the derivation of the differential equations by Doherty (1978), an overall and component mass balance for the rectifying section leads to equation 2.1.

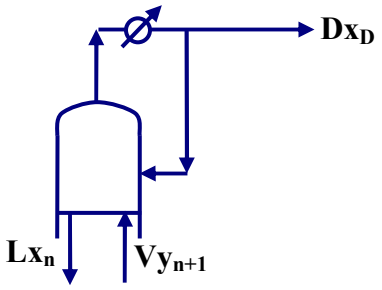

Figure 2.1: Rectifying section of a distillation column

$$\frac{dx_i}{dn} = \frac{\dot{V}}{\dot{L}}(x_i - y_i) + \frac{\dot{D}}{\dot{L}}(X_{Di} - x_i) \qquad \textbf{(2.1)}$$

The overall mass balance is given by

$$\dot{V} = \dot{D} + \dot{L} \qquad \textbf{(2.2)}$$

Traditional approaches to column synthesis involved the calculation of column profiles from the required distillate composition down the column using equation 2.1. Similar compositions were calculated up the column from a similar equation

corresponding to the stripping section. The intersection of the two profiles indicated a feasible column. The DE's are however not valid near the feed stage.

Column profile map theory (Tapp et al. (2003) redefines a column as a series of sections rather than just a rectifying and stripping section. Under the new definition, the column sections are defined as sections with no feed addition or side stream withdrawal.

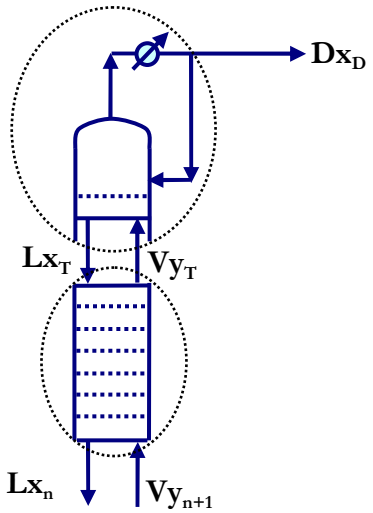

Figure 2.2: Column showing rectifying and general column sections

Analogous to the derivation of the differential equations by Doherty (1978), a component mass balance for the general column section in Figure 2.2 leads to equation 2.3.

$$\frac{dx}{dn} = \frac{\dot{V}}{\dot{L}}(x - y) + (x - x_T) + \frac{\dot{V}}{\dot{L}}(y_T - x) \qquad \textbf{(2.3)}$$

The delta point (composition difference point) and reflux ratio (not to be confused with the traditional reflux ratio $\left(\frac{\dot{L}}{\dot{D}}\right)$ may be defined as:

$$x_{\Delta} = \left(\frac{\dot{V} \cdot y_T - \dot{L} \cdot x_T}{\Delta} \right) \tag{2.4}$$

$$R_{\Delta} = \frac{\dot{L}}{\Delta} \tag{2.5}$$

Where Δ is the flow rate difference point defined as:

$$\Delta = \left(\dot{V} - \dot{L} \right) \neq 0 \tag{2.6}$$

Substituting equations 2.4 and 2.5 into equation 2.3 gives the following:

$$\frac{dx}{dn} = \left(\frac{1}{R_{\Delta}} + 1 \right)(x - y) + \frac{1}{R_{\Delta}}(x_{\Delta} - x) \tag{2.7}$$

The composition difference point and flow rate difference point were first defined by Hoffman (1964) and later adapted by Hauan (1998). The above equation applies to all general column sections and is referred to as the difference point equation.

Rearranging equation 2.4 gives equation 2.8. The analogous interpretation is included for the bottom of a column section.

$$\dot{V} y_T - \dot{L} x_T = \dot{V} y_B - \dot{L} x_B = \Delta x_{\Delta} \tag{2.8}$$

At infinite reflux ($\dot{V} = \dot{L}$; $\Delta = 0$), the difference point equation collapses to

$$\frac{dx}{dn} = (x - y) + \delta \tag{2.9}$$

Where δ is called the difference vector and is defined as:

$$\delta = (x_T - y_T) \tag{2.10}$$

At infinite reflux, δ becomes zero because the stream returning from the total condenser has the same composition as the stream entering it at the top of the column. The equation thus reduces to the residue curve equation:

$$\frac{dx}{dn} = (x - y) \tag{2.11}$$

Thus the difference point equation is a linear transform of the residue curve equation by a scalar and the difference vector.

2.2.2 COLUMN PROFILE MAPS

The difference point equation may be solved by integrating from a starting composition for a specific reflux ratio (R_Δ) and delta point (x_Δ). Integrating in the positive and negative directions yields a complete profile in both directions depending on the number of stages specified. By choosing a number of different starting compositions for the same reflux and fixed delta point, the entire composition space may be populated with column profiles. For finite refluxes, the result is a map of transformed composition trajectories for a fixed delta point at a set reflux.

An example of the resulting transformation is given in Figure 2.3. The residue curves for the system are the dashed lines and the solid lines are the transformed liquid profiles.

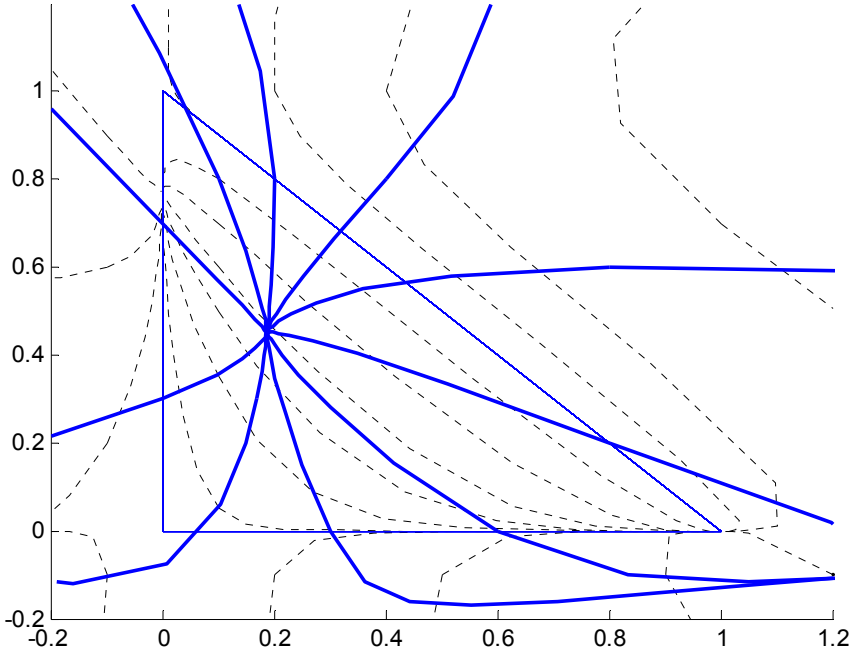

Figure 2.3: Finite reflux column profiles (bold) superimposed on infinite reflux residue curves (dashed).

It should be noted that composition trajectories are not continuous and are defined at discreet points equivalent to stages in the column. Also worth noting is the fact that mathematics of the difference point and residue curve equations are not bound inside the composition space although only profiles inside the composition triangle may be realised. The nature of the profiles outside of the space is very useful however when manipulation of column profiles is to be performed in column profile map synthesis. These may be transformed into realizable composition trajectories within the mass balance triangle.

2.2.3 THEORETICAL PREDICTION MODEL

The acetone, methanol and ethanol system will be considered for this paper. The program for the theoretical calculations and predictions of the system will utilise the Non Random Two Liquid (NRTL) model. The model was used to calculate the

activity coefficients of the components and thus calculate the composition of the vapour in equilibrium with the liquid at each equilibrium stage.

The liquid activity coefficient γ_i may be determined from the NRTL model as follows:

$$\gamma_i = exp\left(\frac{\sum_j x_j \tau_{ji} G_{ji}}{\sum_k x_k G_{ki}} + \sum_j \frac{x_j G_{ij}}{\sum_k x_k G_{kj}}\left(\tau_{ij} - \frac{\sum_m x_m \tau_{mj} G_{mj}}{\sum_k x_k G_{kj}}\right)\right) \quad \textbf{(2.12)}$$

Where $G_{ij} = exp\left(-c_{ij} + d_{ij}\left(T - 273.15K\right)\tau_{ij}\right)$ and $\tau_{ij} = a_{ij} + \frac{b_{ij}}{T} + e_{ij}\, ln\, T + f_{ij} T$

The required binary parameters a_{ij}, b_{ij}, c_{ij}, d_{ij}, e_{ij} *and* f_{ij} for the NRTL model can be determined from the regression of VLE and/or LLE data. ASPEN PLUS™ was used to regress the parameters using data from the Dortmund Databank.

For non-ideal systems the of the component composition of the vapour in equilibrium with corresponding liquid component composition is given by:

$$y_i(x) = \frac{\gamma_i\, x_i\, P_{vap\,i}}{P_{tot}} \quad \textbf{(2.13)}$$

The vapour pressure of each component is calculated from the Antoine equation. The total pressure was set at 1 bar.

$$P_{vap\,i} = \frac{exp\left(A_i - \frac{B_i}{T + C_i + 273}\right)}{P_{tot}\ 760} \quad \textbf{(2.14)}$$

2.3 APPARATUS SELECTION AND JUSTIFICATION

2.3.1 REQUIREMENTS

In the design of experimental apparatus, a process synthesis approach should be adopted. The complexity of probable equipment configurations was a concern from the outset of this undertaking. Engineering design is about finding a simple solution to complex problems. Since the purpose of the investigation was only to pre-empt subsequent more elaborate experiments, the equipment was designed with a high degree of adaptability.

In keeping with the process synthesis approach, the apparatus may be viewed as a series of components in common function areas to that operate achieve the same overall purpose. The main areas of the apparatus are:

- Column Shell and Packing
- Vapour Feed
- Liquid Feed
- Vapour Exit
- Liquid Exit
- Sampling equipment
- Physical property measurement
- Composition analysis

2.3.2 COLUMN SHELL AND PACKING

The following points were important considerations in the construction of the column shell:

- Materials
- Packing and supports
- Sample ports
- Heating

Materials

Potential materials of construction were selected on the basis of their compatibility with a wide range of laboratory chemicals that may be considered in future investigations. The best two candidates are metal and glass. Indeed, the term 'laboratory equipment' invokes a vision of intertwined glass tubes and spectacular cascades of multi-coloured liquids hinged and supported by finely machined metal fixtures. Glass is well established for its thermal properties, resistance to corrosive materials and the fact that it is transparent giving tangible aesthetics to interesting fluid interactions. Metals may be selected for their cost, ease of workability and strength. Both these materials will be used for various applications in the column.

The main disadvantages of glass are that it is brittle and has high costs involved for fabricating custom parts. The column shell is essentially a pipe containing packing material. The boiling points of the components range from 50°C to about 70°C. This suggested that some form of insulation would be required. An additional point was the need for liquid sampling points; clearly frequent sampling would require a strong material to withstand any strains. The final influencing factor was the need for column packing and the substantial mass of such a packing. The interior of the shell would need to support a large amount of packing, again requiring a robust strength in the material and the need to install a custom support grid.

A column shell was available in the lab from previous experiments. The idea was to replicate the existing apparatus so that a coupled column configuration may eventually be investigated. The shell is simply an aluminium pipe. Research by

(Holland, 2003) for coupled columns could be verified much in the same way as one would do column profile maps except for the fact that one would require one or more column sections.

The aluminium tube fulfils all the requirements of the column shell.

- It is relatively cheap and requires no modification.
- Since the column is to be insulated, there is no need for the shell to be transparent.
- Support for the stainless steel packing was easily implemented by inserting flat circular discs above and below the packing that also served to ensure efficient distribution of the liquid and vapour streams.
- The strength of aluminium affords the use of liquid sample ports which need to be moved or orientated fairly often without having to worry about breaks

An aluminium flange was machined to fit on either end of the shell. A corresponding glass flange was made for each aluminium end. The glass flange has two ground glass female joints to accommodate the entering and exiting streams at the top and bottom of the column. A schematic of the column shell ends in shown in Figure 2.4.

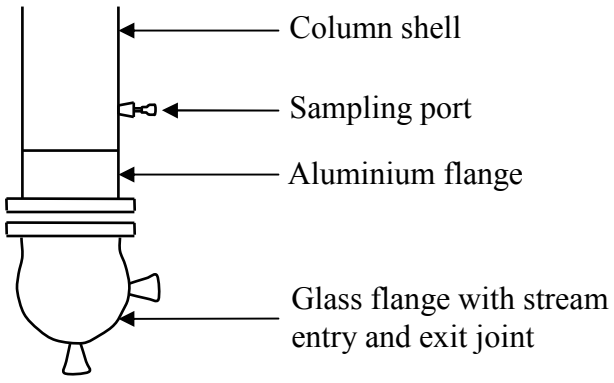

Figure 2.4: Schematic of column shell end (identical top and bottom), showing sample ports and flanges.

Packing and supports

The packing was chosen quite simply by means of availability. Two types of packing were available, namely ceramic raschig rings and stainless steel intalox saddles. The flooding and loading characteristics of both packings were tested in a pre-existing column made of Perspex with a linked water and compressed air supply. The behaviour of both packings may be compared in a plot of pressure drop for increasing gas velocity. This is shown in Figure 2.5 below.

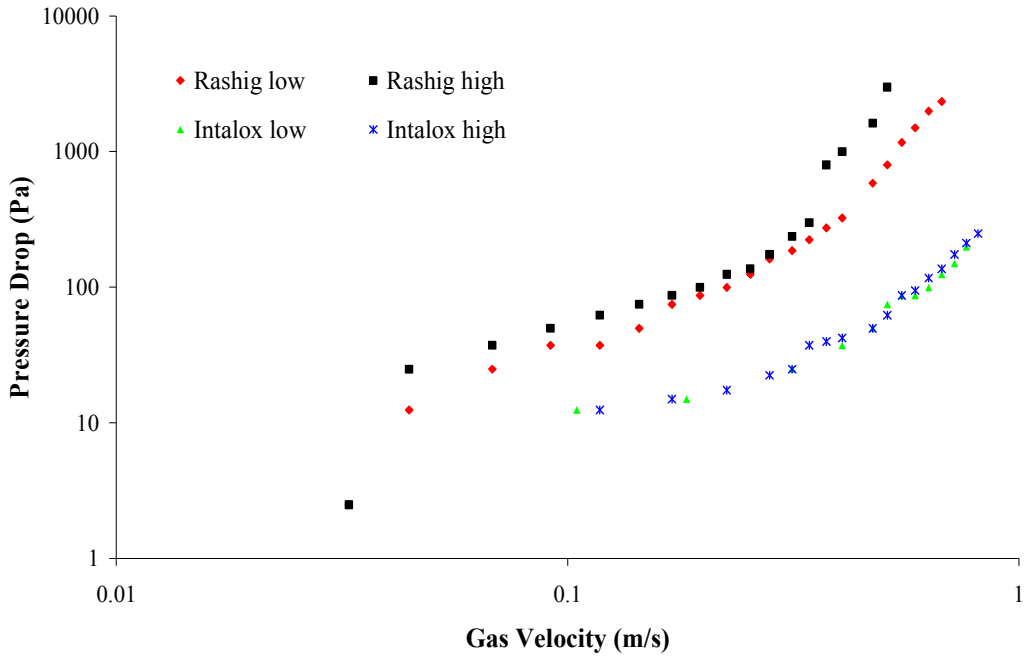

Figure 2.5: Experimental flooding and loading characteristic graph for raschig ring and intalox saddle in identical apparatus for high and low liquid flow rates.

The following may be deduced from Figure 2.5:

- The intalox saddles behave consistently with increased liquid flow rates. The raschig rings flood at lower gas velocities for increasing liquid flow rates.

This difference is due to the sheer volume difference of the two packing types. There is far more free area available in the case of the intalox saddles.

- There is a higher pressure drop associated with the raschig rings for equivalent gas velocities when compared to the intalox saddles. This is again to the volume difference between the two types.

The increased surface area per volume of the intalox saddles compared to the raschig rings results in a far more stable response to operating conditions. The saddles are made of stainless steel and are unlikely to break or deform during loading of the column shell, thus ensuring a uniform packed bed. The raschig rings are brittle and some breakage would likely without loading the column with water prior to adding the packing. The stainless steel intalox packing was thus used in the column.

Perforated aluminium plates above and below the packing provided a means of support and fluid distribution for the entering vapour and liquid streams.

Sample Ports

The sample ports are placed along the length of the column shell. The ports are simply drilled holes into which customized liquid sampling tubes are placed. A sampling tube is shown in Figure 2.6. The rubber plug provides a tight seal in the column shell. The flared end inside the column maximizes the liquid sample catchment area which then collects at the end where the rubber syringe seal is.

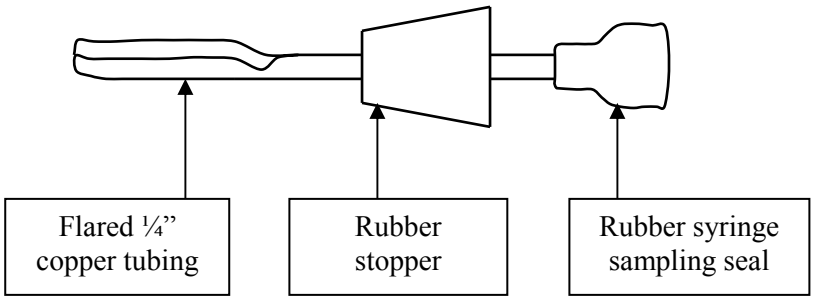

Figure 2.6: Schematic of sampling port in column shell.

Heating

One of the requirements for the assumption of constant molar overflow in the column requires that the column be adiabatic. Any external addition or heat loss would result in localized vaporisation or condensation and consequently, either the vapour or liquid stream having higher or lower flow rates than would be expected.

This means that the column section should be completely insulated to ensure that the temperature profiles of the streams are self regulating according to their own heat content. Deviations from molar overflow manifest as discrepancies in the calculation of the bottom and top delta points for the column section (see Section 2.5.3). Thus by comparing the calculated delta difference composition points at the top and bottom of the column, one has a good measure of how adiabatic the column was for the experimental run if the control on the flow rates of the feed streams was sufficient.

At steady state and thermal equilibrium, a temperature profile will be established along the length of the column. If one were to simply send the pre-heated streams into the insulated column, this would be equivalent to a large heat loss until steady state was reached. This is mainly due to the fact that the experimental apparatus acts a heat sink until an equilibrium temperature is reached.

For an initial time estimate, only vapour feed was sent to the column, the time from the vapour forming at the bottom entry point to the column and the first drop of condensate to form from the vapour product of the top of the column was recorded. This time period was just over 2 hours!

This was unreasonable from a time and economic perspective. Since the streams are not recycled, they pass through the column once and for the purposes of that particular experiment, are classed as waste. 2 hours of waste streams would have meant large amounts of charge for the feed streams to the column, inevitably ending up as waste. Clearly this is unacceptable. A simple solution was the application of heating tape to the shell of the column underneath the insulation material.

The heating tape was temperature controlled by means of a strategically placed thermocouple and a temperature controller. Prior to the establishment of an ideal starting temperature, the thermal equilibrium was checked in two ways during experiments. A handheld digital thermometer was used to monitor the temperatures through the liquid sample points. Samples were analysed during test experimental runs to monitor the change in the compositions of the product streams.

The best temperature was found to be a mid range temperature of 60°C according the component boiling points. The column was heated to this temperature and the heating tape was switched off just prior to the introduction of the feed streams for a particular run. Thermocouple testing and confirmation with product sample analysis revealed that thermal equilibrium and indeed steady state was reached within five minutes of the feed streams having been introduced to the column. Thus for all experimental runs, samples were taken within ten minutes of the experiment having started.

2.3.3 VAPOUR FEED

The simplest method of providing a vapour feed to the column is simply to heat a liquid to its boiling point and provide some means of transport to the column.

The safest solution was to use heating mantles with temperature control and a built in trip mechanism in case of spillages or electric short circuits.

The experiment requires a vapour feed at constant flow rate and of constant composition. If one were to use one mantle and simply charge it with a mixture of the required composition, the composition of the vapour would follow that of a residue curve with a distillate composition of the starting mixture and would thus be changing with time.

If one were to use three pure components, each in their own mantle, the composition of the resulting mixture could be controlled by manipulating the temperature control of the mantles.

Three identical mantles were sourced; their capacity is 3 litres and 450 Watts.

The mantles are temperature controlled by means of a variable resistor graded as a percentage of the total mantle heat output. The linearity of the percentage increments was tested as shown in Figure 2.7.

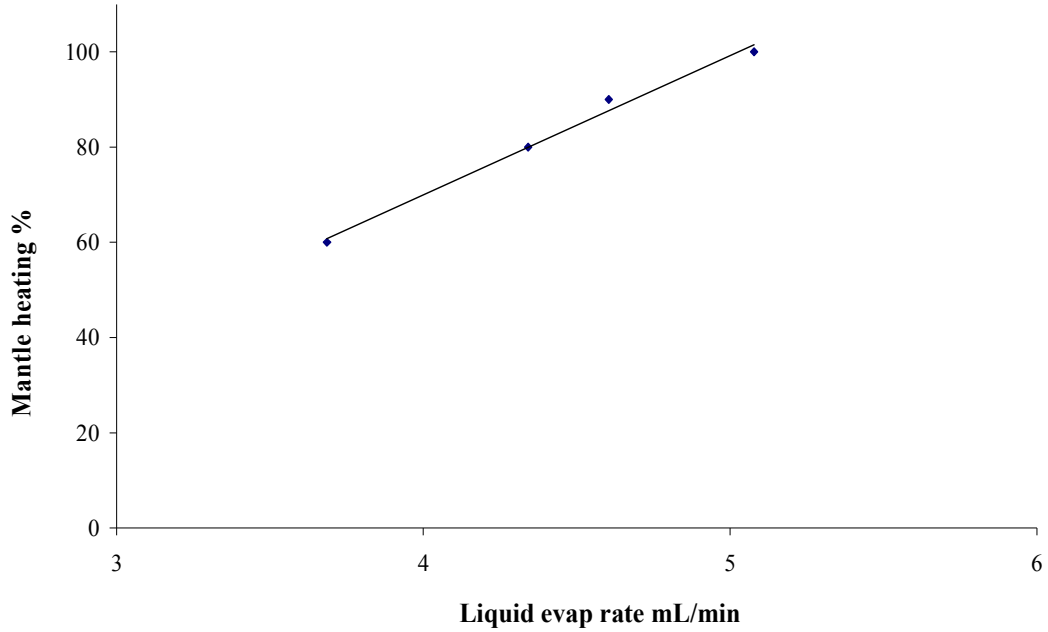

Figure 2.7: Heating mantle temperature control increment linearity tested for various settings and water evaporation rate.

The increments were thus assumed to result in linear increases in heat output from the mantles. The point of this exercise was simply to save chemicals in the calibration of the heating mantles. Now that the linearity of the mantles has been proven, one simply needs to do three boiling experiments with pure acetone, methanol and ethanol and interpolate the resulting evaporation rate to obtain the rates for different heating mantle increments. The result is shown in Figure 2.8.

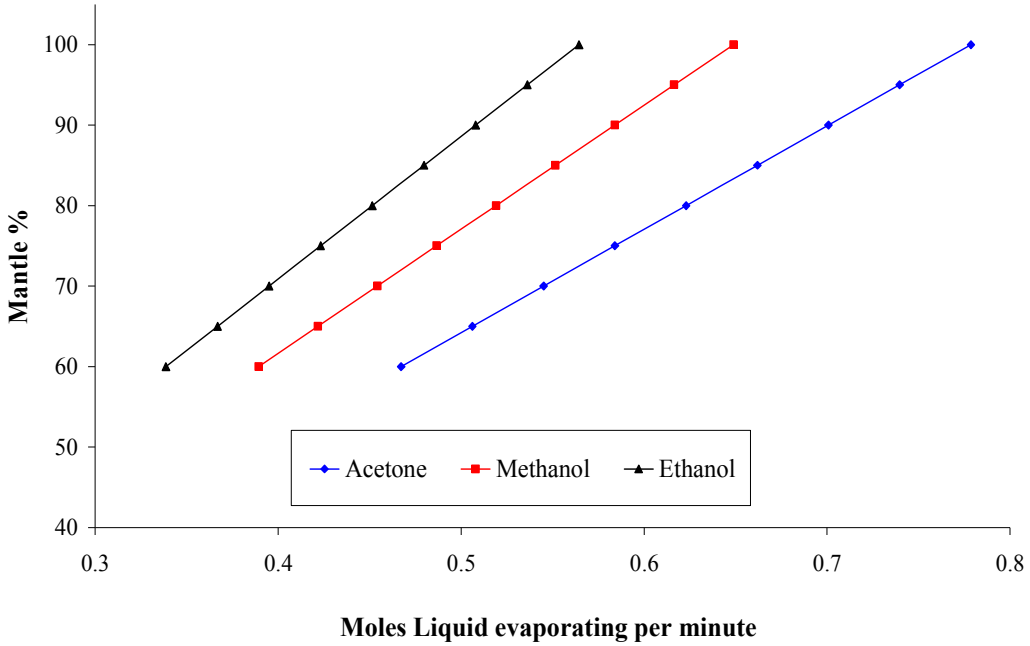

Figure 2.8: Moles of pure components evaporated for different heat settings on heating mantles.

Knowing the maximum heating rates of the mantles gives an idea of the amount of liquid charge required in the still for a certain time period. One solution is simply to have a large excess of liquid charge in the stills.

This would however require a long time for the entire amount to reach its boiling point at start up. A solution to this problem was to only have a small charge in the still and have an external reservoir to top up the liquid in the still, as shown in Figure 2.9. This configuration achieved three main goals:

- The liquid in the stills could indirectly be recharged by adding to the external reservoirs, thus liquid charge could be added without having to stop the experiment. The vapour feed could be analysed during the experiment via a sample port.

- A form of level control was implemented via the tube from the reservoir into the still to ensure a constant composition after the three vapour streams mixed.
- Only a small amount of liquid was present in the still at one time, thus minimizing start up times.

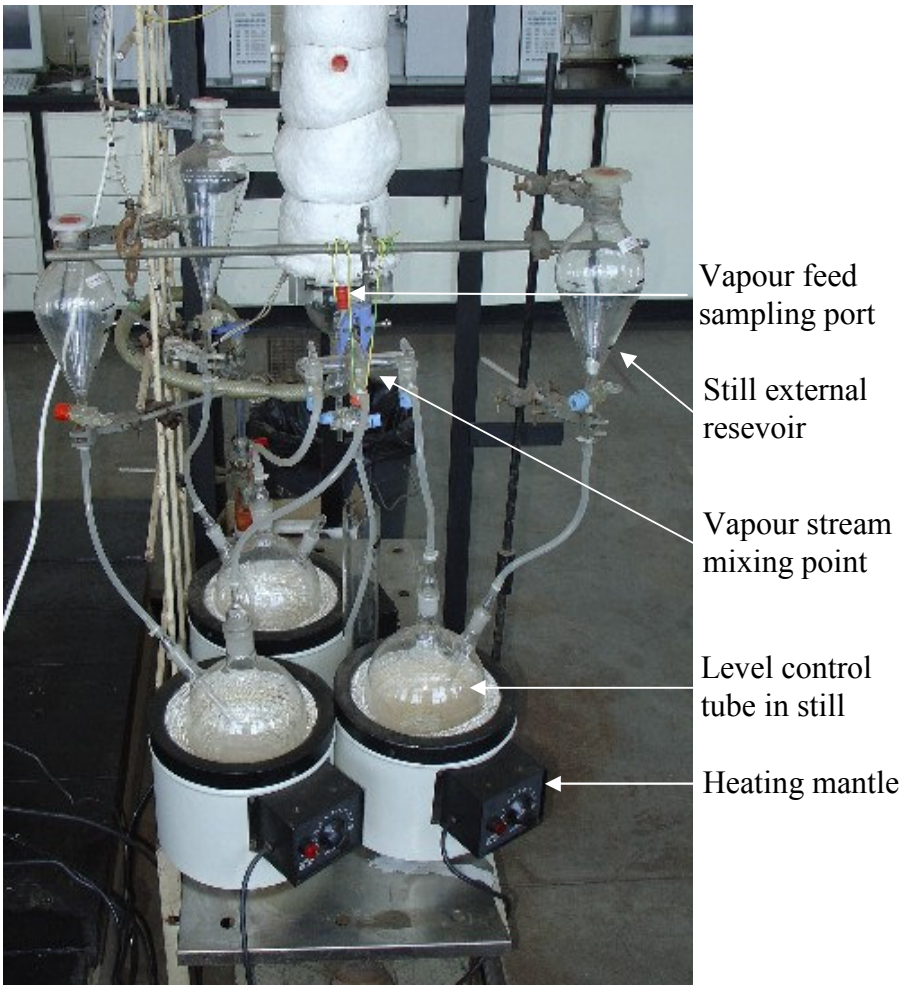

Figure 2.9: Vapour feed apparatus showing three mantles and stills fed by external level controlling reservoirs.

Thus using Figure 2.8, one could select a compositional fraction by setting the three mantles to the required heat settings. The stills were then charged and heated with the

specified pure components. The outlet of the tube from the reservoir acted as a level control by maintaining the liquid level in the still at the level of the tube outlet.

The tube diameters were made greater than 9mm in diameter to ensure that the gravitational force of the liquid in the tube exceeded the surface tension at the bottom meniscus. This ensures that the liquid flows freely from the reservoir. An obstruction occurred at the reservoir tap (somewhat less than 9mm in diameter), but sufficient agitation during boiling allowed the liquid to flow through the tap.

2.3.4 LIQUID FEED

Flow rate and composition

The constraints set by the heat supply capabilities of the heating mantles meant that for a particular selected vapour composition, the flow rate was inherently set. This was only true of course in case where mixtures were desired. In the cases where all three mantles contained the same component then some variation of flow rate was possible.

Theoretical column profiles result from a finite reflux ratio. With the vapour feed flow rate having been set by its composition, the liquid feed flow rate requirements may be determined from the reflux relationship given by:

$$R_{\Delta} = \frac{\dot{L}}{\dot{V} - \dot{L}} \qquad \textbf{(2.15)}$$

Positive reflux ratios thus require a vapour flow rate larger than that of the liquid. In this case however the heating capacity of the mantles was found to be limiting. Positive reflux ratios required small liquid flow rates that were insufficient for wetting of the packing and for consistent liquid sampling.

The column was therefore operated with larger liquid flow rates than vapour flow rates, which of course meant that according to equation 2.15, all the reflux ratios are negative. In complex columns in particular, alternating profiles of positive and negative reflux can exist, (Tapp et al, 2004).

This decision was also favourable from a control perspective as changes in the liquid flow rate are easier to implement as the lag time is only a function of the residence time of the liquid in the column prior to the change. Variations in composition are negligible for a well mixed liquid feed.

For a vapour feed, flow rate changes are a function of the residence time of the vapour entering the column prior to the change and the effective time for the mantle to cool to the specified temperature (heat setting). These changes manifest as more vapour being formed during that time. Thus the changes are not effective immediately. All possible efforts were made to control the composition of the vapour feed, but due to the range of boiling temperatures (approximately 20°C), it is very likely that the vapour feed composition variation would have varied more than that of the well mixed liquid feed when implementing a flow rate change.

The flow rate of the liquid feed was controlled by means of a rotameter and was gravity assisted. The rotameter float was modified by making it slightly heavier so that the intended range of liquid flows could be realized. A rotameter chart was obtained for water and was then corrected for density and temperature depending on the composition of the liquid stream to be used. The rotameter chart is given in Figure 2.10.

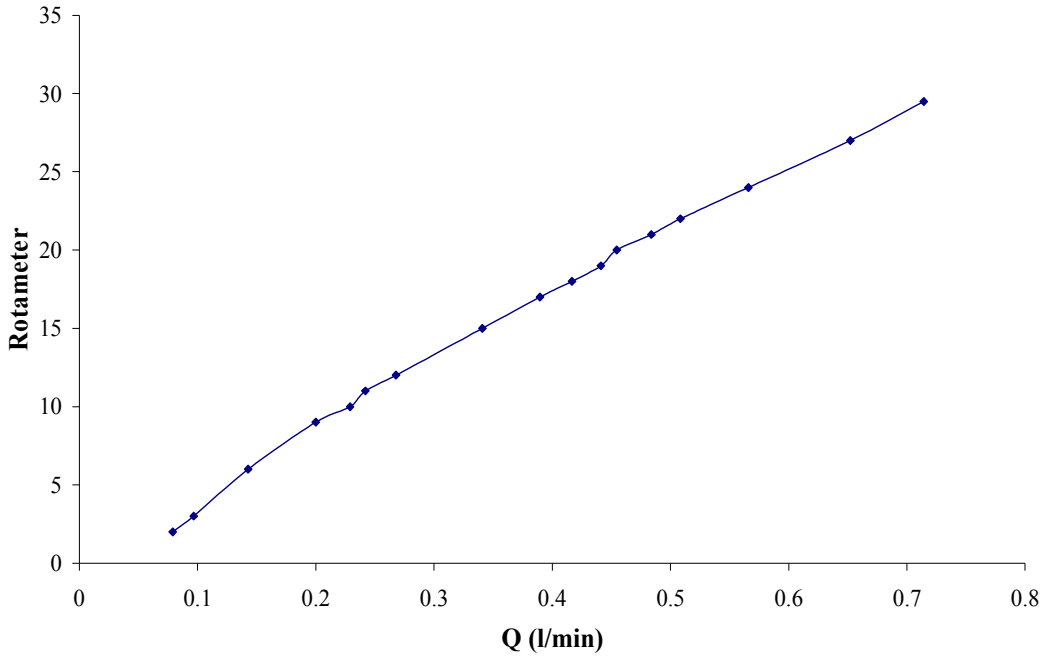

Figure 2.10: Liquid feed rotameter chart calibrated with water

The liquid feed apparatus is shown in Figure 2.11 below.

Liquid Feed Heating

In a column with recycles, the passing streams will eventually reach thermal equilibrium. The loads on the condenser and reboiler will remain constant and so to will the temperatures of the returning streams to the column. In this experiment there are no recycle streams, all streams only pass through the column once.

The purpose of the experiment is to replicate a column section within a column. Remember that a column section is defined as a section of a column in between areas of material addition or removal. The temperatures of all the feed streams in a column section within a column would thus be set by those above or below the particular section, and those would in turn be set by their preceding or following sections. In

effect each feed stream to a column section is indirectly controlled by heat supply to or heat removal from the column.

In order to replicate a column section it should be clear that not only are the flow rates and compositions important, but the temperature of the feed streams too. The temperature of the vapour feed stream is simply the boiling point temperature of the pure component or some combination of them in the case of a mixture. The liquid feed stream is thus the more important of the two as it is not self regulating.

Once having been convinced that the boiling temperatures were correctly predicted by theoretical models, the theoretical models were used to predict those of the various liquid feed mixtures. The boiling point temperature is analogous to the dew point temperature for a condensing vapour. The liquid feed should be at its dew point to simulate a stream having come from a previous column section.

A insulated copper coiled tube was covered with heating tape was used to heat the liquid feed prior to entry into the column. The heating tape was temperature controlled by means of a thermocouple measuring the temperature of the liquid outlet stream from the coil. The heat output of the heating tape and coil combination was found experimentally to be 318Watts. Thus for a particular feed composition, the dew point is known and the temperature of the feed prior to entering the coil can be calculated for a particular proposed feed flow rate. The high dew point temperature of most of the feeds suggested that the feed reservoir would have to be insulated to maintain the temperature required, prior to entering the coil and subsequently the column. The configuration is given in Figure 2.11.

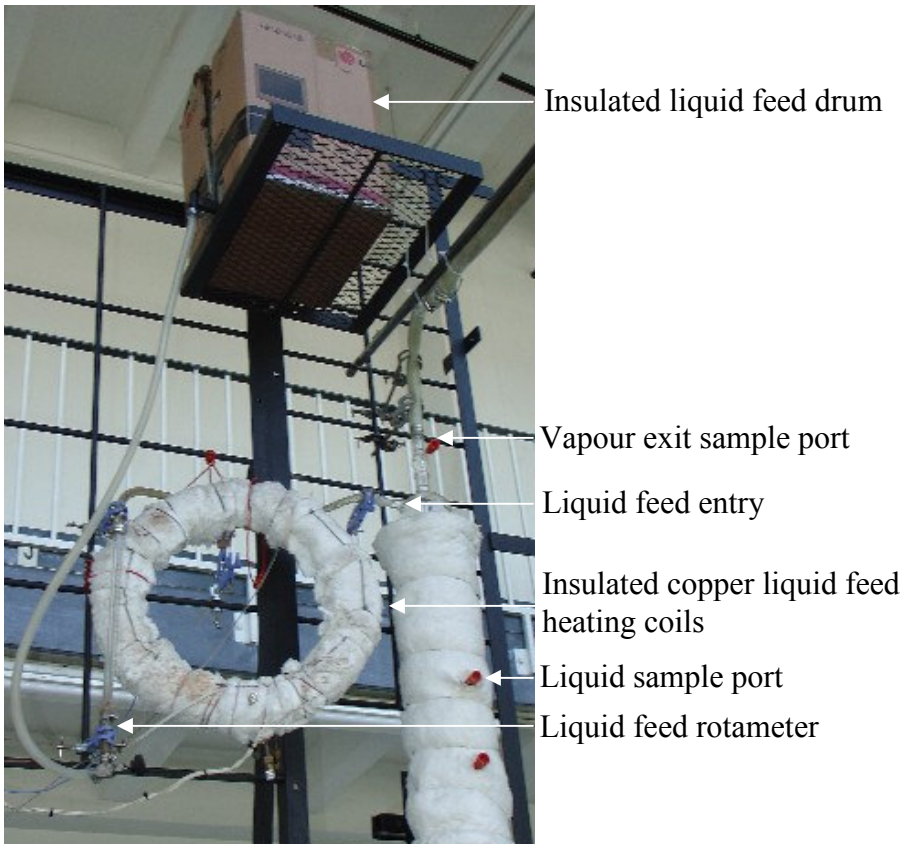

Figure 2.11: Liquid feed apparatus showing insulated reservoir, rotameter and insulated copper heating coils.

2.3.5 VAPOUR EXIT

The vapour exit is included in Figure 2.11. The vapour exits the column and flows to a water cooled condenser after which it is collected in a large flask. The vapour is sampled at the top of the column above the liquid feed entry point.

Analysis of the liquid distillate also gives an overall average vapour distillate composition for the experiment. The vapour exiting at the top of the column is an instantaneous composition, thus comparing this to the average gives an idea whether a constant vapour composition was maintained.

A burette prior to the flask provides a means of measuring the instantaneous flow rate of vapour through the column. This may then compared to the average flow rate calculated from the total condensed liquid and the total experiment time.

2.3.6 LIQUID EXIT

The liquid exiting the column acts as a liquid seal to the entering vapour feed stream by means of a sump. The instantaneous liquid composition may be sampled in the sump. The average composition is sampled from the insulated drum at the base of the column at the end of the experiment. A valve and incremented glass tube provide a means to compare the instantaneous flow rate with the average flow rate. The average bottoms liquid flow rate is the total bottoms liquid volume divided by the total experiment time.

2.3.7 SAMPLING EQUIPMENT

The liquid was sampled with a syringe and size 18 needle. The sample points are along the length of the column. All sample ports were sealed with a special rubber syringe seal.

Vapour samples were taken with a vacuum syringe designed to condense the vapour as the sample is taken.

All samples were cooled in a cooler bag with ice packs prior to being injected into 1.5ml sample vials.

2.3.8 PHYSICAL PROPERTY MEASUREMENT

Liquid feed and GC calibration mixtures were prepared using scales to three decimals. The scales were limited to a maximum load of 1.5kg. For post experimental analysis, the large amounts of liquid proved a problem for mass balance assessments.

A volume basis was thus used. The volume and temperature of all feed mixtures was recorded. The volume of the product mixtures and remaining feed mixtures was then recorded at the same temperature. Temperatures were measured with a handheld digital thermometer to one decimal place.

2.3.9 COMPOSITION ANALYSIS

All samples were analyzed in a Thermal Conductivity Detection (TCD) Gas Chromatograph (GC). The model was the Agilent (Inc.) 6820. The GC works on thermal conductivity differences. Hydrogen and helium have two of the highest thermal conductivities and are therefore superior as carrier gases for the TCD. Hydrogen was used as the carrier gas for this experiment.

A full discussion of the GC configuration and its calibrations offered in APPENDIX B. An example of the output of the GC is given in Figure 2.12.

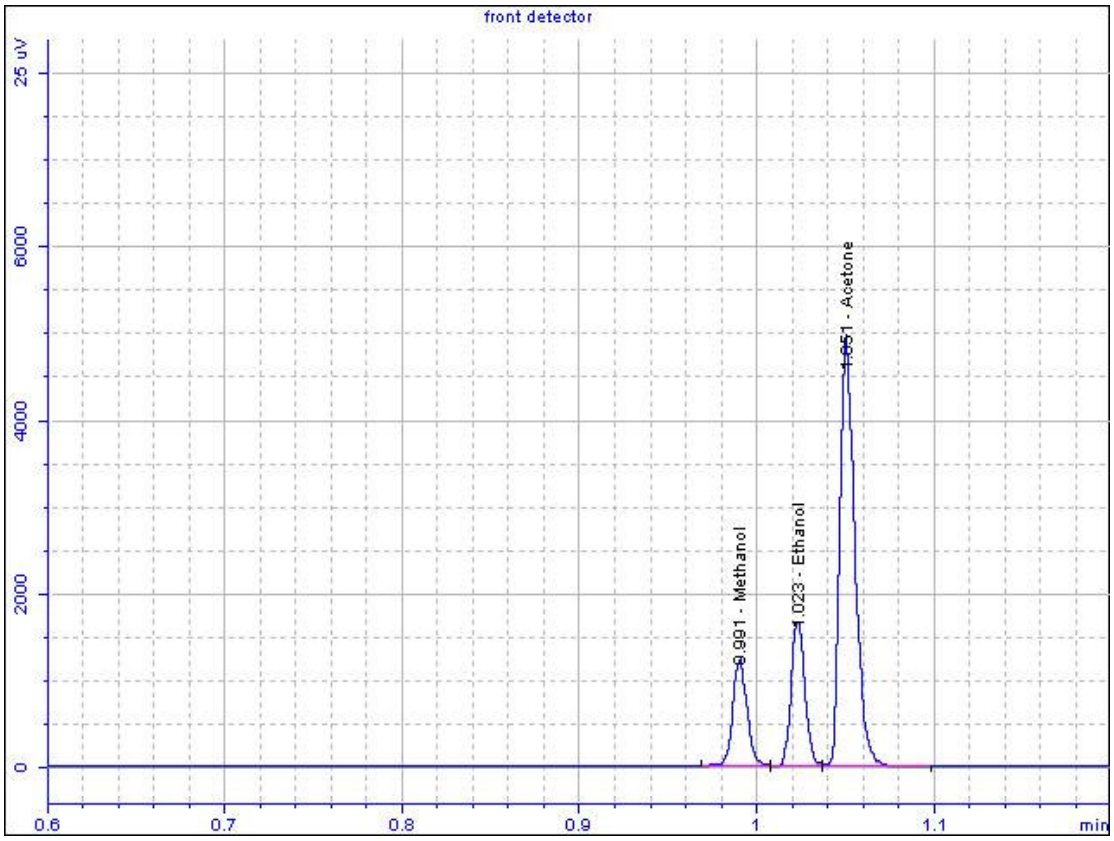

Figure 2.12: Example of GC output showing relative area peaks for a methanol, ethanol and acetone mixture.

2.3.10 APPARATUS OVERVIEW

A photograph showing the overall column apparatus is shown in Figure 2.13. All small diameter tubing was medical grade silicon and the thicker tubing was silicon hosing. All junctions of hose and glass or metal were secured with expandable jubilee clamps.

A qualitative schematic of the apparatus showing the sampling port positions is shown in Figure 2.14.

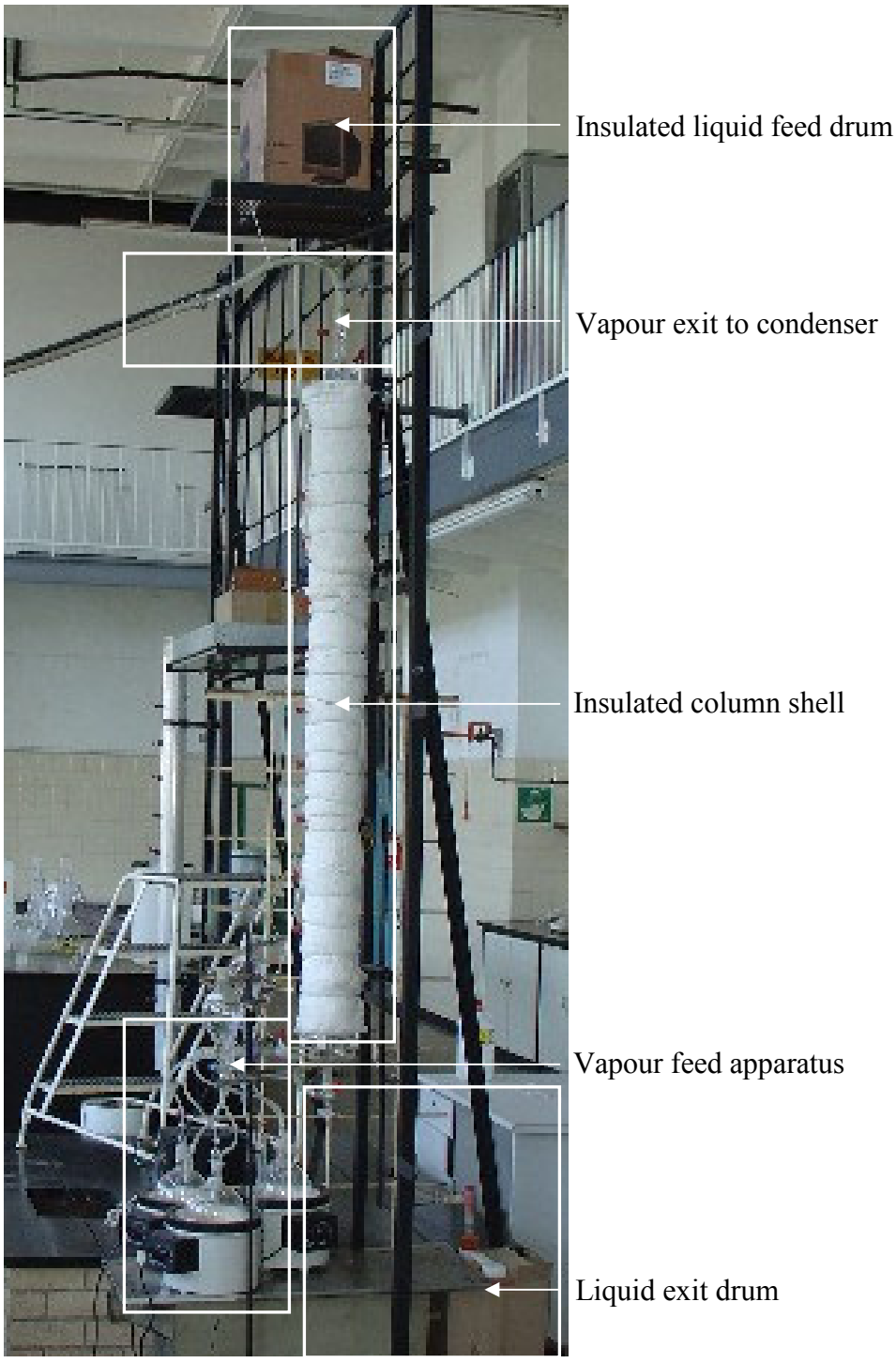

Figure 2.13: Photograph of complete column apparatus showing various column function areas.

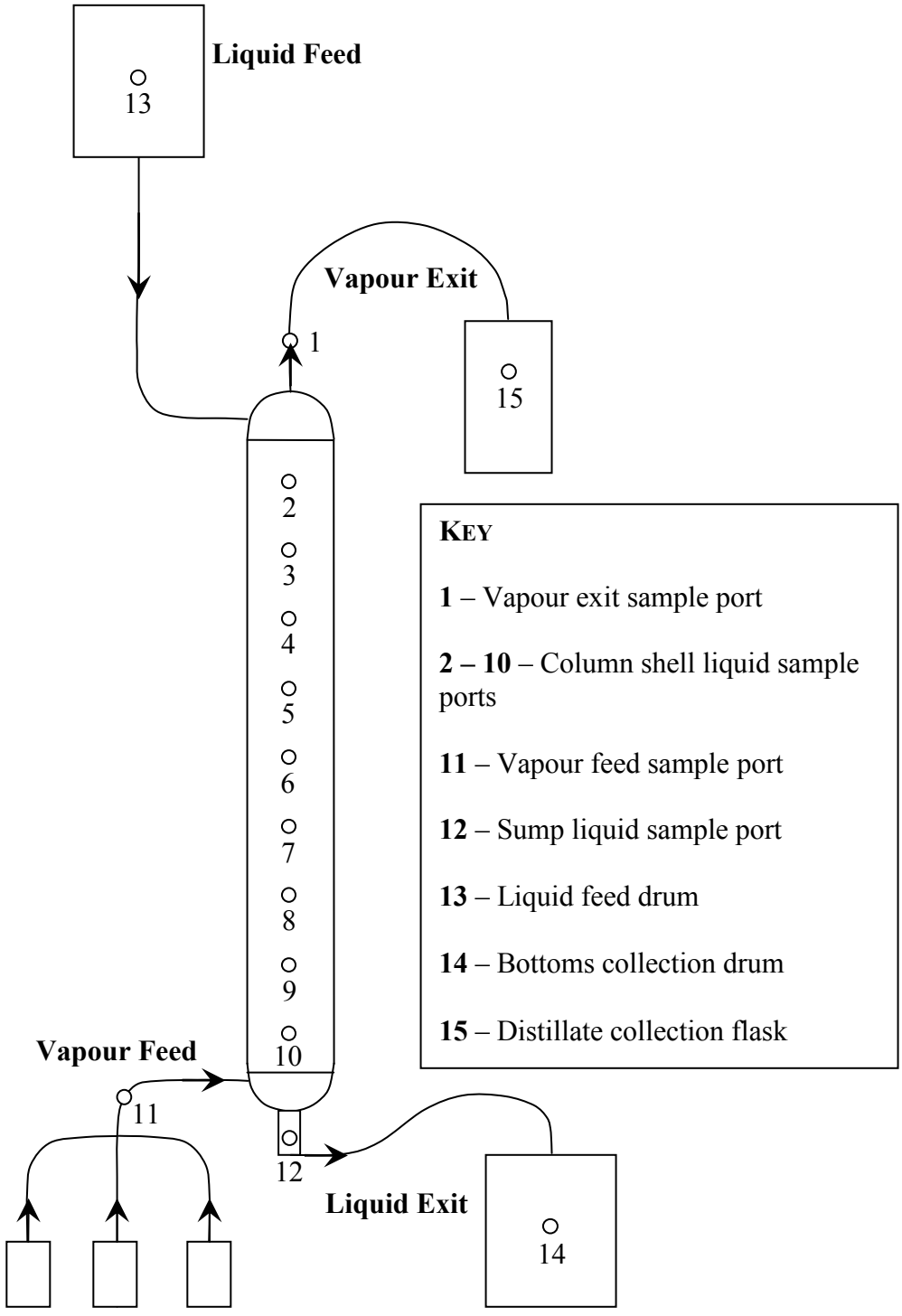

Figure 2.14: Qualitative schematic of column apparatus showing various sampling ports and column function areas.

2.4 EXPERIMENTAL PROCEDURE

2.4.1 PRE-EXPERIMENTAL CALCULATIONS

The feasibility of a potential theoretically predicted column profile needs to be investigated prior to any experimentation.

The liquid and vapour feeds are selected on the basis of a theoretically predicted column profile map for a selected reflux. A theoretical profile was selected on the basis of two main factors.

- The initial concern was the expense of the raw materials, ethanol in particular. Thus profiles were selected conservatively to limit instances where the column profiles may be greatly influenced by small fluctuations in steady state, resulting in useless results. For this same reason, only transformed distillation regions of interest were examined. These were regions where extreme deviations from infinite reflux behaviour were observed.

- The second influencing factor was the achievable vapour bottoms feed to the column. The vapour feed was supplied by three heating mantles where different combinations of heat supply (temperature control) and type of pure component allowed a selection of possible vapour feeds. Thus only composition profiles where the vapour feed to the column could be achieved were considered.

Thus for a feasible column profile, the flow rates and compositions are known. The required temperature of the liquid feed stream needs to be calculated according to the composition. The temperature required in the liquid feed reservoir can then calculated because the heating coil heat output is known and flow rate of the liquid will be set.

2.4.2 START UP

Feed Preparation

The liquid feed composition was prepared by weighing on a scale for new mixtures or by GC analysis for existing mixtures. An amount was prepared according the intended liquid flow rate and experimental time. The volume of the liquid was recorded. The liquid was then heated to the calculated temperature required prior to entry of the heating coils. The heated liquid was then poured into the insulated feed drum. The drum was lifted to the shelf above the column and was connected to the rotameter tube.

The three mantles were charged with the pure components required to make the intended vapour feed composition. The liquids were heated to their boiling points. The liquids in the stills reached their boiling points simultaneously with some careful mantle timing depending on the components. It was also insured that the liquid feed at the top of the column was also ready at this stage. The liquid reservoirs above the vapour stills were also charged with their respective liquids, the lids were put on and the taps opened.

Column Preparation

The column shell heating tape needs to be switched on and the temperature is set on the temperature control box. As discussed in Section 2.3.2, this temperature was found to be 60°C.

The liquid feed heating coil needs to be charged with a small amount of liquid and heated to ensure the calculated dew point temperature of the liquid feed.

The heating of both sets of heating tape should be synchronized to be ready when the liquid and vapour streams are ready for entry to the column.

The column shell heating tape is switched off during an actual experiment, but the heating coil tape is left on to control the liquid feed temperature.

2.4.3 EXPERIMENTAL STEPS

Once the column and feeds are ready, the rotameter valve may be opened as may the vapour entry valve. A stop watch is started.

Steady state is reached when the composition of the vapour and liquid exit streams are unchanging. This was found to occur in less than ten minutes for all experimental runs.

Vapour samples are then taken at the vapour entry and the vapour exit. Liquid samples are taken along the length of the column and in the column sump.

Samples are cooled in the syringes prior to injection into 1.5ml sample vials. The experimental data is tabulated in APPENDIX A.

2.4.4 POST-EXPERIMENTAL ANALYSIS

All heat supply is turned off and the product streams are isolated. The stopwatch is stopped and the total time is recorded.

All liquid vessels are allowed to cool and their volume is recorded at their initial temperature during preparation. They are sealed during this time to prevent evaporation.

The samples in the vials are analysed using the GC.

2.4.5 DATA ANALYSIS

Once the samples have been analysed in the GC, their composition is calculated via the response factors calculated during the GC calibration procedure outlined in APPENDIX A.

A volume balance is performed from the volume data collected to check whether the flows of liquid and vapour through the column are consistent with the intended values. The reflux and delta points for the top and bottom of the column may then be calculated as shown in APPENDIX A.

The composition profile of the liquid and the top and bottom composition of the vapour are then plotted in a mass balance triangle. A theoretical profile is selected according to the reflux for the top and bottom of the column. The initial integration point is then varied to give the best agreement with a superimposed theoretical profile. The theoretical profile may also be plotted as a series of stage points to correlate an experimental number of stages for the equipment.

Using the compositions of the top and bottom streams the delta points are calculated for the experimental run. The agreement of the top and bottom delta points is a good indication of how close the constant molar overflow the column operated.

2.5 RESULTS

2.5.1 DATA INTERPRETATION

The data from the experiments was interpreted in four ways:

- The column liquid and vapour profiles were compared to the theoretical predictions.
- The delta points for the top and bottom of the column were then investigated.
- The number of stages in the column was found by comparing the experimental column profile to the theoretically predicted number of stages.
- In extreme cases the isotherms of the composition space were investigated to check for any temperature inversions

2.5.2 COLUMN PROFILES

Nine experiments were performed where seven column profiles were replicated. Two profiles were repeated for reproducibility. The compositions of the vapour and liquid top and bottom compositions are plotted on a mass balance triangle for the acetone, methanol and ethanol system. The experimental liquid profiles are shown as a series of composition points. The theoretically predicted vapour and liquid curves are included to mark the deviation from the background residue curve maps. The theoretical profile map for each experiment is constructed using the calculated reflux ratio for the experiment. Prior to experimentation, the general trends of the profile map could be gauged to select a potential experimental candidate. This was in part due to the fact that even though one may control the reflux ratio, the delta point is a result of the autonomous regulation of the system by mass balance. Thus once the experiment had been performed the exact corresponding profile map could be found.

Figure 2.15 shows the intended liquid profile and the fully populated column profile map for the resulting reflux calculated from the liquid and vapour flow rate data of experiment 2. The residue curve map is shown to highlight the transformed column profile map and show the shifting of the acetone-methanol binary azeotrope into the space. Experiment 1 is discussed in section 2.5.6.

Figure 2.16 shows the intended liquid and vapour column profiles fitting to the experimental points of experiment 2. The liquid profile points clearly lie between the limits of the top and bottom compositions. The same comparison is shown for experiments 3 to 9 in Figures 2.17 to 2.28. Figures 2.16 to 2.28 are annotated to indicate the top and bottom streams in the column. The liquid enters at the top (L_T) and exits at the bottom (L_B). The vapour stream enters the column at the bottom (V_B) and exits at the top (V_T).

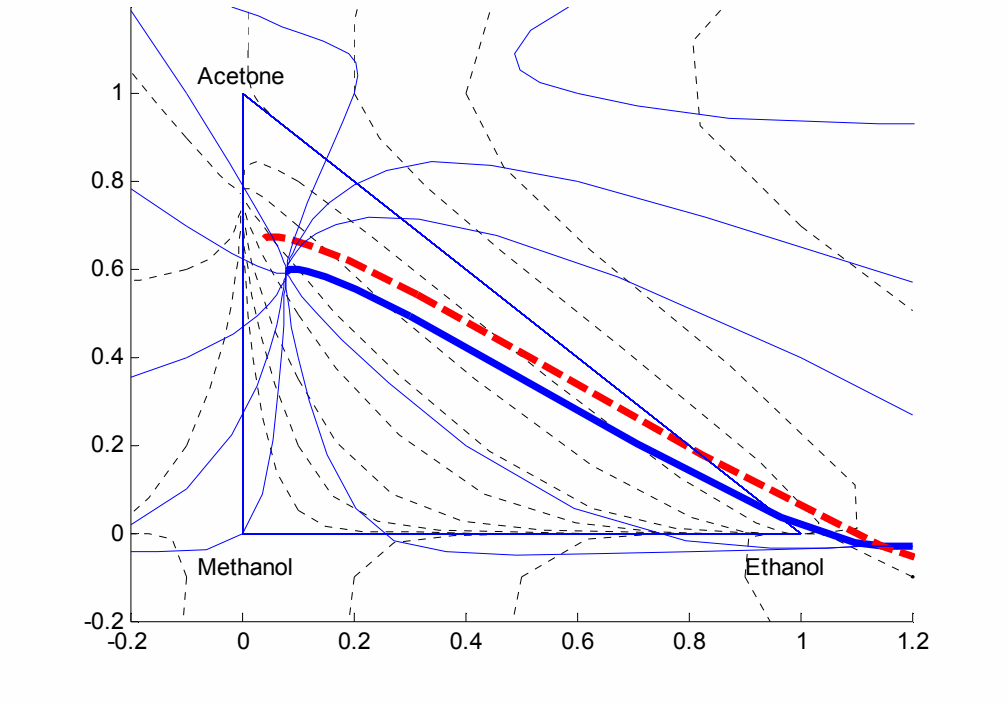

Figure 2.15: Comparison of shifted column profiles with residue curves for experiment 2. Intended liquid (bold) and vapour (dashed) profiles are highlighted. x_{Δ}=[0.304; 0.247], Reflux=-3.8

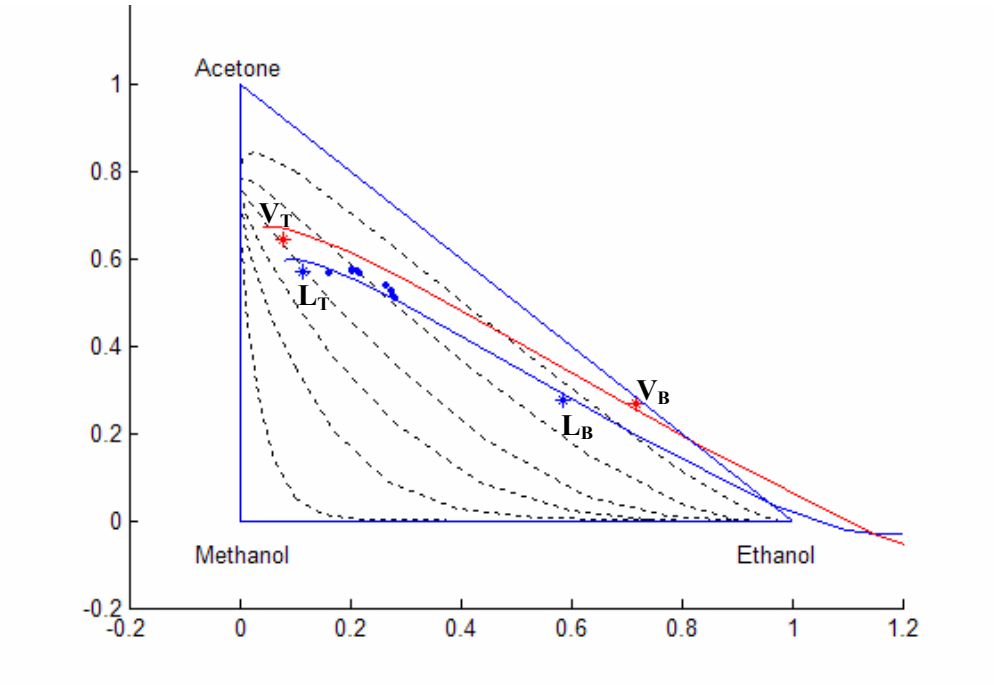

Figure 2.16: Experiment 2 profile points and corresponding theoretical liquid and vapour profile. x_{Δ}=[0.304; 0.247], Reflux=-3.8

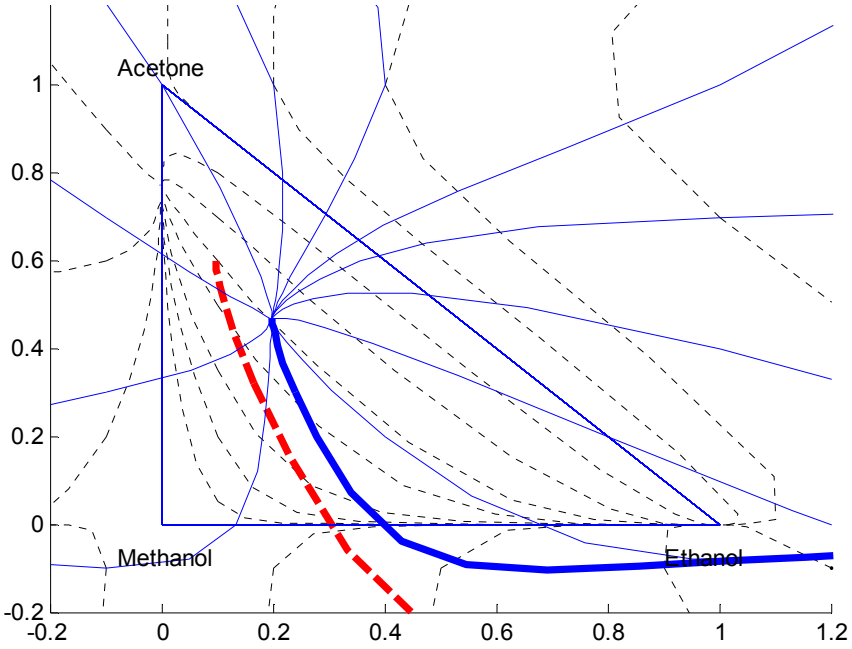

Figure 2.17: Comparison of shifted column profiles with residue curves for experiment 3. Intended liquid (bold) and vapour (dashed) profiles are highlighted. x_{Δ}=[0.269; 0.351], Reflux=-2.5

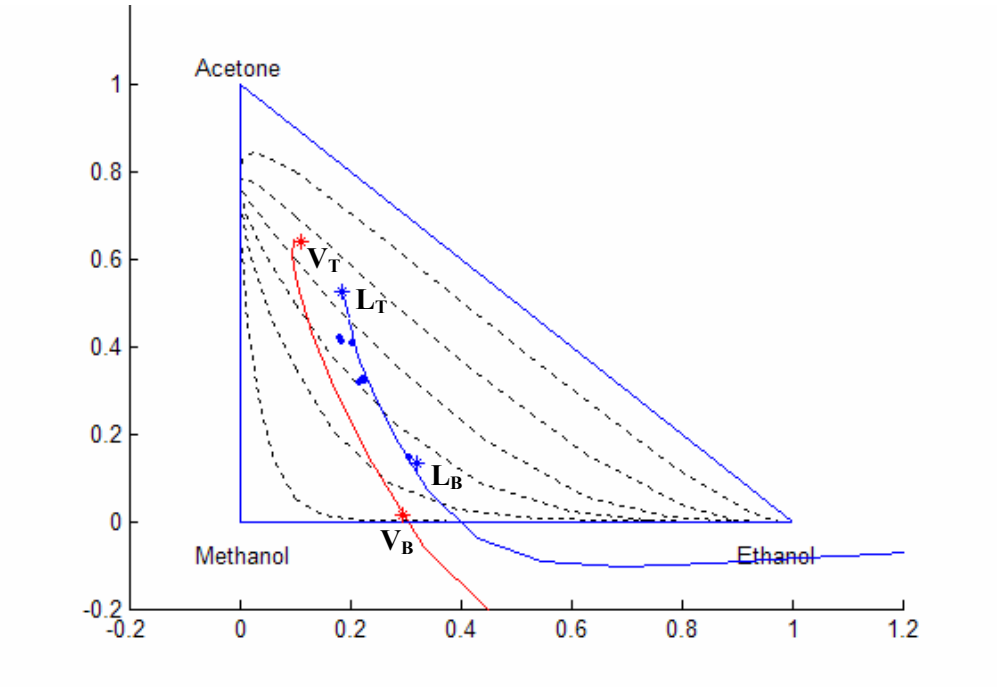

Figure 2.18: Experiment 3 profile points and corresponding theoretical liquid and vapour profile. x_{Δ}=[0.269; 0.351], Reflux=-2.5

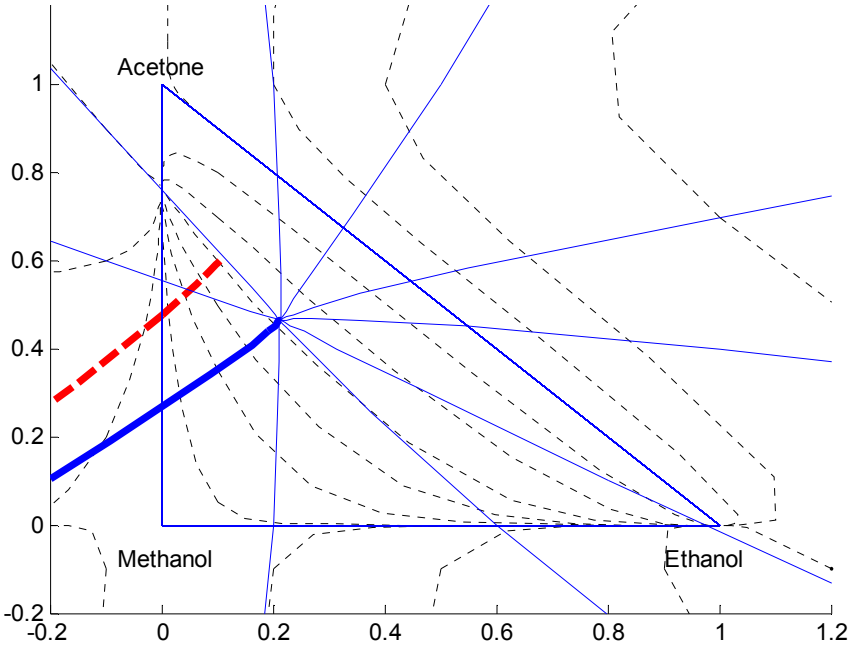

Figure 2.19: Comparison of shifted column profiles with residue curves for experiment 4. Intended liquid (bold) and vapour (dashed) profiles are highlighted. x_{Δ}=[0.431; 0.240], Reflux=-1.38

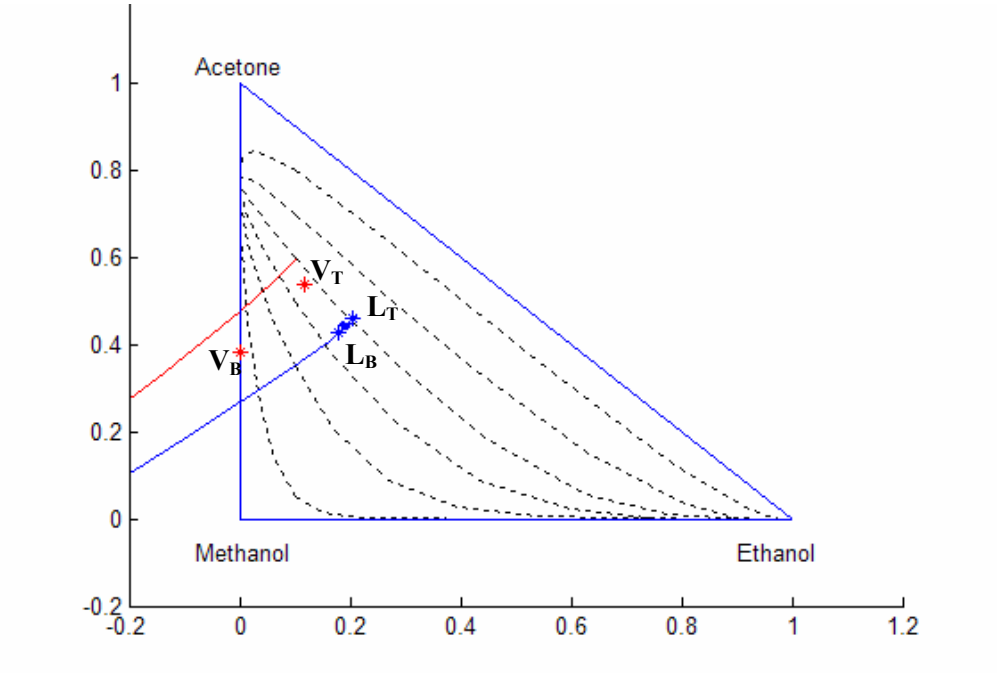

Figure 2.20: Experiment 4 profile points and corresponding theoretical liquid and vapour profile. x_{Δ}=[0.431; 0.240], Reflux=-1.38

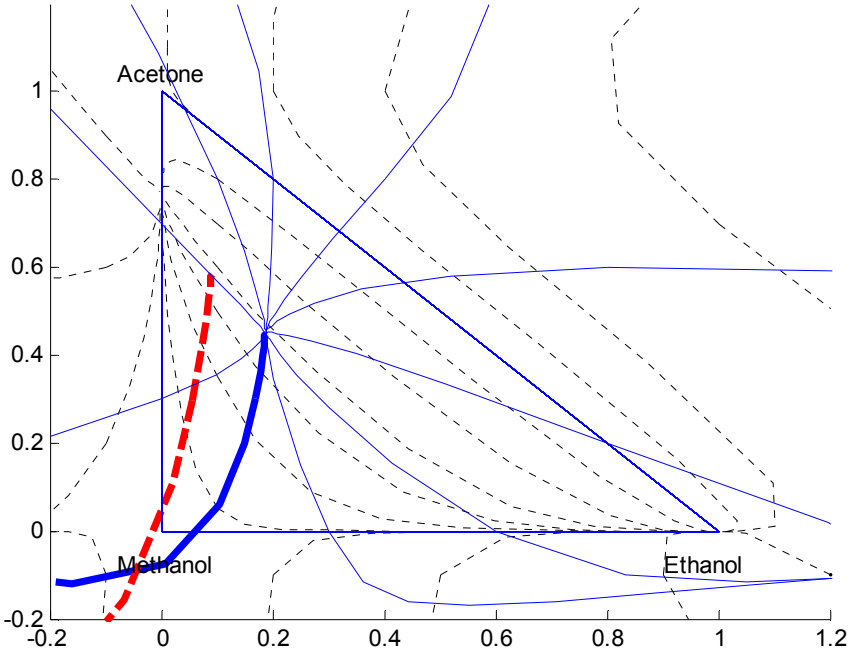

Figure 2.21: Comparison of shifted column profiles with residue curves for experiment 5. Intended liquid (bold) and vapour (dashed) profiles are highlighted. x_{Δ}=[0.303; 0.294], Reflux=-2

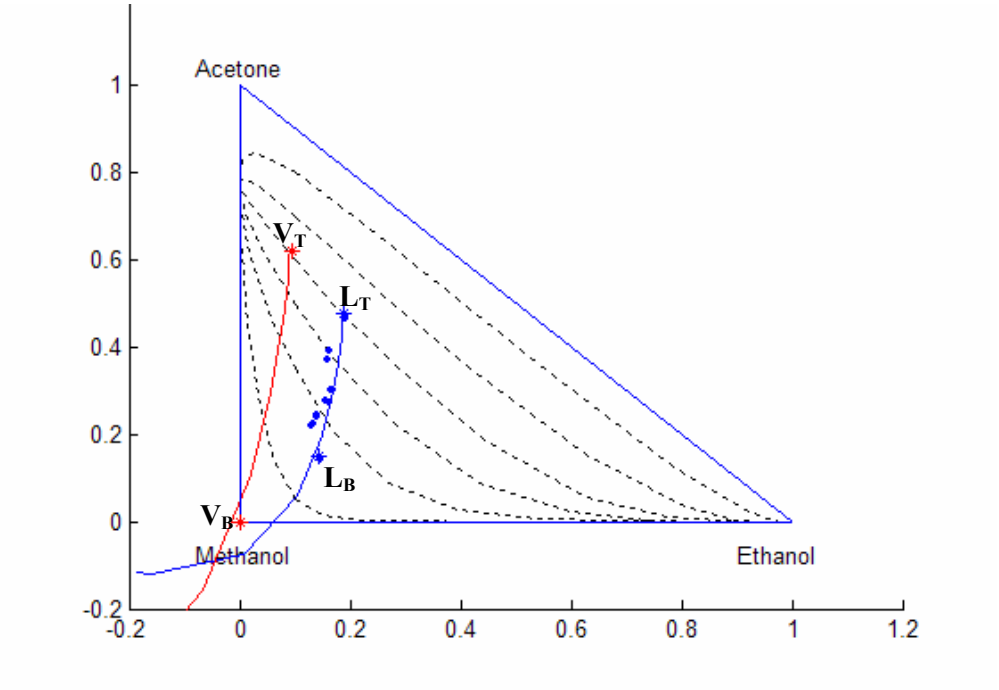

Figure 2.22: Experiment 5 profile points and corresponding theoretical liquid and vapour profile. x_{Δ}=[0.303; 0.294], Reflux=-2

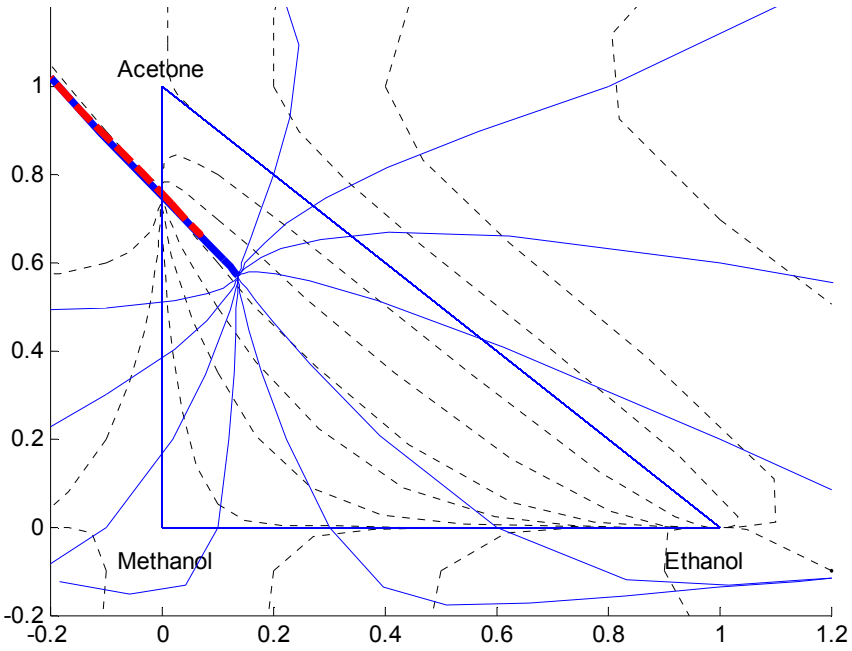

Figure 2.23: Comparison of shifted column profiles with residue curves for experiments 6 and 7. Intended liquid (bold) and vapour (dashed) profiles are highlighted. x_{Δ}=[0.445; 0.232], Reflux=-2.3

With experiments 6 and 7 the reproducibility of the experimental results was tested. Two identical experiments were performed with the same liquid and vapour feed compositions and corresponding flow rates as shown in figures 2.24 and 2.25.

The intended profile shown in Figure 2.23 is rather extreme in that the top vapour and liquid compositions begin near the shifted azeotrope composition and end (in the composition space) at the original minimum boiling acetone-methanol azeotrope. *In other words the column profiles are completely opposite in direction to the residue curves.*

The two experiments are shown in Figures 2.24 and 2.25. The two resulting profiles are barely discernible. Reproducibility of the results was specifically tested in this extreme case to verify that the results are quite easily reproducible.

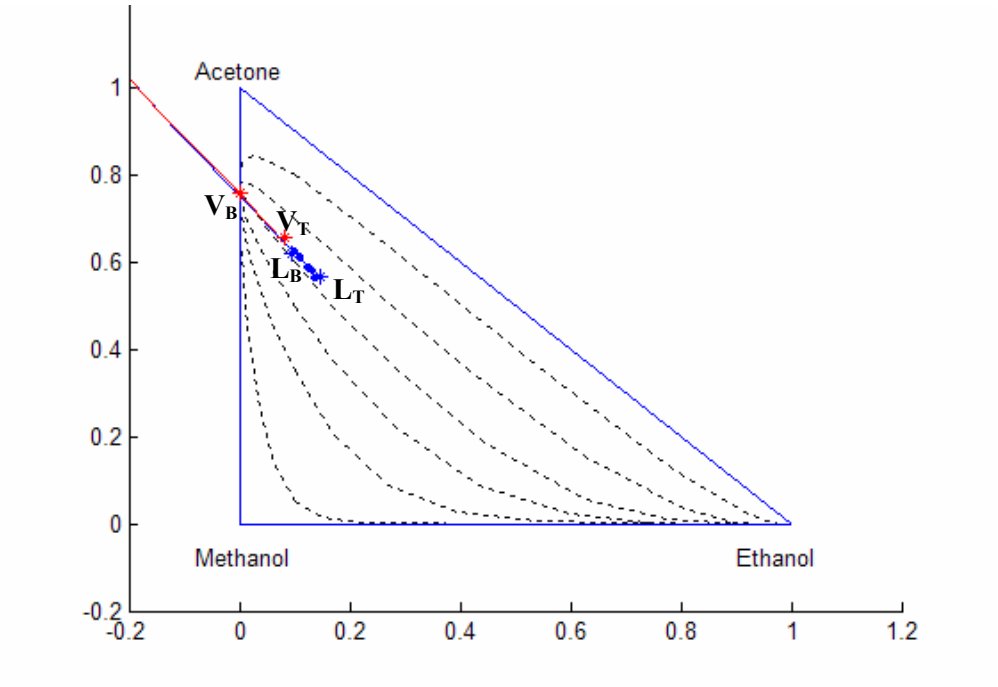

Figure 2.24: Experiment 6 profile points and corresponding theoretical liquid and vapour profile. x_Δ=[0.445; 0.232], Reflux=-2.3

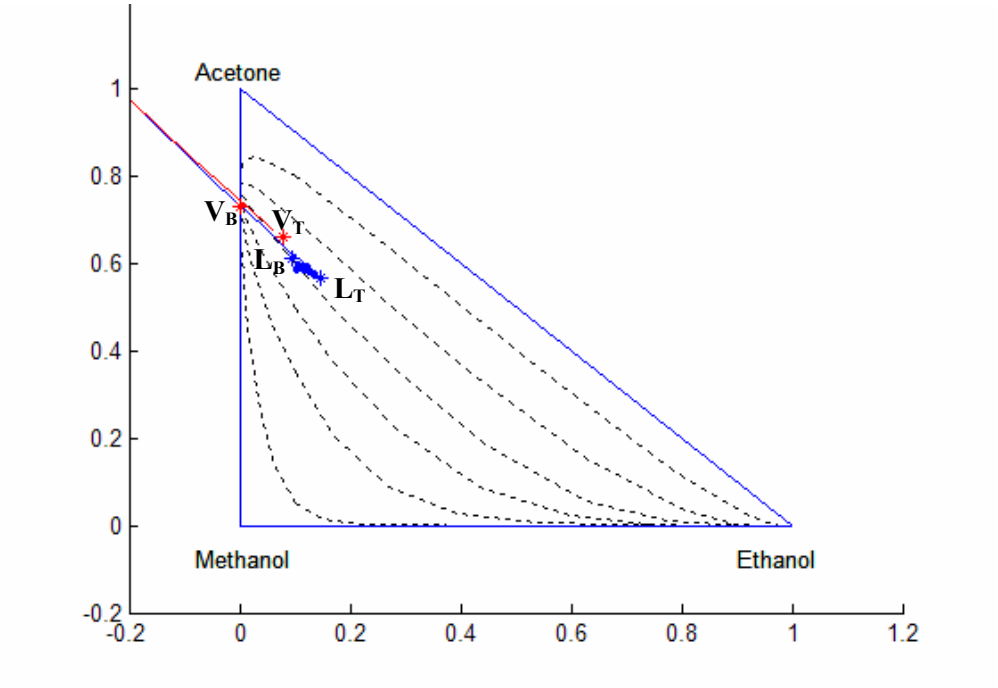

Figure 2.25: Experiment 7 profile points and corresponding theoretical liquid and vapour profile. x_Δ=[0.474; 0.212], Reflux=-2.1

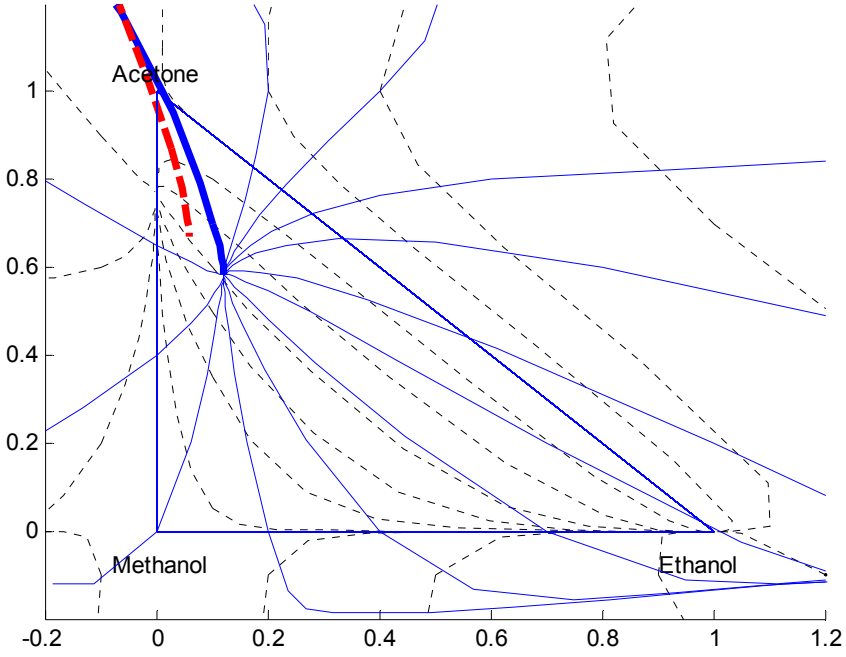

Figure 2.26: Comparison of shifted column profiles with residue curves for experiments 8 and 9. Intended liquid (bold) and vapour (dashed) profiles are highlighted. x_{Δ}=[0.492; 0.188], Reflux=-1.96

For experiments 8 and 9, identical column profiles were chosen. Two identical experiments were performed with the same liquid and vapour feed compositions and corresponding flow rates as shown in figures 2.27 and 2.28.

The two experiments are shown in Figures 2.27 and 2.28. The two resulting profiles are slightly different to illustrate a point. The liquid flow rate is larger than the vapour flow rate for all experiments. A large liquid flow rate is not sensitive to a small vapour flow rate in that only a small range of liquid compositions will result from the interaction by sheer mass balance. Thus adjusting the reflux ratio slightly can lengthen (or shorten) the liquid profile without having a significant effect on the shifted column profile map. The two profiles in Figures 2.27 and 2.28 illustrate this where the second liquid profile is slightly longer.

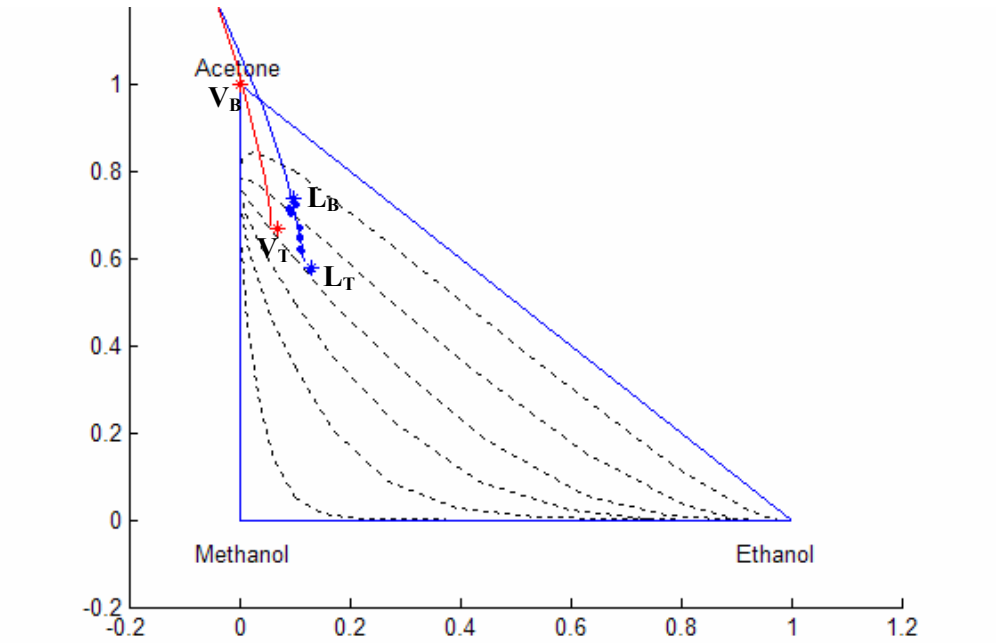

Figure 2.27: Experiment 8 profile points and corresponding theoretical liquid and vapour profile. x_Δ=[0.492; 0.188], Reflux=-1.96

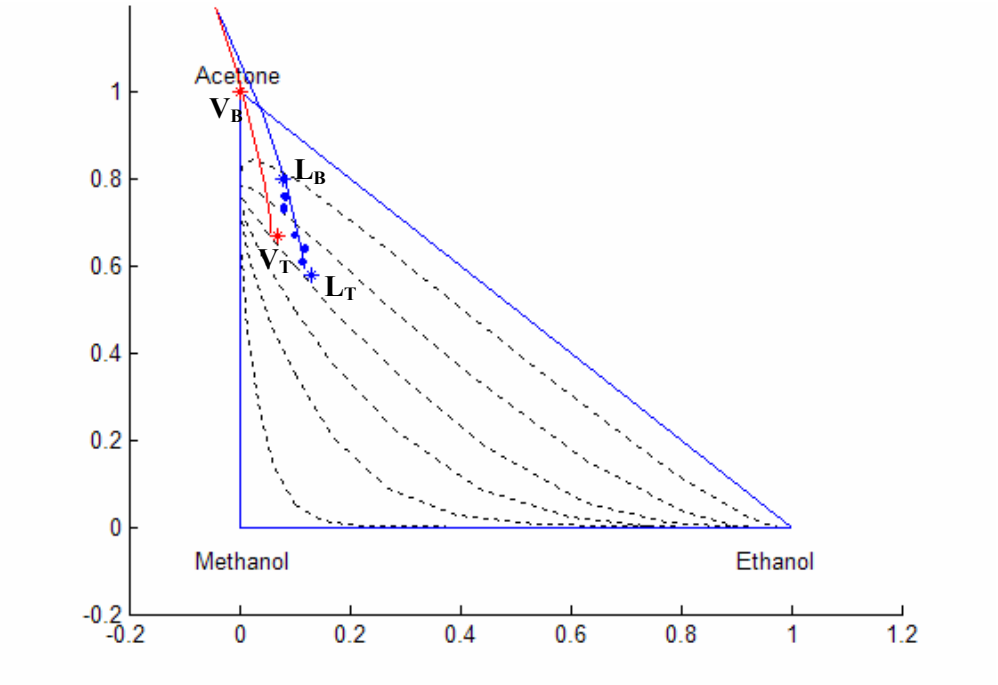

Figure 2.28: Experiment 8 profile points and corresponding theoretical liquid and vapour profile. x_Δ=[0.492; 0.188], Reflux=-2.3

2.5.3 DELTA POINTS

The delta points corresponding to the top and bottom of the column for each experiment may be calculated using equation 2.4 and the molar flowrates and compositions of the liquid and vapour streams at the top or bottom of the column. The experimental data is available in APPENDIX A for each experiment.

Agreement between the top and bottom delta points is a consistency check for the experiments. Equivalent delta points for the top and bottom of the column imply constant molar overflow and adiabatic operation of the column. The delta point is calculated from equation 2.4.

The delta points were calculated for the top and bottom of each experiment (except experiment 1) and are shown in Figures 2.29 to 2.36 below.

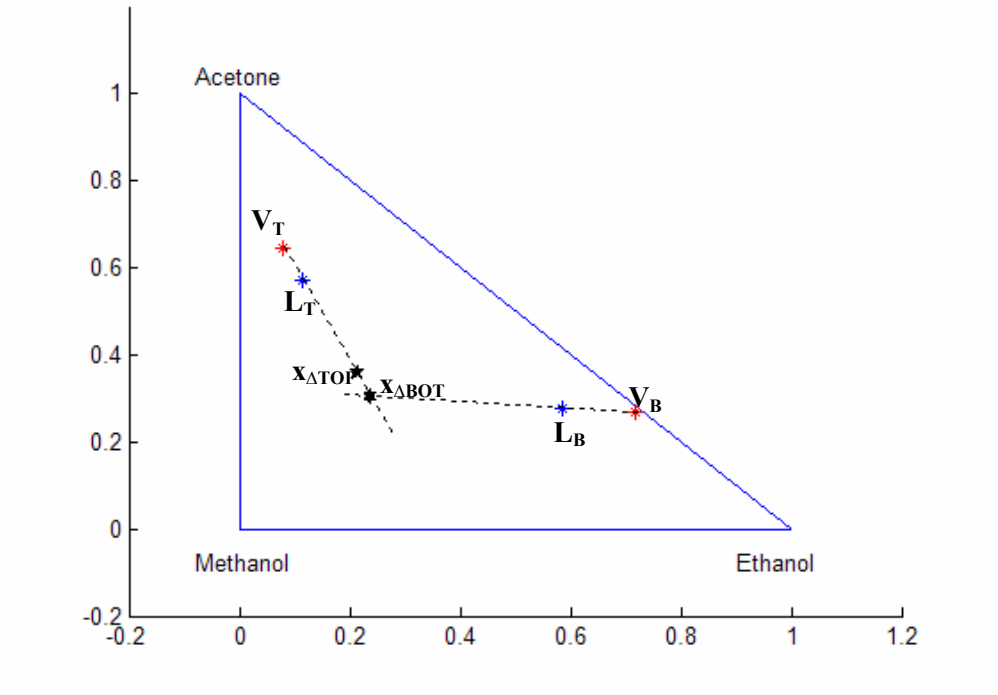

Figure 2.29: Delta points for top and bottom passing streams for experiment 2.

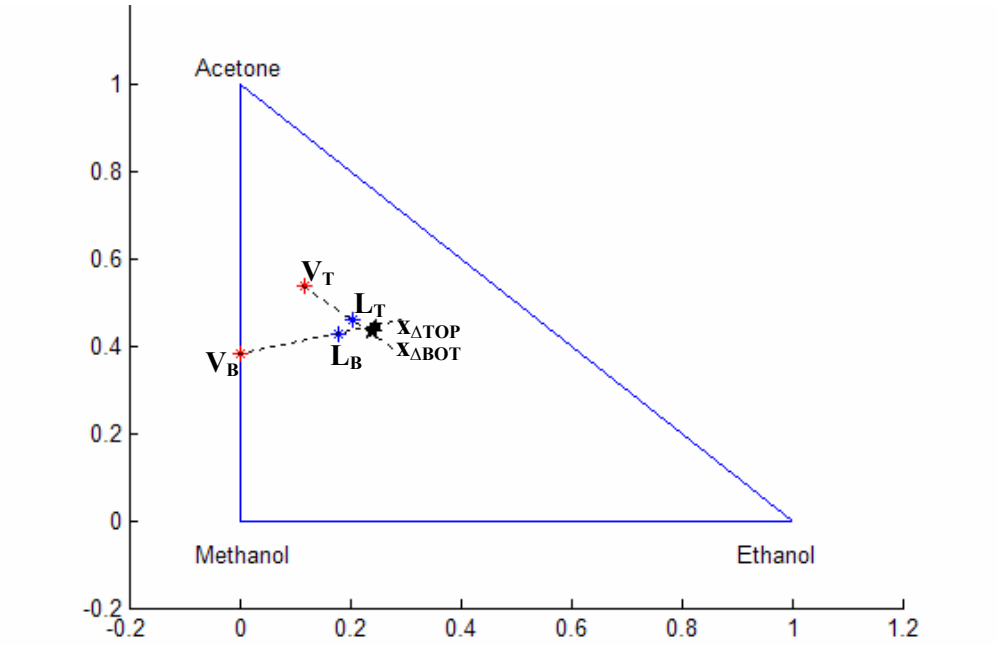

Figure 2.30: Delta points for top and bottom passing streams for experiment 3.

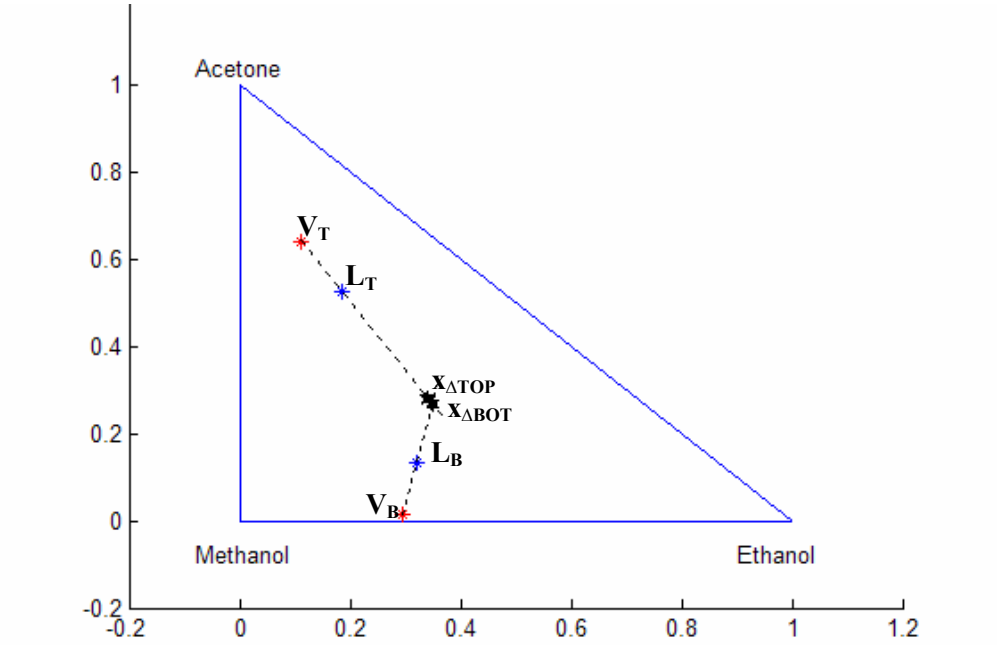

Figure 2.31: Delta points for top and bottom passing streams for experiment 4.

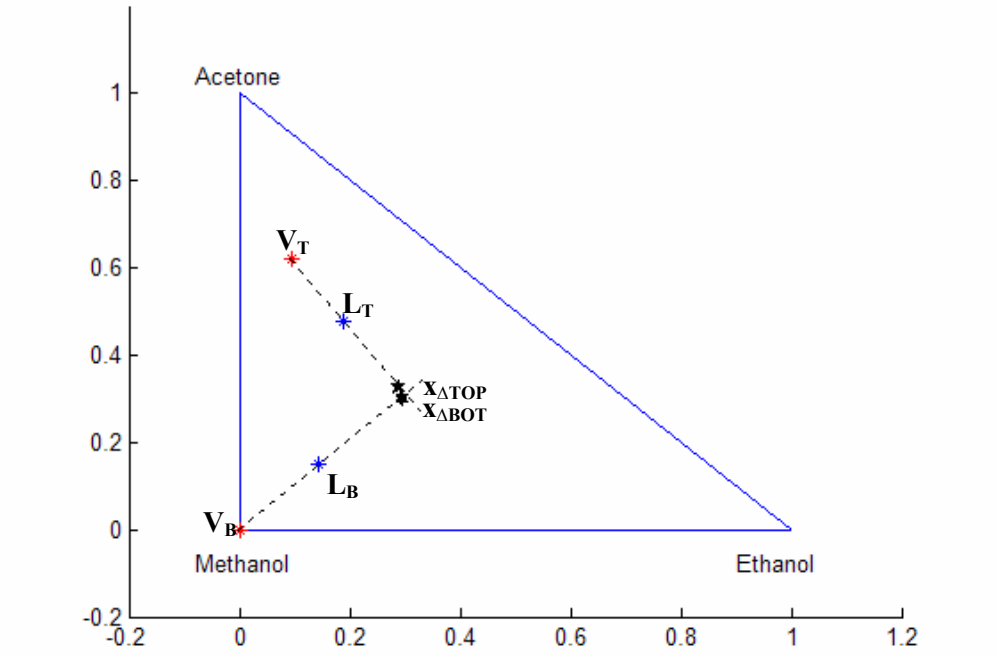

Figure 2.32: Delta points for top and bottom passing streams for experiment 5.

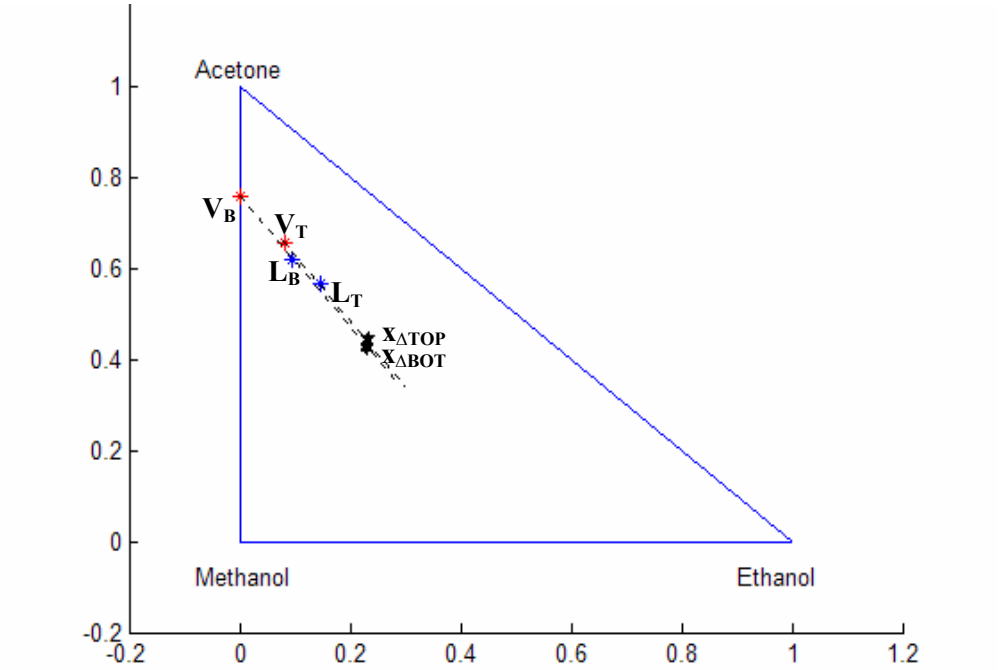

Figure 2.33: Delta points for top and bottom passing streams for experiment 6.

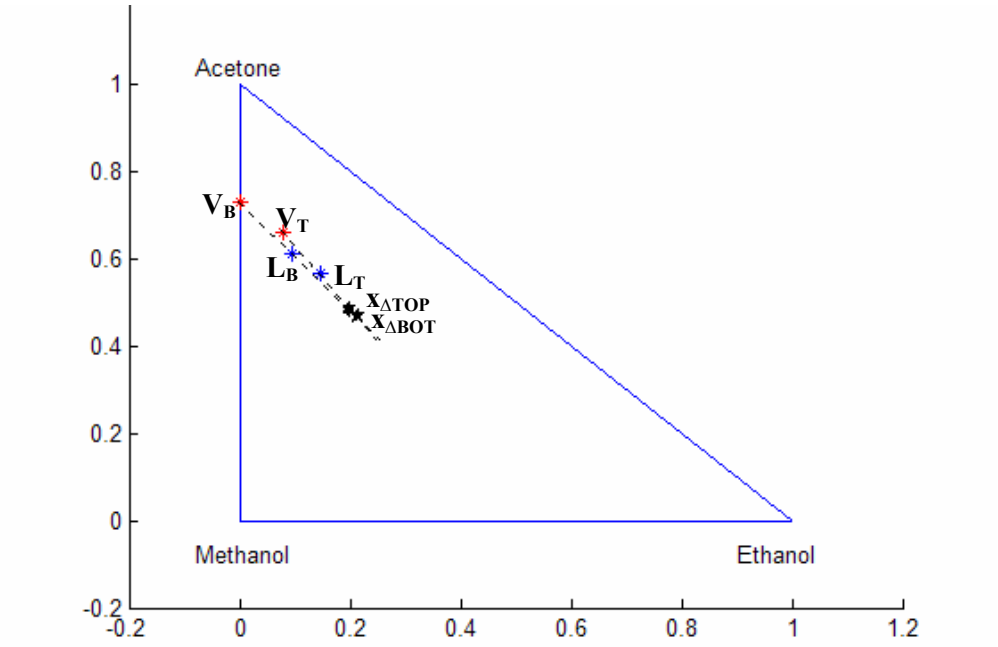

Figure 2.34: Delta points for top and bottom passing streams for experiment 7.

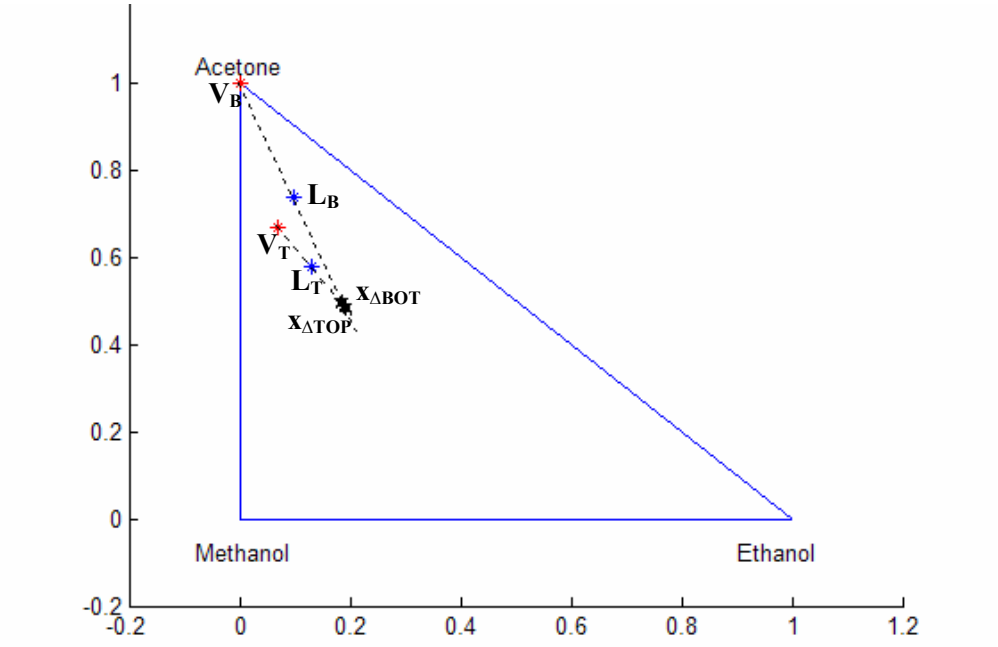

Figure 2.35: Delta points for top and bottom passing streams for experiment 8.

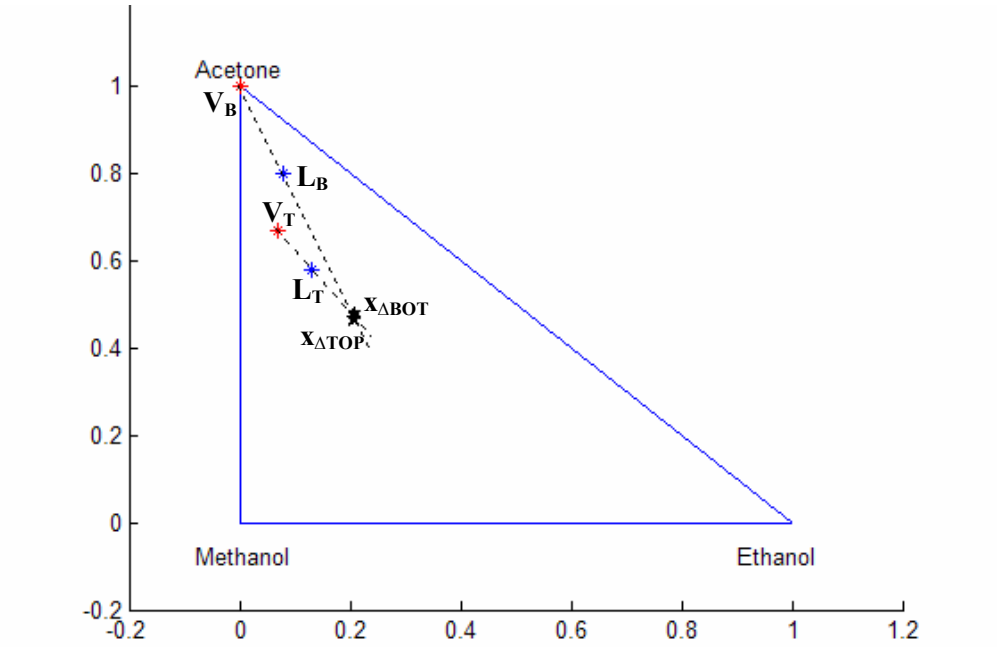

Figure 2.36: Delta points for top and bottom passing streams for experiment 9.

2.5.4 NUMBER OF STAGES

The theoretical column profiles are calculated according to equation 2.7. A number of time steps are specified for this calculation. The theoretical profile may be represented as a series of points where each point represents a dimensionless time step or equilibrium stage.

The theoretical time steps may then be superimposed on the limits of the experimental liquid and vapour profiles. A correlation is sought between the actual number of stages and the experimentally predicted number for a particular experiment.

The procedure is performed for experiments 2, 3, 5 and 9 in Figures 2.37 to 2.40 below.

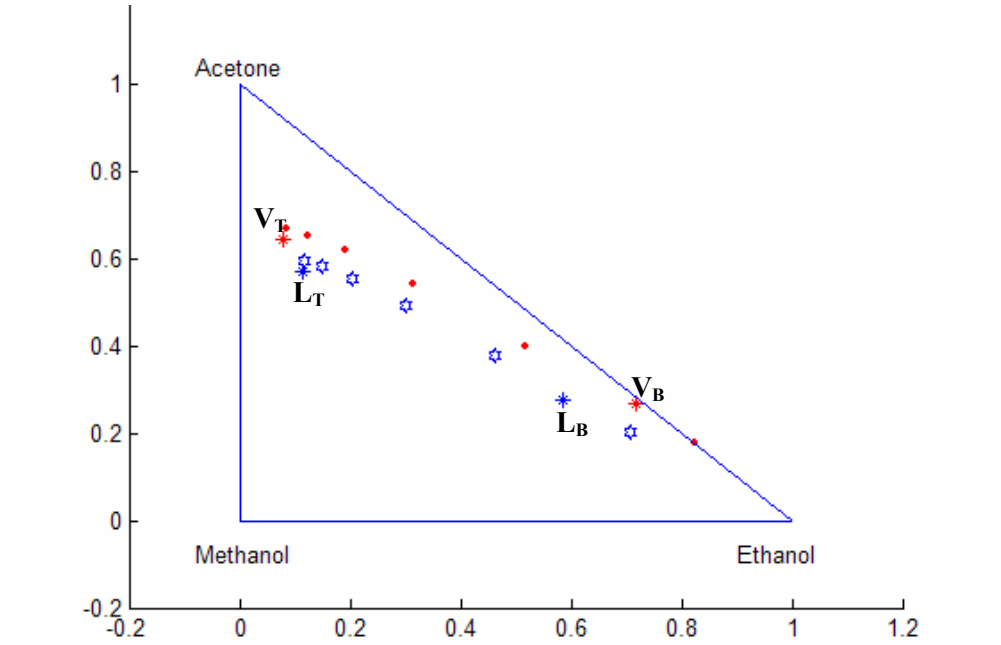

Figure 2.37: Theoretical stages superimposed on liquid and vapour column profile limits for experiment 2. There are approximately 6 stages in the profile.

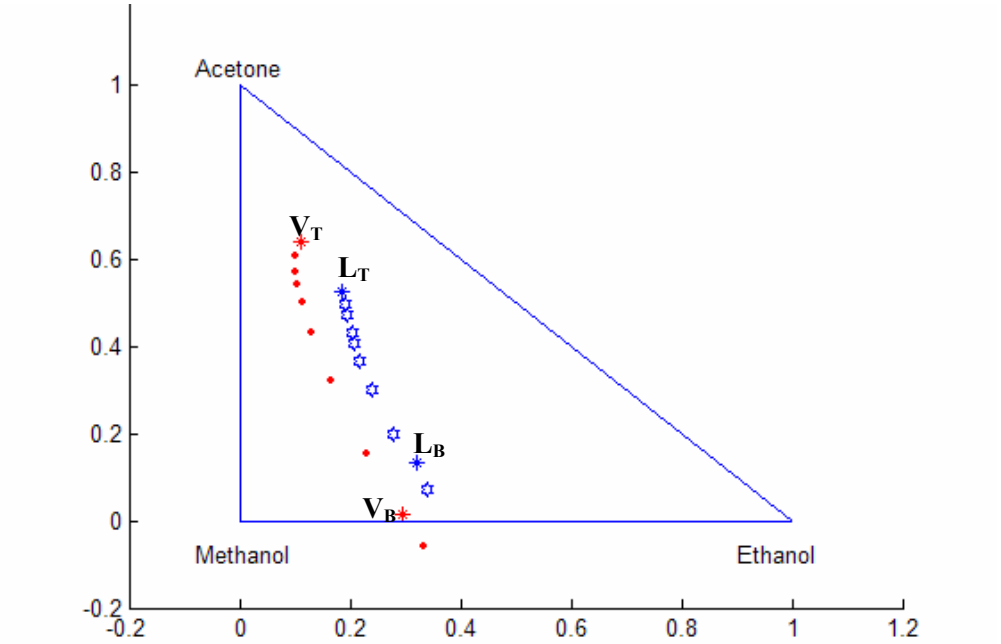

Figure 2.38: Theoretical stages superimposed on liquid and vapour column profile limits for experiment 3. There are approximately 8 stages in the profile.

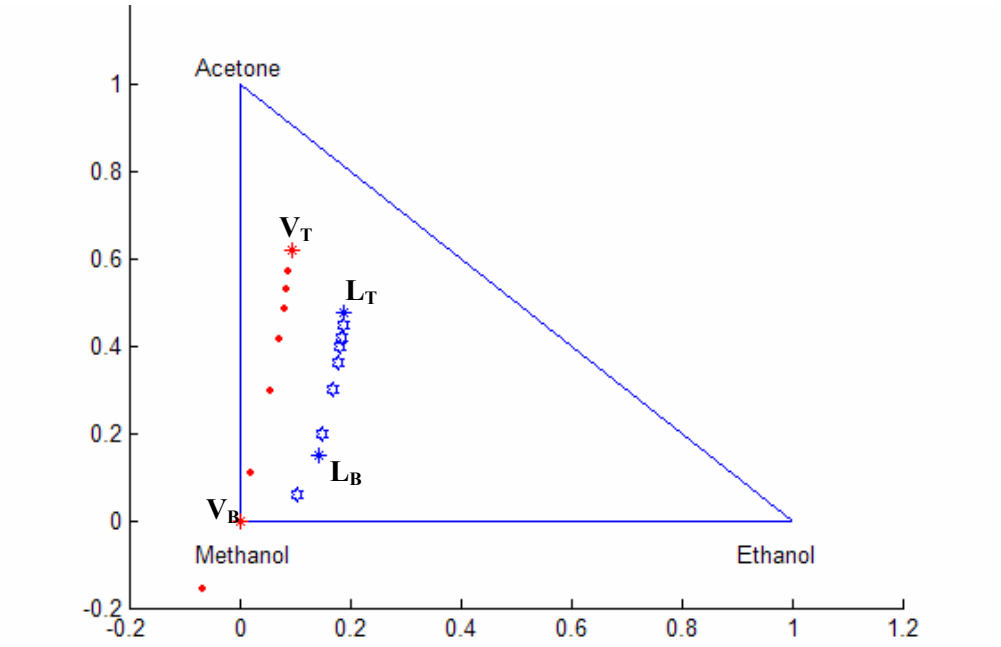

Figure 2.39: Theoretical stages superimposed on liquid and vapour column profile limits for experiment 5. There are approximately 7 stages in the profile.

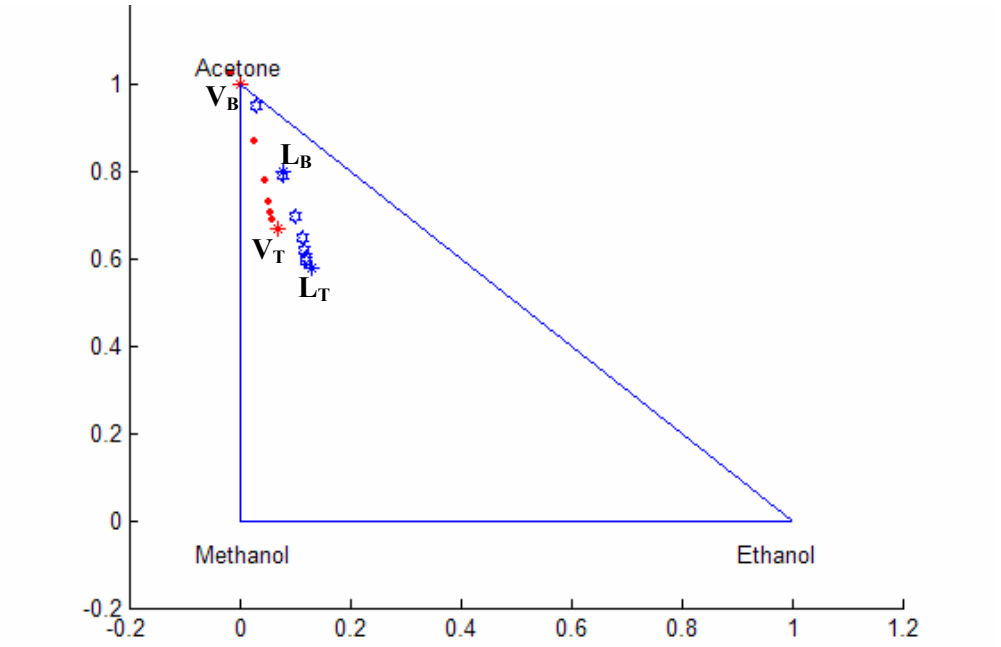

Figure 2.40: Theoretical stages superimposed on liquid and vapour column profile limits for experiment 9. There are approximately 6 stages in the profile.

From Figures 2.37 to 2.40, one can deduce that the column has between 6 and 8 equivalent stages. The other experimental profiles are not shown as the profiles are too short to distinguish successive stages from each other.

2.5.5 INVERSE TEMPERATURE PROFILES

Experiments 6, 7, 8 and 9 were shown to run completely opposite to the residue curves in that region as shown in figures 2.23 to 2.28. The deviation of the profiles from the residue curves is not however limited to the compositions.

Isotherms are only dependent on composition. Transformed singular points do not retain their original temperature assignments. Usually the distillate of a column has a lower boiling point that the bottoms. *In this case the experimental profiles have an inverse temperature profile as the distillate is warmer than the bottoms.* Inverse temperature profiles have been reported by Lee and Westerberg (2000).

The isotherms for the acetone, methanol and ethanol system are plotted along with the experimental profiles for experiments 7 and 9 in figures 2.41 and 2.42 respectively. Since experiments 6 and 7 are identical and experiments 8 and 9 follow the same trend, only the two plots are shown. As can be seen in figures 2.41 and 2.42, the top temperatures for the vapour and liquid streams are at higher boiling isotherms than their corresponding bottom stream isotherms.

Note that the theoretical profiles are shown for clarity. This is sufficient as their equivalence to the experimental profiles was already verified in section 2.5.1.

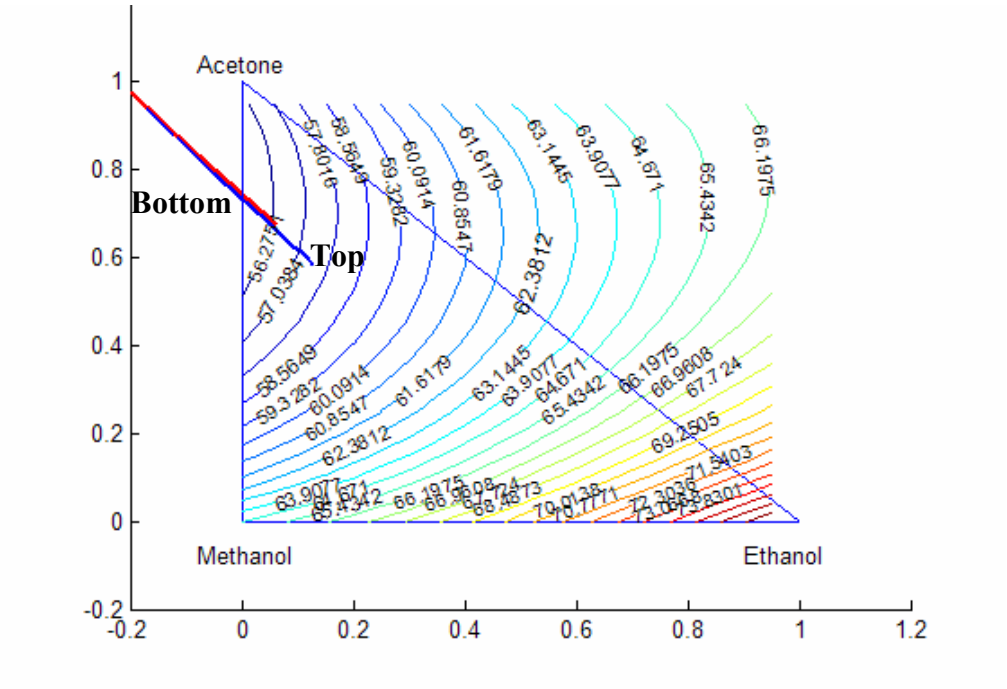

Figure 2.41: Theoretical profiles for experiment 7 with isotherms to show a temperature profile inversion in the column.

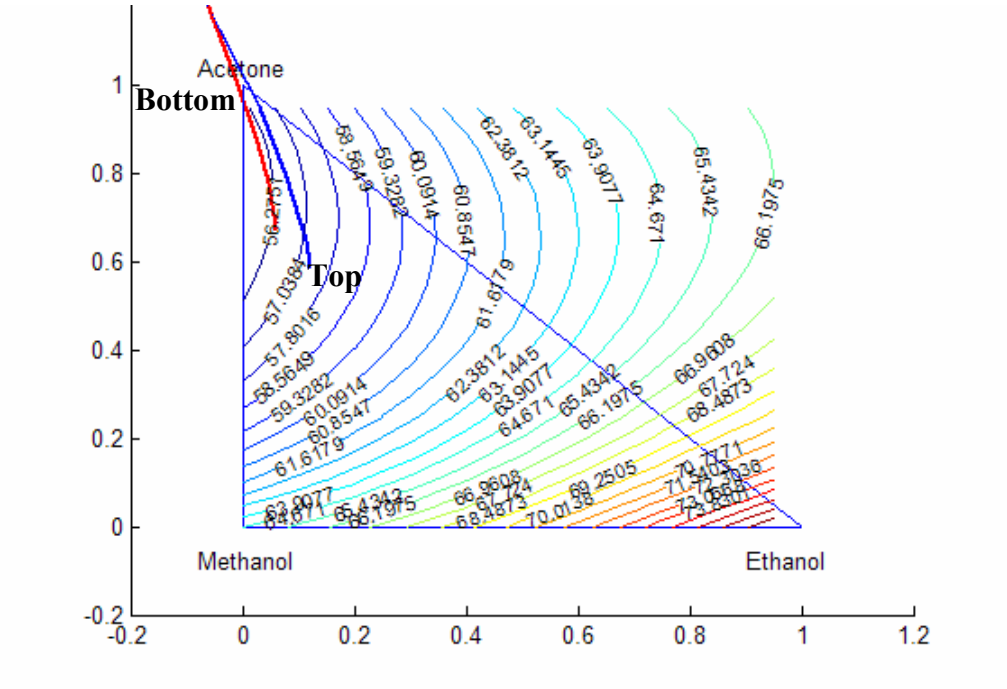

Figure 2.42: Theoretical profiles for experiment 9 with isotherms to show a temperature profile inversion in the column.

2.6 DISCUSSION

Section 2.5.1 aimed to show the equivalence of the theoretical column profiles to the experimentally obtained data points. The composition profiles for experiments 2 to 9 have a corresponding theoretical profile that characterises the data almost perfectly. This equivalence for experiments 2 through 9 is shown in figures 2.15 to 2.28.

Initially an intended trend of a theoretical profile was selected. The profiles were selected on the basis of exhibiting the highest degree of deviation from the infinite reflux residue curves. This was done to assist with feed composition and flow rate selection. Once the intended experiment was performed the reflux was re-calculated to give a more accurate theoretical representation. The reproducibility of the experiments was verified by the repetition of experiments 6 and 8. The differences in the profiles are barely discernible as shown in figures 2.23 to 2.28.

Although column profiles are not mathematically bounded to the composition space it should be clear that the experimental profiles are. It should also be noted that the entire space is not populated by a discreet number of profiles, but rather a surface of infinite ones. Each profile map is unique to a delta point and reflux, but the curves may be traversed by means of the initial composition from which integration takes place. In this way, the best fitting profile to the experimental data may be found.

In section 2.5.3, the delta points for the top and bottom of the column for each experiment are represented. In the constant molar overflow assumption, it is assumed that the net molar flow composition of passing streams remains constant along the length of the column. The assumption is quantified by the delta point. The delta point is a composition point along a straight line for passing streams. At infinite reflux the delta point is merely a composition difference of the passing streams, but at finite reflux, the difference point is scaled by the inclusion of the molar liquid and vapour flow rates of the passing streams. The agreement of the delta points calculated for the

top and bottom of the column indicates the degree to which thermal and mass steady state was achieved.

The top and bottom delta points for experiments 2 to 9 are shown in figures 2.29 to 2.36. Their agreement is within a few percent and gets progressively better for successive experiments as operating techniques were fine tuned.

Section 2.5.4 investigates the correlation between the theoretically predicted stages and the experimental profiles. This is possible because the DE's describing the column profiles are not continuous but rather are defined at discreet points or stages. The theoretical profiles are plotted as discreet points between the limits of the top and bottom experimental liquid and vapour compositions. The resulting correlations are shown in figures 2.37 to 2.40, corresponding to experiments 2, 3, 5 and 9. The other experiments had profiles that were too short to graphically distinguish the number of discreet steps.

From the results, the packed column has a theoretical number of stages between 6 and 8. For a qualitative comparison of the actual position of the theoretical stages relative to the experimental sampling point compositions one may compare figures 2.37 to 2.40 to the corresponding plots in section 2.5.1. For the most part, it can be seen that there is no clear relationship. This is intuitively correct as there should be no correlation between equally spaced sampling ports and actual equivalent stages in the column.

Section 2.5.5 reports two extreme proposed column profiles that are the diametrical opposites of their corresponding residue curves. The theoretical profiles are represented having already shown their equivalence to their corresponding experimental profiles. Superimposed on the theoretical profiles are the isotherms for the acetone, methanol and ethanol system. The isotherms are independent of singular point transformations and thus remain unique for the system. The profiles for

experiments 6, 7, 8 and 8 are shown to adopt an inverse temperature profile relative to the isotherms.

In terms of column profile map theory, this is the equivalent of modifying the orientation of the components within a column section. In this case acetone was made to strip instead of forming the distillate. In other words one could achieve pure acetone in the bottoms of the column! This phenomenon is an excellent example of how the delta point can be used to manipulate the system to achieve desired separations within mass balance constraints.

2.7 CONCLUSIONS

An apparatus has been built for an experimental verification of column profile map theory. The acetone, methanol and ethanol system was investigated for a number of reflux ratios to demonstrate the deviation of column profile maps from infinite reflux behaviour. The different experiments resulted in various delta points in the composition space. Only profiles of considerable deviation were considered to highlight the agreement of the theoretical predictions with the experimental findings.

Residue curve maps had previously been used to gain a qualitative understanding of finite reflux systems and batch experiments were done to investigate singular point complexities. The introduction of column profile maps advanced the understanding of finite reflux systems by demonstrating the transformation of residue curves for deviations from total reflux. *This experiment has verified these transformations in a fairly simple continuous apparatus.*

The vapour flow rates were found to be limiting for the capacity of the column thus a larger liquid flow rate than vapour flow rate was used. This ensured sufficient wetting of the packing for consistent results and liquid sampling. *Careful pre-heating of the*

column and high quality insulation contributed to start-up times of less than 10 minutes for an experimental run. Temperature control of the liquid feed ensured minimal temperature disturbances to the column temperature profiles.

Incorrect control of the input parameters of the experiment namely feed compositions, flow rates and temperatures manifested as discrepancies in the calculated delta points for the top and bottom of the column. A fluctuating rotameter float for the liquid feed and unavoidable residual liquid hold-up in the column were two of the main reasons for the calculated delta points being different, nonetheless they never differed by more than 5% and constant molar overflow was observed to within 8% for the liquid and vapour streams. *The delta point thus provides a useful internal check for constant molar overflow and adiabatic operation of the column.*

This experimental CPM investigation would be applicable in cases where discrepancies arise in the position of predicted singular points for different thermodynamic models. By doing a few simple carefully designed experiments, the best model for a particular system could be selected. Including potential mass transfer limitations could increase the accuracy of the method further.

An investigation at finite reflux for this system has given rise to an understanding of the column behaviour that would never have been realised with traditional qualitative techniques. The result has been obtained in a continuous apparatus where the equivalent results of batch experiments were slow to be accepted due to their batch nature.

2.8 PRECAUTIONS AND RECOMMENDATIONS

An example of incorrect experimentation is shown in Figure 2.14 for experiment 1. Incorrect sampling technique and heating of the column shell resulted in the sampled

liquid profile lying outside the bounds of the liquid top and bottom composition. A combination of local vaporisation and simultaneous vapour-liquid sampling resulted in sample points outside of the intended liquid profile.

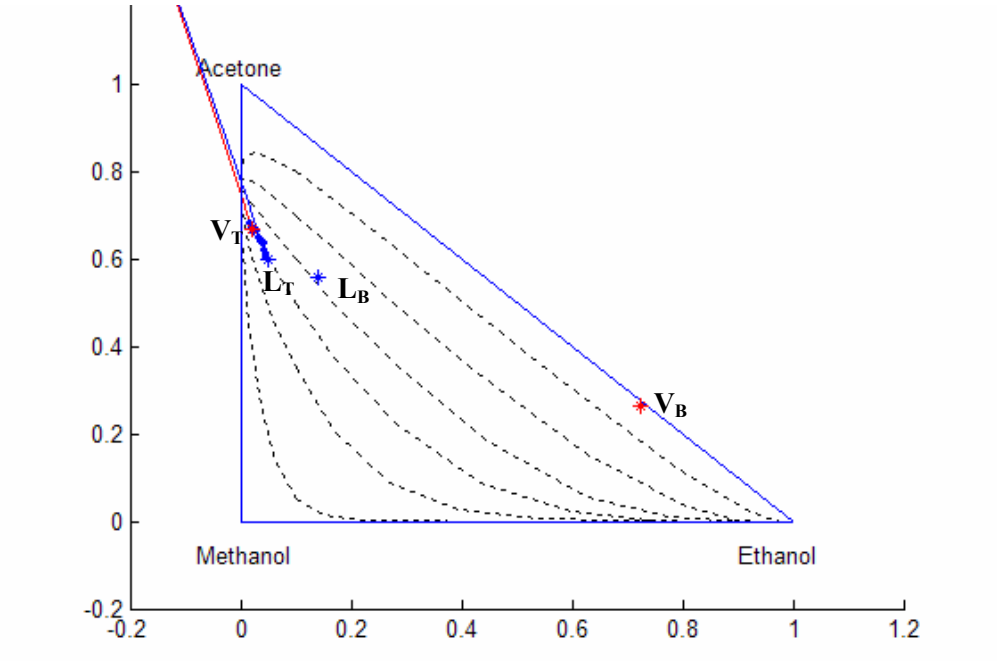

Figure 2.43: Column profile map with superimposed residue curves (dotted). The liquid profile lies outside the top and bottom compositions. x_{Δ}=[0.592; 0.051], Reflux=-1.1

An optimal column shell pre-heating temperature was found and the heating was stopped during experimental runs. The sample ports were tilted downward to ensure sufficient liquid collection for consistent liquid sampling.

The following are the main two recommendations for future experimentation:

- Higher capacity heating mantles should be sourced to increase the possible variations in flow rate capabilities.
- The flow rate of the liquid feed should be controlled by means of a pump or the feed drum placed higher to provide more head to overcome pressure build up in the column and allow the liquid to flow consistently. This problem occurred mainly during startup.

CHAPTER 3: TOPOLOGICALLY BASED SHORT CUT METHODS IN MULTI-COMPONENT DISTILLATION SYSTEMS

ABSTRACT

Residue curves at infinite reflux are used for the synthesis of column sequences or the analysis of existing column configurations. The use of residue curves is however usually limited to systems with four or less components. The important information is contained in the topology of the map. The curvature represented in the visual map is only important for sizing.

An alternative representation is proposed that utilizes temperature sequencing and combinatorial techniques to obtain a maximal structure for a distillation system having only known boiling temperatures and azeotropes. The structure contains all the relevant information and can be extended into higher dimensions.

A direct consequence of the structure is the representation of the sequence of component separation in complex column configurations. The method provides a quick and simple pre-design evaluation tool. The representation is then shown to be useful in subsequent analysis methods such as P-graph analysis or manifolds.

3.1 INTRODUCTION

Process synthesis techniques, whether heuristic, algorithmic or combinations of both can usually be interpreted and analyzed by some form of graphical representation. The graphical approach provides a simple means to communicate potentially complex interactions between system variables. In distillation systems the relationship between the vapour liquid equilibrium of a mixture and the open evaporation residue curves for ternary mixtures was established (Schreinemakers, 1902; and Ostwald, 1902). Shreinemakers (1902) suggested that the interior of the composition space was populated with residue curves to form a Residue Curve Map.

Residue curve maps provided one of the first graphical means of understanding three-component batch evaporative distillation although their relationship to the composition profile of a packed column at infinite reflux was later shown (Hausen, 1952; and Rische, 1955). Early work (Zharov, 1967, Zharov, 1968) gave a more mathematically rigorous foundation to residue curves and expanded the analysis to multi-component mixtures. The usefulness of residue curve maps in interpreting multi-component systems is usually limited to four components. However, the important information in residue curves is in the topology of the maps or rather the structure of the map. A structural residue curve map represents the topology of the residue curve map as given by the residue curves' singular points; the residue curves along the edges of the composition space and the saddle separatrices located in the interior of the space (Serafimov, 1968d). The curvature of the composition profiles in the visual map is only important for column sizing.

The analysis of highly non ideal azeotropic systems is exceedingly difficult due to the severe non-linearity of the system (Feng, 2003). The majority of the analysis methods are heuristically based, and reliant on residue curve maps. These are applicable to homogeneous and heterogeneous systems. Algorithmic synthesis has been limited to

homogeneous systems (Feng 2003). Simulation packages also provide a means to investigate azeotropic separation schemes. By using geometrical methods in conjunction with design by simulation methods, feasible separations for highly non-ideal systems may be found by considering the separation space, singular points and residue curves (Wasylkiewicz, 2000).

The use of combinatorial topology has been suggested for exploration of multi-component mixtures with more than four components (Rev, 1994). Residue curves are trajectories of the first order explicit autonomous system of the ordinary differential equation:

$$\frac{dx}{d\tau} = \vec{x} - \vec{y}(x, P) = \vec{x}(y, P) - \vec{y} \qquad \textbf{(3.1)}$$

Where vectors **x** and **y** are vectors of the equilibrium liquid and vapour mole fractions of mixture. The vector **y** is a unique function of **x** and equilibrium pressure and the vector **x** is also a unique function of the vector **y** and equilibrium pressure (P). This property whereby the **y** and **x** vectors are both continuously differentiable and linked by a unique scalar is termed homeomorphism (Rev 1994). A direct result of the homeomorphism is that the topological structure in higher dimensions remains unchanged under phase transformations.

There is another unique scalar parameter unique to each **x** and **y** and their corresponding equilibrium pressure in Equation 3.1, namely the equilibrium temperature. Temperature increases monotonically along any trajectory of Equation 3.1, i.e.

$$\frac{dT}{d\tau} > 0 \qquad \textbf{(3.2)}$$

Work by Doherty and Perkins (1978, 1979) showed that only a finite number of singular points may exist for a particular distillation system. Stable and unstable

points are local maxima and minima in temperature respectively. Saddle nodes may be explored by noting that there are a finite number of trajectories arriving or departing from a saddle point and these are tangent to some eigenvectors in the neighbourhood of the saddle. The trajectories connect singular point pairs.

As a consequence of the simultaneously existing temperature function, given by Equation 3.2, a natural partial ordering appears amongst the singular points. This partial ordering has been used to formulate temperature sequences as a complete method of categorizing the feasible distillation boundary maps for ternary systems which commonly have unique binary and ternary azeotropes (Peterson and Partin, 1997). These simplified versions of RCM's are termed Distillation Boundary Maps (DBMs). The method requires the boiling temperatures of pure components and azeotropes at system pressure and the components are thus ranked resulting in the temperature sequence. Thus the type of mixture can be determined and the distillation behaviour can be qualitatively predicted for various feed components of a mixture by knowing the boiling points of the pure components and any azeotropes (Kiva et al. 2003).

Further combinatorial work has been extended into process synthesis systems by the use of bipartite graphs, termed P-graphs (Friedler, 1992; Feng, 2000; Feng 2003). An axiom system underlying the approach is constructed to define combinatorial feasible process structures. Individual solution structures are then embedded in a maximal structure for the process.

Another method for higher dimension mixtures has been investigated by Thong and Jobson (2001a, b, c) using a modified form of the rectification body method developed by Bausa (1998). Feasibility tests were developed and subsequently extended to test the feasibility of a proposed class of split. Algorithms for computer-aided determination of multi-component VLE diagram structures were developed by

Petlyuk, Kievski and Serafimov (1975a; 1977a, b, c; 1978) and are also given by Julka and Doherty (1993), Rooks et al. (1998) and Safrit and Westerberg (1997).

This work proposes a unique graphical combinatorial approach adapted from Henley and Williams (1973) for developing a representation for higher dimension mixtures. The work derives from a likening between residue curve map binary component boundaries and simple distillation column component splits. A number of heuristic rules are introduced to obtain a maximal chain structure to represent a distillation system having only known the component boiling temperatures and those of any azeotropes.

The method is initially developed for four component mixtures for ease of comparison and verification of the resulting representation with existing methods. A six component example is then completed to show the robustness of the method in its application to assist in the necessary steps for the rectification body and column feasibility design approach (Thong and Jobson 2001a, b, c); and as a precursor to P-graph methods (Friedler, 1992).

3.2 DEVELOPMENT OF CHAIN MAP REPRESENTATION

3.2.1 ACETONE, METHANOL, ETHANOL AND WATER SYSTEM

Consider a four component mixture containing acetone, methanol, ethanol and water. There are two binary azeotropes in the system. The acetone/ethanol azeotrope is a minimum boiling azeotrope and the ethanol/water azeotrope is an intermediate boiler. The four components yield four possible Residue Curve Maps (RCM's) when each of the ternary combinations of the components is considered.

The acetone, methanol, water RCM is given in Figure 3.1. Note the minimum boiling azeotrope is the unstable node, the pure acetone and methanol are saddle nodes and pure water is the stable node. For simple distillation, all feasible separations may be viewed as a sequence of binary splits. These binary splits are given by the outer boundaries of the RCM. If one begins at the lowest boiler of the system and traces out increasing temperature profiles along the binary edges of the RCM, the result will be a list of paths that a sequence of simple columns would essentially follow.

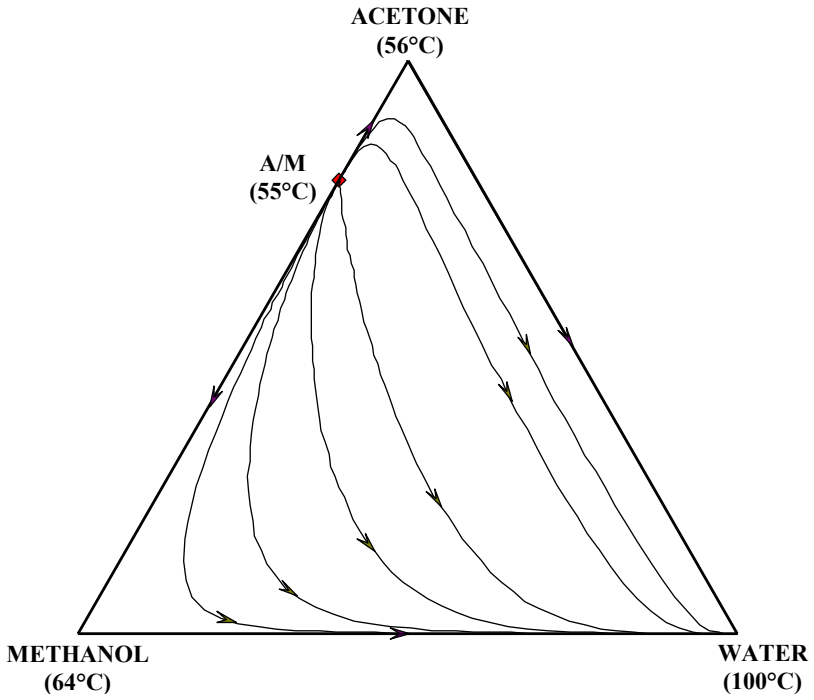

Figure 3.1: Residue Curve Map for acetone, methanol and water system.

Using Figure 3.1 and following this procedure yields two possible paths, namely:

AM → A → W

AM → M → W

Inspection of the two paths reveals a common starting and end point, thus the two paths may then be combined to yield the condensed maximal structure in Figure 3.2:

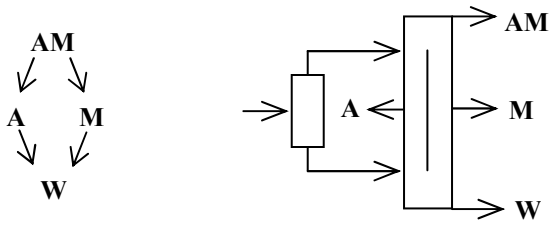

Figure 3.2: Maximal chain structure for acetone, methanol and water system and corresponding complex column configuration.

The maximal structure may be used to formulate the separation order in a complex column configuration (Petlyuk, 1975, 1977a, 1977b) as shown in Figure 3.2. The same procedure may now be applied to the acetone, water and ethanol system to obtain the chain structure as shown in Figure 3.3. Acetone is the lowest boiling component followed by the water/ethanol azeotrope, ethanol and then water. Note that the azeotrope splits the maps into two distillation regions.

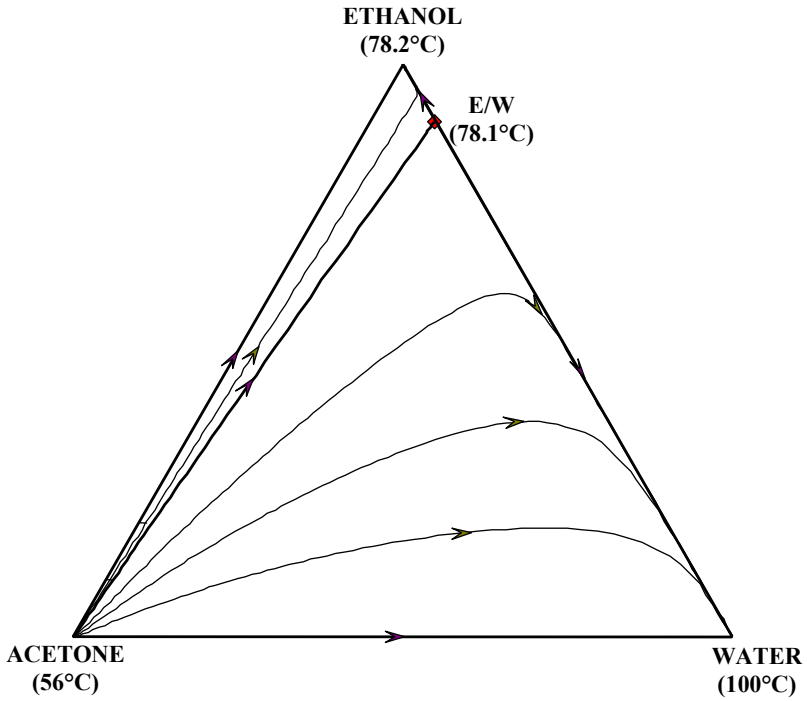

Figure 3.3: Residue Curve Map for acetone, ethanol and water system.

Therefore beginning at the lowest boiling component (acetone) and tracing out all possible binary paths, one arrives at two possible paths which have a common starting point (the pure acetone node) and may thus be combined to give Figure 3.4. The presence of an azeotrope has induced the resulting split of the composition space into two distillation regions.

Figure 3.4: Maximal chain structure for acetone, ethanol and water system.

For a four component system there are four different RCM's that represent the four faces of the 3-D tetrahedron that contains the composition space for the four components. The two remaining RCM's for the system under consideration, namely those for ethanol, methanol and water; and the acetone, methanol, and ethanol are shown below in Figure 3.5 and Figure 3.6 respectively. Note that the same methods have been applied to obtain the final chain representations.

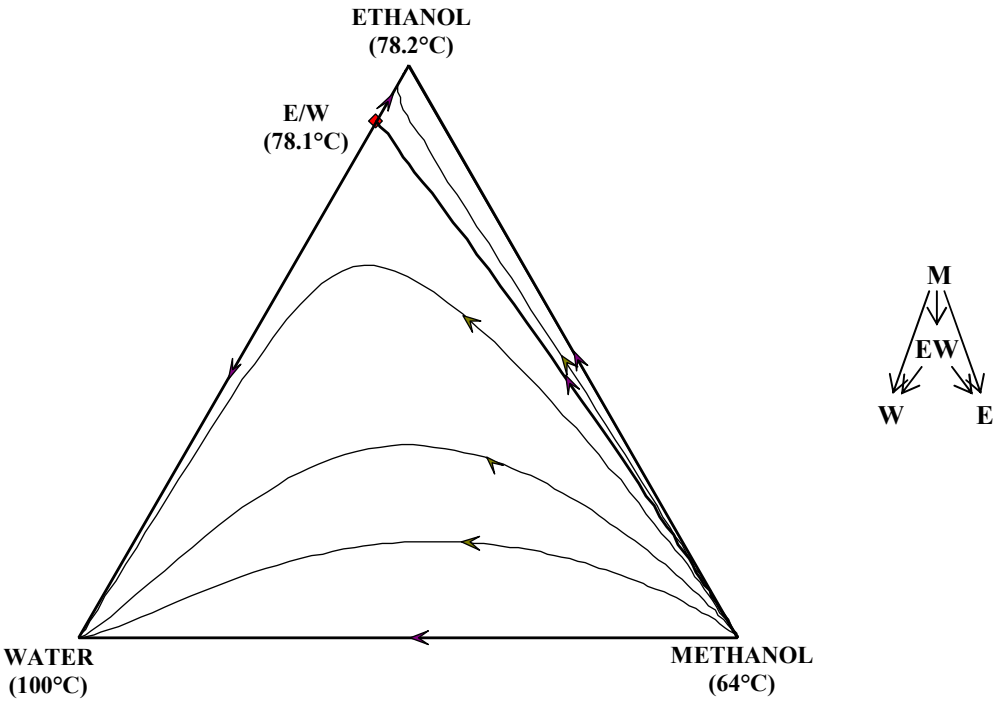

Figure 3.5: Residue Curve Map and resulting maximal chain structure for methanol, ethanol and water system.

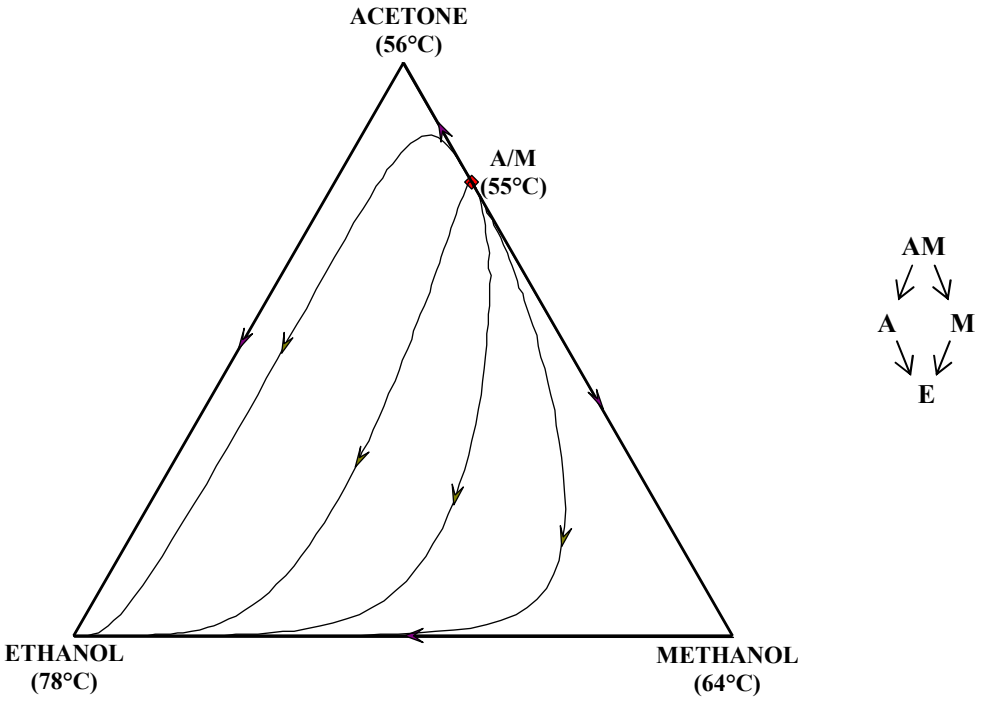

Figure 3.6: Residue Curve Map and resulting maximal chain structure for acetone, methanol and ethanol system.

The open tetrahedron for the system is given by Figure 3.7. By combining the chain paths given by Figure 3.2 and Figure 3.4 and the resulting chains from Figure 3.5 and Figure 3.6, a maximal chain structure may be found by combining the common nodes for the chains given for each of the four residue curve maps. The maximal chain path structure for the acetone, methanol, ethanol and water system is thus given by Figure 3.8.

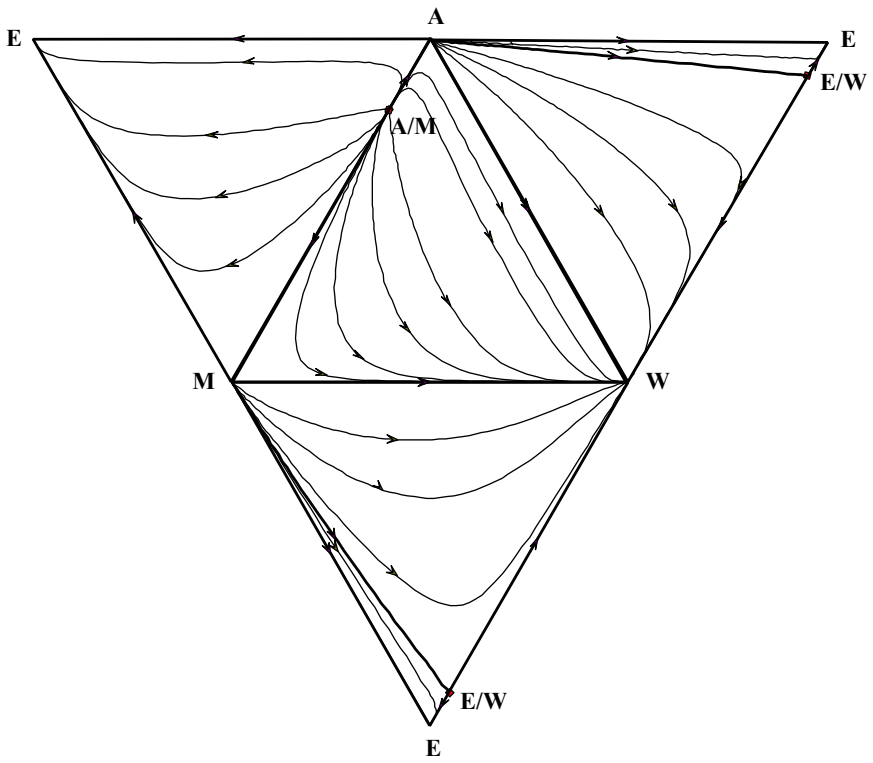

Figure 3.7: Open tetrahedron for acetone, methanol, ethanol and water system.

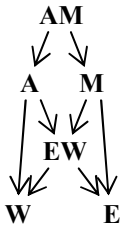

Figure 3.8: Maximal chain structure for acetone, methanol, ethanol and water system.

In this chain representation method, the azeotropes may themselves be considered as components because they satisfy the conditions necessary to be classed as nodes. Complexities in the system are introduced by the addition of azeotrope forming components and result in a branched structure for the maximal chain path. The series of component separations may thus be formulated from this graphical representation.

3.3 INVESTIGATION OF COMPONENT ADDITION

A theoretical system will now be considered to investigate the effects of introducing new components to a system and the effect on the chain structure. Consider a fourth component added to the acetone, methanol and water system given in Figure 3.1. This new component 'D' introduces no new azeotropes to the system. The boiling of point of 'D' may assume five different temperatures for the purposes of investigation, namely:

A. Lowest boiling – 40°C (Figure 3.9)
B. Between A/M and Acetone – 55.5°C (Figure 3.10)
C. Between Acetone and Methanol – 60°C (Figure 3.11)
D. Between Methanol and Water – 70°C (Figure 3.12)
E. Highest boiling – 120°C (Figure 3.13)

Using an open form tetrahedron, the five cases may be investigated and the resulting chain structures shown.

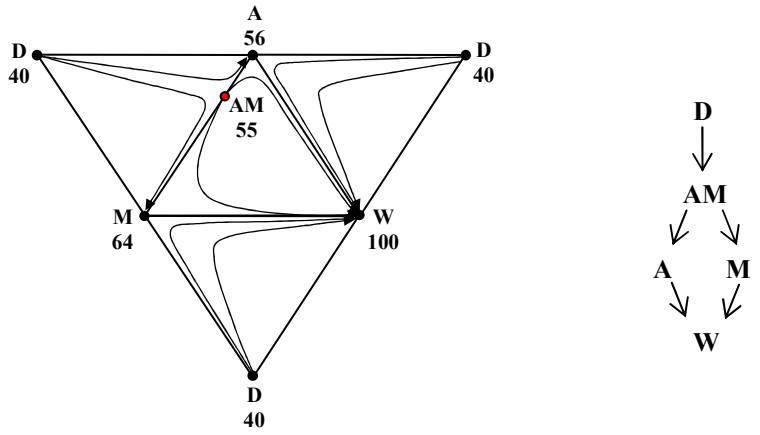

Figure 3.9: Case A: the addition of a lowest boiling component to the acetone, methanol and water system.

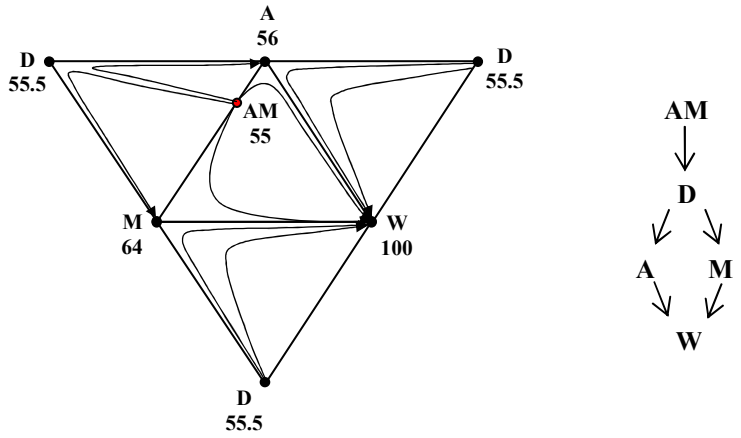

Figure 3.10: Case B: the addition of a component of boiling point between the acetone-methanol azeotrope and acetone; to the acetone, methanol and water system.

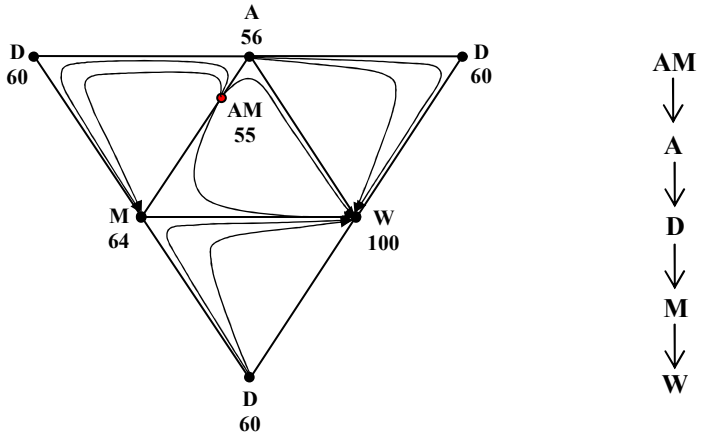

Figure 3.11: Case C: the addition of a component of boiling point between acetone and methanol; to the acetone, methanol and water system.

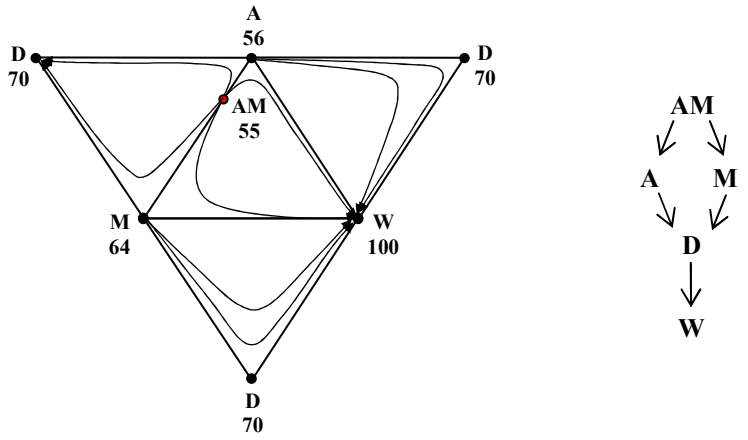

Figure 3.12: Case D: the addition of a component of boiling point between methanol and water; to the acetone, methanol and water system.

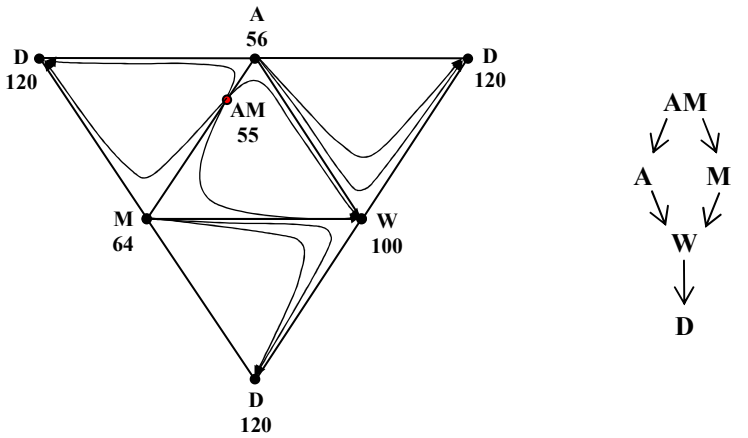

Figure 3.13: Case E: the addition of a highest boiling point component to the acetone, methanol and water system.

From Figures 3.9 to 3.13 above it can be seen that although the additional component does not introduce an azeotrope, the resulting graphical interpretation can be quite different. The basic ternary prior to the addition of 'D' was shown in Figure 3.2.

From the resulting chain structures for the differing boiling points of 'D' it is clear that the original ternary structure remains unaffected when 'D' is a minimum or

maximum boiler relative to the original structure, as in Figure 3.9 and Figure 3.13 respectively. As the temperature order of 'D' gets more or less by one, than the following or preceding component, 'D' only displaces those components but the original structure is essentially intact.

Case C is the special case where the boiling point of 'D' is between that of acetone and methanol. It should also be noted that an azeotrope exists between these two components. From the resulting chain structure in Figure 3.11 it is clear that the branch induced originally by the azeotrope has been collapsed according the chain structure by the introduction of 'D'. The result is a topographically ideal composition space where component 'D' has become a pseudo-component. This is the industrial equivalent of finding a suitable entrainer whereby the relevant binary azeotrope may be bypassed. *It should be clear that a complete separation yielding four pure components and pure azeotrope could be achieved in one column given enough stages and correctly placed side draws.*

The following observations are worth noting:

1. Addition of lowest or highest boiling components that are non-azeotrope forming simply lengthens the chain structure without adding any complexity.
2. The presence of azeotropes introduces complexity in the form of branching. The number of branches is equivalent to the number of azeotropes and their order, unless components equivalent to entrainers are present.
3. To follow a particular path allowable by the maximal structure, one does not need to pass through all the nodes. Along any path, a preceding component has a direct split path with any of the higher order boiling components reachable within the constraints of that path.
4. *With infinite stages at infinite reflux, and correctly placed side draws the column separation would follow the chain structure and pure product streams could be obtained.*

3.4 IMPROVED REPRESENTATION

3.4.1 DEVELOPMENT

As shown before in Sections 3.2 and 3.3, the approach of simple binary separations from a known RCM up to a quaternary mixture may be used to obtain the alternative chain representation. The uses of the chain representation are clear but the methods whereby they are obtained have been heavily reliant on specific topographical knowledge of the relevant RCM.

The purpose of the chain map representation is to allow the investigation of higher order component mixtures while still allowing a graphical user interface. The usefulness of a graphical method that extends to higher dimensions but that still requires the use of the preceding dimensionally limited representation is questionable. The point has been to prove that the resulting structure obtained by the chain method is equivalent to the information in the RCM.

The next task will be to introduce the reader to a systematic approach for determining the chain structure without having a RCM for the particular system or for systems with more than four components. The combinatorial method has been adapted from Henley and Williams (1973). The temperature ordering aspect is similar to that used in the construction of Distillation Boundary Maps (Peterson and Partin, 1997) whereby temperature sequencing is utilized, but this method is extended to higher dimensions.

For ease of comparison, the initial examples will be limited to four component systems. A prior assimilation of boiling point temperatures and existing azeotropes is required for any system that is to be investigated.

3.4.2 BINARY AZEOTROPE FOUR COMPONENT MIXTURE

The azeotrope has the classification of a node and thus there are five components in the system. The components are ordered by numbers corresponding to their boiling temperature. The same ordering can be used for real systems where the components are simply denoted by a number. The azeotrope (between components 2 and 3) has the lowest boiling point of the system. If the components are ordered according to their boiling temperatures from lowest to highest boiler, the following chain is obtained in Table 3.1. Note that if the component is an azeotrope, its constituent components are denoted below the chain entry.

1 2/3	**2**	**3**	**4**	**5**

Table 3.1: Temperature ordered sequence for four component mixture with single minimum boiling azeotrope.

In the previous method the information in Table 3.1 would have been contained in the boundaries of the residue curve map. *All the relevant topological behaviour is contained in the temperature sequencing of a system, the curvature of the residue curves is only important for sizing in simple distillation column sequences*.

The azeotrope information below the first component serves three purposes. Firstly it alerts the reader to the fact that this component is an azeotrope. The second purpose is to indicate the direction of the path out of that component. In this case the paths out of component 1 can lead directly to component 2 or directly to component 3. The third property of this notation is less obvious but paramount to understanding the structure. As a rule, if there is a binary azeotrope, then the two constituents of that azeotrope can never be separated directly by simple distillation. In other words there will be no direct path from component 2 to component 3 or vice versa if they are consecutive nodes in the temperature sequence.

The next step is to write all the possible binary splits in the sequence of components while being mindful of the azeotrope information. The erroneous binary splits are avoided by beginning with the lowest boiling component, then writing all possible binary splits with immediately adjacent components in the temperature sequence. The same procedure is then completed for the product components of the lowest boiling component. This procedure is repeated until all the binary splits that terminate in the highest boiling components are completed. The following splits are obtained for the first component according to Table 3.1:

1 → 2
1 → 3

The next splits should begin from the product components of the preceding step of binary splits. Components 2 and 3 can never be linked as per the azeotropic information under component 1 in Table 3.1, so the following are the next series of splits:

2 → 4
3 → 4

The temperature chain shows no complications between components 4 and 5. Thus the final binary split is:

4 → 5

The next step involves a combinatorial approach that will yield the final resulting chain structure. The initial set of binary splits is considered and then the binary splits from the second series are simply linked to the first by means of the repeated corresponding number:

1 → 2
1 → 3

---

1 → 2 → 4
1 → 3 → 4

The remaining binary split may then be combined in a similar fashion for the final result:

1 → 2 → 4 → 5
1 → 3 → 4 → 5

As shown in Section 3.3, the presence of a single azeotrope results in a branch chain structure with two disjoint paths. The two paths are descriptions of the two distillation regions that are present within the composition space due to the division by the azeotrope. Thong and Jobson (2001a) refer to these as compartments or regions within the composition space where ideal component behaviour is observed. The two subsets of the maximal structure are straight chains denoting ideal component behaviour. The overall process may be summarised as shown in Table 3.2.

1	**2**	**3**	**4**	**5**
2/3				

Possible Binary Splits	**Obtaining Combinatorial Paths**
1 → 2	1 → 2
1 → 3	1 → 3
2 → 4	
3 → 4	1 → 2 → 4
4 → 5	1 → 3 → 4
	1 → 2 → 4 → 5
	1 → 3 → 4 → 5

Table 3.2: Summary of steps in obtaining the final subsets of a chain structure for the four component temperature sequence specified.

The single binary azeotrope introduced a single branch to the system, resulting in two subsets of the maximal structure as shown in Table 3.2. These subsets describe the ideal component behaviour in the two compartments or distillation regions of the composition space. Since the system is comprised of four pure components it may be

represented by an open tetrahedron to verify the obtained result. The tetrahedron and the maximal chain structure for this system are given in Figure 3.14.

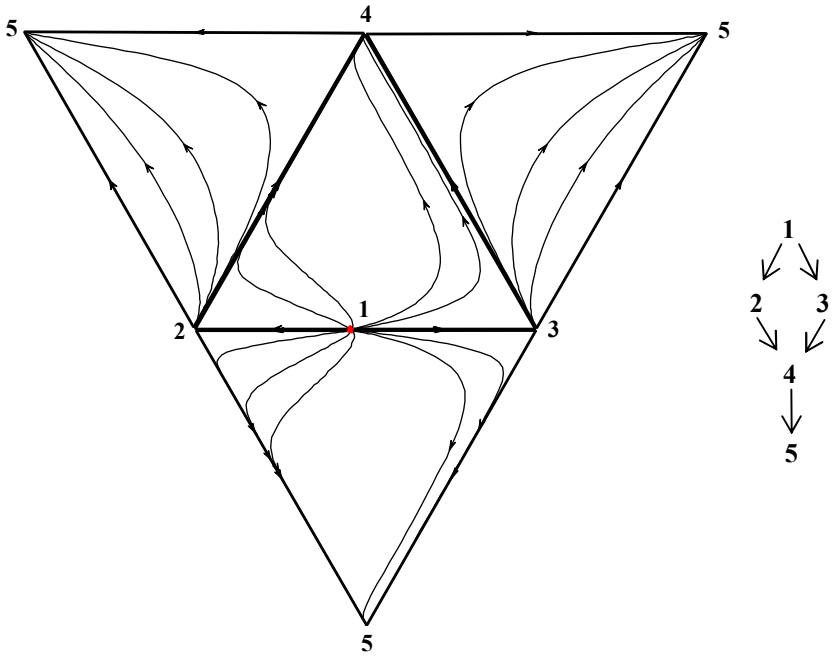

Figure 3.14: Open tetrahedron and maximal chain structure for four component, single minimum boiling azeotrope system.

By considering the tetrahedron as four separate residue curve maps, one would have arrived at four unique chain paths which when combined would have yielded the same result as that given in Figure 3.14. The azeotrope has divided the composition space into two regions where the distillation boundary is a planar triangular surface within the tetrahedron where its vertices are components 1, 4 and 5.

Also verifiable are the possible direct links between components 1 – 5; 1 – 4; 2 – 5 and similar paths for the other subset. This is indicative of the condition whereby all nodes along a particular path need not be passed through.

3.4.3 COMPLEX FOUR COMPONENT MIXTURE

The following example considers a four component mixture with three binary azeotropes and a minimum boiling ternary azeotrope.

The components are ordered according to their temperatures and the corresponding azeotrope information is included in the construction of the temperature sequence, given in Table 3.3.

1	**2**	**3**	**4**	**5**	**6**	**7**	**8**
2/3/4 5/6/7	5/6	6/7	5/7				

Table 3.3: Temperature ordered sequence for four component mixture with ternary minimum boiling azeotrope (5,6,7) and three corresponding binary azeotropes (2,3,4).

Component 1 is the ternary azeotrope, it is directly adjacent to the three binary azeotropes, and thus the initial information underneath component 1's entry is 2/3/4. This denotes the three paths to components 2, 3 and 4 and the fact that there will be no direct path between any of these components.

A second piece of information may be included for component 1. The ternary azeotrope lies on a face of the tetrahedron bounded by the components 5, 6 and 7. In the previous examples it was seen that components within a system that lie outside of an azeotropes influence form a straight 'ideal' chain. The extra information is thus included to indicate that the azeotropes influence must terminate at these components, thus one would expect the branches to converge into one path after components 5, 6 and 7.

Components 2, 3 and 4 are the binary azeotropes for their respective entries in Table 3.3. The information included with these entries yields the paths from the components and again, shows that an azeotrope between components prohibits a direct path between those components.

The same method is used whereby successive binary splits are sequentially combined to yield the subsets of the maximal structure constrained by the distillation regions. A summary of the results is shown below and the tetrahedron and maximal chain structure for the system are offered in Figure 3.23 for comparison and verification of the results.

1	**2**	**3**	**4**	**5**	**6**	**7**	**8**
2/3/4 5/6/7	5/6	6/7	5/7				

Possible Binary Splits	**Obtaining Combinatorial Paths**
$1 \rightarrow 2$	$1 \rightarrow 2$
$1 \rightarrow 3$	$1 \rightarrow 3$
$1 \rightarrow 4$	$1 \rightarrow 4$
$2 \rightarrow 5$	———
$2 \rightarrow 6$	$1 \rightarrow 2 \rightarrow 5$
$3 \rightarrow 6$	$1 \rightarrow 2 \rightarrow 6$
$3 \rightarrow 7$	$1 \rightarrow 3 \rightarrow 6$
$4 \rightarrow 5$	$1 \rightarrow 3 \rightarrow 7$
$4 \rightarrow 7$	$1 \rightarrow 4 \rightarrow 5$
$5 \rightarrow 8$	$1 \rightarrow 4 \rightarrow 7$
$6 \rightarrow 8$	———
$7 \rightarrow 8$	$1 \rightarrow 2 \rightarrow 5 \rightarrow 8$
	$1 \rightarrow 2 \rightarrow 6 \rightarrow 8$
	$1 \rightarrow 3 \rightarrow 6 \rightarrow 8$
	$1 \rightarrow 3 \rightarrow 7 \rightarrow 8$
	$1 \rightarrow 4 \rightarrow 5 \rightarrow 8$
	$1 \rightarrow 4 \rightarrow 7 \rightarrow 8$

Table 3.4: Summary of steps in obtaining the final subsets of a chain structure for the four component temperature sequence specified.

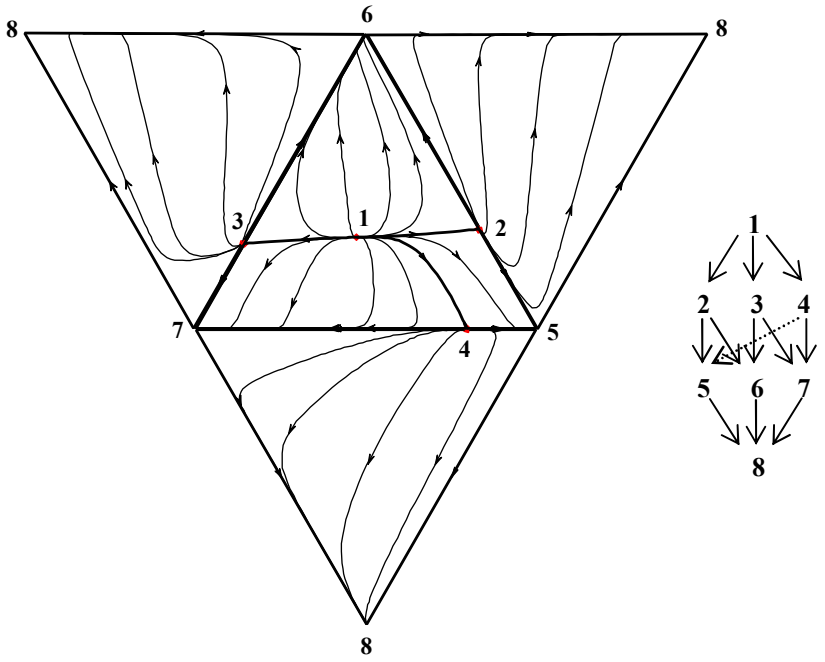

Figure 3.15: Open tetrahedron and maximal chain structure for four component mixture with ternary minimum boiling azeotrope and three corresponding binary azeotropes.

3.5 APPLICATIONS IN EXISTING METHODS

3.5.1 EXISTING METHODS

This method may be used as the precursor in two main methods of distillation synthesis, namely general applications of the rectification body method and P-graph analysis.

3.5.2 RECTIFICATION BODY METHOD

To demonstrate the applicability of this method, the procedure will be performed on a six component example. The same example is discussed in Thong and Jobson (2001a). The aim is not to replicate the method, but merely to show that the techniques may by useful in the primary steps for assessing product feasibility.

The boiling temperatures of the components and their azeotropes are listed in Table 3.5 below.

Temperature Order Number	Component; Azeotrope	Boiling Temperature °C
1	Methanol	64.5
2	Ethanol - Water	77.9
3	Ethanol	78.2
4	2-Propanol - Water	79.8
5	2-Propanol	82.2
6	2-Butanol – Water	88.4
7	Water - 1-Butanol	93.5
8	2-Butanol	99.8
9	Water	100
10	1-Butanol	117.9

Table 3.5: Temperature order numbers and boiling points for the singular points in a six component mixture.

An overview of the procedure in obtaining the subsets of the maximal structure for the distillation compartments of the system is shown in Table 3.6.

1	**2**	**3**	**4**	**5**	**6**	**7**	**8**	**9**	**10**
	3/9		5/9		8/9	9/10			

Possible Binary Splits	**Obtaining Combinatorial Paths**
$1 \rightarrow 2$	$1 \rightarrow 2$
$2 \rightarrow 3$	
$2 \rightarrow 4$ hidden link	$1 \rightarrow 2 \rightarrow 3$
$\underline{2 \rightarrow 9}$	$1 \rightarrow 2 \rightarrow 4$
$3 \rightarrow 5$	
$4 \rightarrow 5$	$1 \rightarrow 2 \rightarrow 3 \rightarrow 5$
$4 \rightarrow 6$	$1 \rightarrow 2 \rightarrow 4 \rightarrow 5$
$\underline{4 \rightarrow 9}$	$1 \rightarrow 2 \rightarrow 4 \rightarrow 6$
$5 \rightarrow 8$	
$6 \rightarrow 7$ hidden link	$1 \rightarrow 2 \rightarrow 3 \rightarrow 5 \rightarrow 8$
$6 \rightarrow 8$	$1 \rightarrow 2 \rightarrow 4 \rightarrow 5 \rightarrow 8$
$\underline{6 \rightarrow 9}$	$1 \rightarrow 2 \rightarrow 4 \rightarrow 6 \rightarrow 7$
$7 \rightarrow 9$	$1 \rightarrow 2 \rightarrow 4 \rightarrow 6 \rightarrow 8$
$7 \rightarrow 10$	
$8 \rightarrow 10$	$1 \rightarrow 2 \rightarrow 3 \rightarrow 5 \rightarrow 8 \rightarrow 10$
	$1 \rightarrow 2 \rightarrow 4 \rightarrow 5 \rightarrow 8 \rightarrow 10$
	$1 \rightarrow 2 \rightarrow 4 \rightarrow 6 \rightarrow 7 \rightarrow 9$
	$1 \rightarrow 2 \rightarrow 4 \rightarrow 6 \rightarrow 7 \rightarrow 10$
	$1 \rightarrow 2 \rightarrow 4 \rightarrow 6 \rightarrow 8 \rightarrow 10$

Table 3.6: Summary of steps in obtaining the final subsets of a chain structure for the six component temperature sequence specified.

Note in Table 3.6, that the 'hidden links' are possible due to a common component in the respective binary azeotropes. Remember that azeotropic components are labeled with the two components of which they are comprised. The combinatorial nature of the sequence implies that in this case the two azeotropes with a common pure component are linked in the temperature sequence.

Note again that the subsets of the maximal structure indicated in Table 3.6 are actually the structures denoting the compartments of the system.

The maximal structure is then constructed by combining the substructures and their common singular points as shown in Figure 3.24.

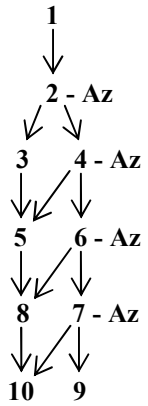

Figure 3.16: Maximal chain structure for six component example from Thong and Jobson (2001a).

The adjacency and reachability matrices may now be obtained from the maximal chain structure utilizing a few simple rules.

There are 10 rows and 10 columns in each of the two matrices that correspond to each ordered component, i.e. row 5; column 6 indicates information about component 5 relative to component 6.

The reachability matrix, as proposed by Knight and Doherty (1990) identifies neighbouring points for a particular singular point. It is a representation of all the singular points that a composition profile may pass through along any of the possible paths given by the chain structure.

The rows of the **reachability matrix** are constructed as follows:

Row 1: From Figure 3.16 it is clear that component 1 may 'reach' any of the other components, resulting in a row of 1's.

Row 2: By the same argument for Row 1, component 2 may reach any higher boiling component than itself.

Row 3: Component three may only pass through components 5, 8 and 10.

Row 4: Component 4 can pass through all higher boiling components than itself.

Rows 5, 8, 10: These rows are simply subsets of the larger subset comprising the 3, 5, 8, 10 chain.

Rows 6, 7, 9: These rows are simply subsets of the larger subset given by the reachable singular points of point 4.

The rows of the **adjacency matrix** are constructed as follows:

Row 1: As can be seen from Figure 3.24 component 1 is not directly bounded by any branches. From the properties of the chain structure it should be reiterated that not all points need to be included in every path and an unbound component will have a direct path to all the higher boiling components. This is the case for component 1 and thus a direct path exists to all other components resulting in their adjacency to component 1.

Row 2: Component 2 is in the immediate vicinity of components 3 and 4. Component 4 is an azeotrope and is thus treated as a saddle point, thus the next point would be component 6. By the same argument, component 6 is passed and thus component 7 is included. Component 9 is included by the

same argument. Components 5, 8 and 10 are not adjacent as they simply constitute a continuation of the unbranched component 3 chain.

Row 3: Component 3 begins an unbranched path to component 10. As mentioned before a composition profile need not pass through all points, thus all the components in the linear chain after component 3 are adjacent to component 3.

Row 4: Following from the argument for Row 2, component 4 is adjacent to components 6, 7 and 9. Component 5 is adjacent, but components 8 and 10 are not, as they are the next two singular points in the linear chain that started with component 3.

Rows 5, 8, 10: These are simply a continuation of a linear chain and are simply adjacent to the next component in the chain.

Row 6, 7, 9: These rows follow the same arguments as those given for Row 4.

$$R = \begin{bmatrix} 1 & 1 & 1 & 1 & 1 & 1 & 1 & 1 & 1 & 1 \\ 0 & 1 & 1 & 1 & 1 & 1 & 1 & 1 & 1 & 1 \\ 0 & 0 & 1 & 0 & 1 & 0 & 0 & 1 & 0 & 1 \\ 0 & 0 & 0 & 1 & 1 & 1 & 1 & 1 & 1 & 1 \\ 0 & 0 & 0 & 0 & 1 & 0 & 0 & 1 & 0 & 1 \\ 0 & 0 & 0 & 0 & 0 & 1 & 1 & 1 & 1 & 1 \\ 0 & 0 & 0 & 0 & 0 & 0 & 1 & 0 & 1 & 1 \\ 0 & 0 & 0 & 0 & 0 & 0 & 0 & 1 & 0 & 1 \\ 0 & 0 & 0 & 0 & 0 & 0 & 0 & 0 & 1 & 0 \\ 0 & 0 & 0 & 0 & 0 & 0 & 0 & 0 & 0 & 1 \end{bmatrix} \qquad A = \begin{bmatrix} 0 & 1 & 1 & 1 & 1 & 1 & 1 & 1 & 1 & 1 \\ 0 & 0 & 1 & 1 & 0 & 1 & 1 & 0 & 1 & 0 \\ 0 & 0 & 0 & 0 & 1 & 0 & 0 & 1 & 0 & 1 \\ 0 & 0 & 0 & 0 & 1 & 1 & 1 & 0 & 1 & 0 \\ 0 & 0 & 0 & 0 & 0 & 0 & 0 & 1 & 0 & 1 \\ 0 & 0 & 0 & 0 & 0 & 0 & 1 & 1 & 1 & 0 \\ 0 & 0 & 0 & 0 & 0 & 0 & 0 & 0 & 1 & 1 \\ 0 & 0 & 0 & 0 & 0 & 0 & 0 & 0 & 0 & 1 \\ 0 & 0 & 0 & 0 & 0 & 0 & 0 & 0 & 0 & 0 \\ 0 & 0 & 0 & 0 & 0 & 0 & 0 & 0 & 0 & 0 \end{bmatrix}$$

Figure 3.17: The Reachability (R) and Adjacency (A) matrices for the six component example in Thong and Jobson (2001a).

The procedure in Thong and Jobson (2001a, b) continues to divide the various distillation regions into compartments from which feasible and potentially feasible classes of splits are identified. Potentially feasible cross-compartmental splits are also identified. Once identified, these splits may be used in a column sequencing procedure, as outlined in Jobson and Thong (2001c).

As can be seen from Table 3.6, the compartments are a direct result of the combinatorial approach of this method. Each of these compartments is equivalent to a distillation region of a non-azeotropic mixture, in that the residue curves in each compartment behave in the same manner as residue curves in the composition space of a non-azeotropic mixture. Using a few simple rules, the information has been represented in the reachability and adjacency matrices.

3.5.3 P-GRAPH ANALYSIS

In P-graph terminology the chain structure given by Figure 3.24, is known as a directed bipartite graph (Friedler et al., 1992, Friedler et al., 1995 and Feng et al. 2000). Its vertices may be partitioned into two disjoint sets, and no two vertices in the same set are adjacent. This is evident in the branching of the chain and the non-adjacency of non-connected terms in the two parallel chains.

P-graph analysis has been extended to process synthesis problems as a tool for selecting optimal process system configurations with minimum waste. The method has selected the bipartite graph for effective structural representation of a process system. The graph contains additional details for process synthesis processes.

Materials in the process graph are termed M-type vertices and operating units are symbolized by a horizontal bar, designating an O-type vertex.

An example of a P-graph for a simple separation of an ideal three component system is given as follows in Figure 3.18:

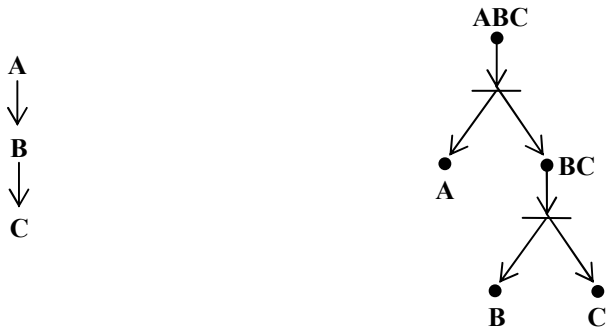

Figure 3.18: Comparison of chain structure with P-graph structure for an ideal three component system.

A few important results arise from the axioms underlying P-graph analysis that are applicable to the chain structure method:

- The union of two solution structures remains a solution structure. Thus the set of solution structures is finite and closed.
- The maximal structure is an element which is the union of all the elements. In this structure, each vertex belongs to at least one solution structure and each solution structure is a subgraph.

From Figure 3.18, the chain structure may be viewed as a condensed form of a P-graph. The P-graph is then an expanded maximal structural form of the chain graph where all possible binary splits are viewed. The chain construction method would be useful in higher order complex systems where the expanded P-graph may be complicated and difficult to visualise.

3.6 CONCLUSIONS

A new graphical representation for multi-component mixtures has been developed. The method is based on combinatorial techniques and the fundamental characteristics of distillation systems. The main characteristic is the presence of a natural temperature ordering among the components in any mixture. The result is a qualitative topographical equivalent of a residue curve map that can be extended to higher dimensions.

The method requires only the specification of the system singular points and their boiling temperatures. A chain map structure may then be constructed as a complete representation of all simple distillation pathways.

Ideal component mixtures form additive linear chains, where additional non-azeotropic forming components simply lengthen the chain. Complexities in the form of azeotropes present in highly non-ideal distillation mixtures manifest in the form of branching in the chain structure representation. In this respect, the chain structure is a bipartite graph and the branches are disjoint sub-sets of the maximal chain structure.

The branches are subsets of the maximal chain structure and are shown to be equivalent to describing the simple residue curve lines in ideal regions within the composition space or compartments. Included in the sub-set structures are sharp splits whereby all nodes need not be passed through.

This method is useful for a qualitative analysis of higher order systems whereby feasible column sequence configurations may be easily identified. The resulting structure is constructed with little effort and minimal data is needed. The combination of temperature ordering, feasibility and higher order representation is a new approach to initial design methodologies. Feasible candidate process synthesis is achieved in

the initial stages of design thereby avoiding undue erroneous results in subsequent analyses.

The representation is also shown to be useful as a precursor for other existing methods that are used for more rigorous subsequent analyses of distillation systems.

CHAPTER 4: THE INVESTIGATION OF A COSTING FACTOR FOR AN IDEAL BINARY DISTILLATION SYSTEM USING ATTAINABLE REGION THEORY

ABSTRACT

Attainable region (AR) theory is applied to an ideal binary distillation system for a geometrically based method of cost analysis. The costing variable, kappa, ('κ'), is derived from a unique balance over a 'flash step' for a process, and acts as a capacity variable for the vapour produced in any equilibrium stage. Having defined the costing variable, the method is applied to various distillation configurations such as a rectifying section, distributed reflux addition and distributed feed addition.

The resulting attainable regions are a series of equilibrium step compositions with varying reflux and corresponding cost associations. Thus multiple paths to achieving product specifications may be evaluated with costing as a primary influence on the decision. The extremities of the attainable region are traversed by considering various combinations of mixing and separation.

The constructed AR shows the trends of varying the number of column stages and reflux on composition and cost. One may exploit the convexities of the attainable region for the system to optimize potential separations at minimum cost for a minimum number of equilibrium stages.

4.1 INTRODUCTION

In preliminary process design synthesis steps, a multitude of decisions often face the designer. The complexity is not lessened when sub-structures of the process are considered. Once the fundamental physical processes that are involved in the particular process are identified, another degree of complexity is revealed by their interactions. At each decision making point there may be one or many options for utilizing these fundamental processes to achieve a predefined objective. In the case where there are many options, there exist a number of paths that the design may follow.

The paths need to be viewed as a series of alternatives and thus some form of comparison is required. Graphical methods are especially effective for conveying complex relationships in an easily interpretable manner. Comparing the alternatives is in effect an indirect optimization exercise. A relatively new optimization tool called attainable region (AR) analysis has been pioneered by Hildebrandt and Glasser (Godorr, Hildebrandt & Glasser, 1994; Hildebrandt & Bieglar, 1995; Jobson, Hildebrandt & Glasser, 1996; Glasser & Hildebrandt, 1997; McGregor, 1998).

The AR method relies on geometric principles and aims to find the region of all attainable outcomes for a particular system (McGregor, 1999). It was first defined by Horn (1964), as the full set of product composition vectors that can be produced in principle by means of all possible steady state designs that employ only reaction and mixing. This includes points that cannot actually be realized but which nevertheless can be approached arbitrarily closely (Feinberg and Hildebrandt, 1997). These are the extreme points of the attainable region and form a manifold or protrusion.

Of special interest is the boundary of the AR (Feinberg, 1999). The boundary points of the AR are extreme points if their associated vectors point inward. Outward

pointing vectors suggest a possible expansion of the region. The vectors may point outward in the case of a constrained AR where the boundary is itself a constraint. Feinberg & Hildebrandt (1997) showed that manifolds of extreme points (protrusions) on the attainable region's boundary of reactor networks are invariably made up of plug flow reactor trajectories. The plug flow reactor trajectories provide access to the attainable regions extreme points and the boundary formed by these points may be traversed by continuous-flow stirred-tank reactors (CFSTRs) and differential sidestream reactors (DSRs).

AR methods are primarily used to view process alternatives at the conceptual design of flowsheet development but costing may be included to extend the feasibility analysis to become an optimisation tool. Jobson et al. (1996) introduce the concept of capacity variables as cost indicators for processes involving vaporisation and condensation. The dimensionless variables are shown to be valid for any vapour liquid equilibrium separation process in batch or continuous applications. The capacity variables are analogous to the mean residence time of a process involving reaction.

Kauchali et al. (1999) introduce a modified form of the capacity variables formulated by Jobson et al. (1996) for use in a complex countercurrent distillation column developed by McGregor (1998). The reflux ratio policy is optimized along the length of the column by differential cooling and condensing along the length of the column thereby minimizing the cost variable. The costs in controlling the optimum reflux ratio were neglected in minimizing the objective function. AR theory was used as a tool to minimise the objective function containing elements representing vectors of the fundamental processes involved for the separation of an ideal binary mixture. The costs associated with the differential condensers and reboilers were later included in the investigation (Kauchali, 2000).

The AR considers the fundamental processes that can occur rather than the flowsheet configuration being considered. If the state variables are expressed as rates for a particular process area, an AR may be formulated with the use of an overall vector describing the changes in the system. Gadewar et al. (2002) use the AR approach for a system with simultaneous separation, reaction and mixing. A model is developed for a countercurrent cascade of two-phase continuously stirred tank-reactors (CSTRs) that replicate the stripping or rectifying sections of a reactive distillation column. Two important results arise from this work. When one of the fundamental processes is mixing, the region is convex as a line that joins any two points in the region also lies in the region. The boundary of the feasible region for the countercurrent cascade of CSTRs is shown to be the trajectory for two phase CSTRs in series. This is in agreement with universal properties of the AR (Feinberg & Hildebrandt 1997).

This work introduces a modified or rather manipulated version of the original capacity variable by Jobson et al. (1996). The manipulated version of the capacity variable definition is as a pseudo balance that tracks the vapour formation for successive equilibrium flash steps and thus provides a cumulative measure of cost. The equivalence to the original is verified by the use of examples.

The new method is applied to the rectifying section of a binary distillation column by a further modification to allow for the number of stages in successive column sections (Kauchali et al. 1999). An AR is constructed from the composition vector and the capacity difference vector for an ideal binary mixture. Convexities are shown to be apparent in the region indicating the optimal reflux policies could be selected to minimise the number of stages and cost simultaneously.

Mixing is then included in the investigation in the form of differential side stream addition of the distillate. The mixing is shown to expand the AR into a lower cost region. The boundary of the AR is seen to be equivalent to a number of optimised column sections in series.

The work is not limited to binary systems and a ternary equivalent is offered. This work shows that a costing function included in an AR analysis can prove to be a valuable optimization tool.

4.2 BACKGROUND

4.2.1 DERIVATION

Jobson et al. (1996) introduce the definition of the boiling capacity variable, κ, for an equilibrium stage as:

$$\kappa = \kappa_f + \frac{moles\ \ of\ \ vapour\ \ product\ \ leaving\ \ the\ \ stage}{moles\ \ fed\ \ to\ \ the\ \ stage} \tag{4.1}$$

The condensing capacity variable is defined analogously for the liquid products of an equilibrium stage as shown in Jobson et al. (1996), but is not used in this work. Both variables are dimensionless.

The variables are valid in batch and continuous processes for any feed conditions thus providing a cumulative measure of the costs associated with cooling and condensing in the upstream process.

Two more of the definitions related to capacity variables by Jobson et al. (1996) will be important in this work, namely:

1. Each equilibrium stage has a single vapour and a single liquid product and the capacity variables of both products leaving that stage are by definition, equal.

2. The capacity variables obey the linear mixing rule. If two streams F_1 and F_2 with associated capacity variables κ_1 and κ_2 respectively are mixed, the mixture is a weighted average of the capacity variables of the constituent streams.

$$F * \kappa^* = F_1\kappa_1 + F_2\kappa_2 \qquad \textbf{(4.2)}$$

By rearranging Equation 4.2, the following balance is obtained:

$$\begin{aligned} &(moles\ \ of\ \ feed\ \ of\ \ all\ \ phases)(\kappa - \kappa_f) \\ &= vapour\ \ flow\ \ rate\ \ leaving \end{aligned} \qquad \textbf{(4.3)}$$

Although Equation 4.3 is a direct manipulation of the definition of the boiling capacity variable, it does not allow a link between the mass balance and the κ balance given by Equation 4.1 for steady state problems that are represented by a Differential Equation (DE). An alternative form of Equation 4.1 is proposed. This form serves to facilitate a direct balance with all the required information to construct a DE for any steady state separation process.

The proposed form of the κ balance is:

$$\begin{aligned} &\Sigma F_i\kappa_i\ \ Streams\ \ entering\ \ flash + Vapour\ \ produced\ \ in\ \ flash \\ &= \Sigma F_i\kappa_i\ \ Streams\ \ leaving\ \ flash \end{aligned} \qquad \textbf{(4.4)}$$

The validation of the proposed alternative is given by means of a series of examples culminating in the equivalent result for a batch still as that obtained in Jobson et al. (1996). The first example is a single flash step as shown below.

4.2.2 EXAMPLE 1: A SINGLE FLASH STEP

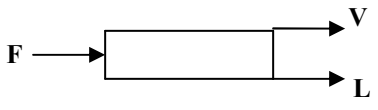

Figure 4.1: A single flash equilibrium stage with single feed and single vapour and liquid products

The mass balances and component mass balances for Figure 4.1are given as

$$\dot{F} = \dot{V} + \dot{L} \tag{4.5}$$

$$\dot{F}x_F = \dot{V}y + \dot{L}x \tag{4.6}$$

Substituting Equation 4.5 in Equation 4.6 gives the relationship between the feed and the vapour product stream.

$$\dot{F}(x - x_F) = \dot{V}(x - y) \tag{4.7}$$

The κ balance for the component streams is then written according to Equation 4.8 below.

$$\dot{F}\kappa_F + \dot{V} = \dot{V}\kappa_V + \dot{L}\kappa_L \tag{4.8}$$

From Figure 4.1 and additional definition 1, it should be clear that the capacity variables for the vapour and liquid are identical as they both leave the same equilibrium stage.

$$\boldsymbol{\kappa}_V = \boldsymbol{\kappa}_L = \boldsymbol{\kappa} \tag{4.9}$$

Thus using Equation 4.8 and Equation 4.9, the resulting balance is:

$$\dot{F}(\boldsymbol{\kappa} - \boldsymbol{\kappa}_F) = \dot{V} \tag{4.10}$$

Note the main difference between equation 4.7 and the final κ balance, equation 4.10, is the absence of the composition difference vector in equation 4.10. This is an expected result, as the purpose of the κ variable is to track the vapour formation in successive flash steps and it does so by encompassing the composition difference vector.

4.2.3 EXAMPLE 2: TWO STREAM MIXER FLASH STEP

Consider the equilibrium step shown in Figure 4.2. The configuration in mathematically analogous to the stage feed stage in a distillation column. A small strip of length Δz is considered in the plug flow flash step.

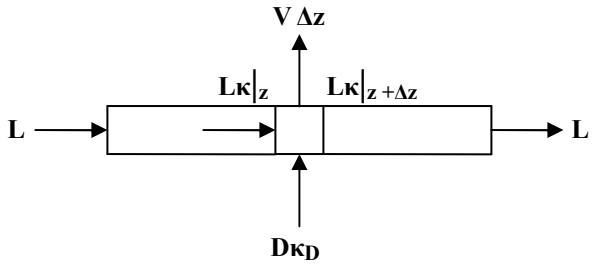

Figure 4.2: Differential equilibrium step for double feed mixing and single vapour and liquid products in a plug flow configuration.

With the assumption of steady state, the mass balance for the system in Figure 4.2 over the strip Δz is given as:

$$\dot{L}\Big|_z + \dot{D}\Delta z = \dot{L}\Big|_{z+\Delta z} + \dot{V}\Delta z \qquad \textbf{(4.11)}$$

The resulting DE from Equation 4.11 is:

$$\frac{d\dot{L}}{dz} = \dot{D} - \dot{V} \qquad \textbf{(4.12)}$$

The component mass balance for the system in Figure 4.2 is given in Equation 4.13 below. The final mass balance DE given by Equation 4.14 is found by using the relationship in Equation 4.12 in the resulting DE from Equation 4.13.

$$\dot{L}x\Big|_z + \dot{D}x_D\Delta z = \dot{L}x\Big|_{z+\Delta z} + \dot{V}y\Delta z \qquad \textbf{(4.13)}$$

$$\dot{L}\frac{dx}{dz} = \dot{V}(x - \mathrm{y}) + \dot{D}(x_D - \mathrm{x}) \tag{4.14}$$

The κ balance for the component streams is then written according to Equation 4.15.

$$\dot{L}\kappa\Big|_z + \dot{D}\kappa_D\Delta z + \dot{V}\Delta z = \dot{L}\kappa\Big|_{z+\Delta z} + \dot{V}\kappa\Delta z \tag{4.15}$$

The resulting DE in Equation 4.16 may then be manipulated and the relationship in Equation 4.12 substituted to yield the final form in Equation 4.17.

$$\frac{d\dot{L}\kappa}{dz} = \dot{D}\kappa_D + \dot{V} - V\kappa \tag{4.16}$$

$$\dot{L}\frac{d\kappa}{dz} = \dot{D}(\kappa_D - \kappa) + \dot{V} \tag{4.17}$$

Note again the absence of the composition difference vector in the final κ balance DE, Equation 4.17, compared to the final mass balance DE, Equation 4.14.

4.2.4 EXAMPLE 3: A BATCH STILL

Consider a batch still containing a liquid mixture. At time *t*, heat is introduced to the system and a vapour is formed as shown in Figure 4.3.

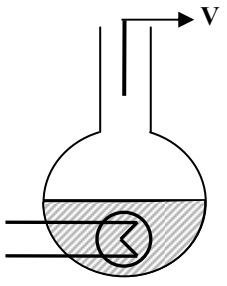

Figure 4.3: Heated batch still containing liquid mixture forming vapour.

The mass balance and the resulting equation describing the change in liquid amount with time are shown below.

$$L\big|_t = L\big|_{t+\Delta t} + \dot{V}\Delta t \tag{4.18}$$

$$\frac{dL}{dt} = -\dot{V} \tag{4.19}$$

The component mass balance is performed and the final DE after substitution of the relationship in Equation 4.19 may be found.

$$Lx\big|_t = Lx\big|_{t+\Delta t} + \dot{V}y\Delta t \tag{4.20}$$

$$L\frac{dx}{dt} = \dot{V}(x - y) \tag{4.21}$$

The κ balance for the batch still is performed according to Equation 4.22 and the final DE is obtained by substitution of Equation 4.19.

$$L\kappa\big|_t + \dot{V}\Delta t = L\kappa\big|_{t+\Delta t} + \dot{V}\kappa\Delta t \tag{4.22}$$

$$L\frac{d\kappa}{dt} = \dot{V} \tag{4.23}$$

Equation 4.23 is the equivalent mathematical result obtained by Jobson et al. (1996) for the same example and thus the proposed modified κ balance will be used for the duration of this work.

4.3 APPLICATION OF AR THEORY TO DISTILLATION

4.3.1 CASE STUDY 1: RECTIFYING DISTILLATION COLUMN

The rectifying section of a simple distillation column will be used to illustrate the application of the κ variable and its implications in an attainable region. The column setup is illustrated in Figure 4.4 below. The column section is assumed to operate at steady state; to be adiabatic and the heats of vaporisation are assumed to be constant. Thus there is constant molar overflow for the entire column section, resulting in only mass transfer having been considered for the construction of the AR.

Previous work with AR concentrated on reactor networks and cost measures had not been included in the attainable region as its main purpose was to determine process alternatives and to determine which of these were feasible, (Gadewar, 2002). By producing column profiles at different reflux ratios while considering cost implications, a cost scaled attainable region is obtained.

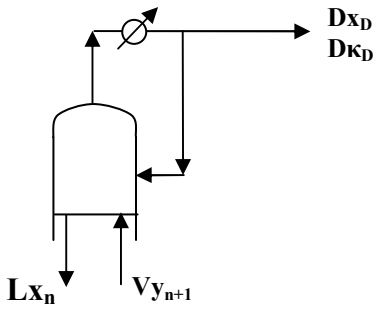

Figure 4.4: Rectifying column section for simple distillation column.

The mass balance and component mass balance for the rectifying section of a simple distillation column as shown in Figure 4.4 are given by:

$$\dot{V} = \dot{L} + \dot{D} \qquad \textbf{(4.24)}$$

$$\dot{V}y_{n+1} = \dot{L}x_n + \dot{D}x_D \qquad \textbf{(4.25)}$$

An algebraic trick is employed so that limits may be applied and the balance differentiated to obtain the overall mass balance DE for the system, given by Equation 4.26.

$$\dot{V}y_{n+1} + \dot{L}x_{n+1} = \dot{L}x_n + \dot{L}x_{n+1} + \dot{D}x_D \qquad \textbf{(4.26)}$$

$$\dot{L}\frac{dx}{dn} = \dot{V}(x - y) + \dot{D}(x_D - x) \qquad \textbf{(4.27)}$$

The previous examples involved single step equilibrium separation steps. The construction of a composition profile for a column requires that a number of consecutive equilibrium stages be considered. Solving Equation 4.27 is made easier by the use two dimensionless variables that are defined below.

Firstly the reflux ratio relationship, where *r*, is the column reflux ratio, equivalent to $\left(\frac{\dot{L}}{\dot{D}}\right)$. Thus:

$$\frac{\dot{D}}{\dot{V}} = \frac{1}{1+r} \qquad \textbf{(4.28)}$$

and secondly a dimensionless time variable, τ, a dimensionless time variable for the integration. The dimensionless time steps are equivalent to the stages in the column.

$$d\tau = \frac{\dot{V}dn}{\dot{L}} \qquad \textbf{(4.29)}$$

Substitution of Equations 4.28 and 4.29 yields:

$$\frac{dx}{d\tau} = (x - y) + \frac{1}{1+r}(x_D - x) \qquad \textbf{(4.30)}$$

By choosing a distillate composition x_D, and a reflux ratio, Equation 4.30 may be integrated for a specified number of time steps, or stages. The vapour (y) composition in equilibrium with the liquid on each stage is calculated using the following relationship:

$$y_i = \frac{\alpha_i x_i}{\alpha_i x_i + \alpha_i x_i} \tag{4.31}$$

Where α_i, is the relative volatility of component i. Components 1 and 2 have relative volatilities of 3 and 1 respectively. The solution to equation 4.30 is shown in Figure 4.5 for a number of reflux ratios ranging from 0.01 to 110.

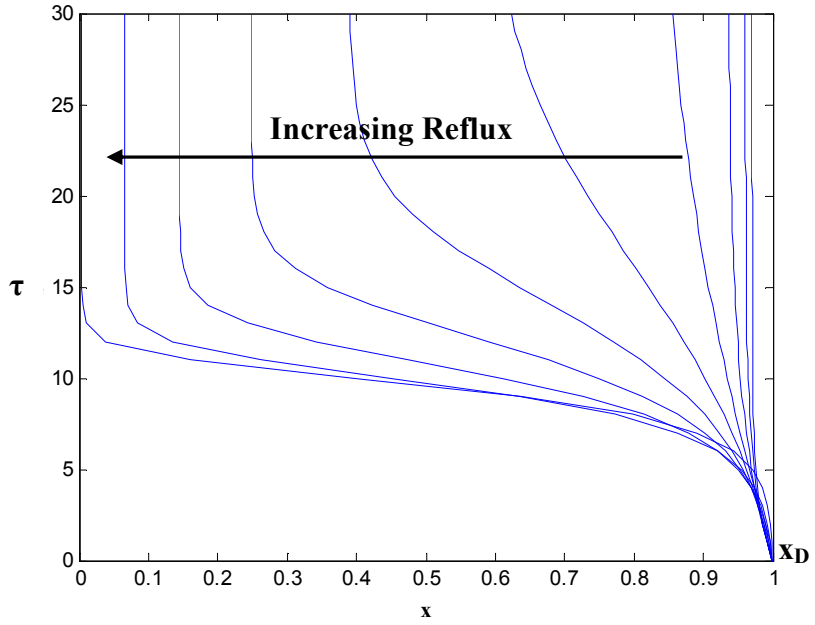

Figure 4.5: Change in component composition with respect to time/stages for a range of reflux ratios from 0.01 to 110. x_D is the distillate composition equal to 0.99.

Figure 4.5 shows the effect of increasing the reflux ratio on the (exit) pinch composition for a set number of stages and constant distillate composition (x_D). Higher reflux ratios result in a complete composition profile whereas lower refluxes pinch. It should be noted that the profiles are merely rectifying profiles for the

column and thus it is not necessary to obtain a complete separation. This would be achieved by finding an intercepting stripping profile for a specified feed composition.

The aim is to link the composition change for a given reflux to the cost associated with that separation. Kauchali et al. (2000), proposed the use of a modified form of Equation 4.1 for a distillation column. The modified capacity variable for a rectifying section was defined as:

$$\kappa = \frac{\dot{V}}{\dot{D}} \times n \tag{4.32}$$

The additional factor, n, accounts for the number of stages in the column. This addition will be applied to the modified definition of the capacity variable given by Equation 4.4 in the construction of the overall mass and component mass balances for the configuration in Figure 4.5.

The component mass balance for κ is given by Equation 4.33 and Equation 4.34. The same algebraic trick is used in Equation 4.34 in preparation of forming the DE. Note the addition of the, n, to the vapour term to designate the particular stage for that step of the eventual integration in obtaining the composition profile.

$$\dot{V}\kappa_{n+1} + Vn = \dot{L}\kappa_n + \dot{D}\kappa_D \tag{4.33}$$

$$\dot{V}\kappa_{n+1} + Vn + \dot{L}\kappa_{n+1} = \dot{L}\kappa_n + \dot{L}\kappa_{n+1} + \dot{D}\kappa_D \tag{4.34}$$

In the construction of an attainable region, all state variables are required to be expressed as rates. Equation 4.34 is put into differential form (Doherty & Perkins, 1978) and the overall mass balance relationship given by Equation 4.24 is substituted to yield:

$$\dot{L}\frac{d\kappa}{dn} = \dot{D}(\kappa_D - \kappa) - \dot{V}n \qquad \textbf{(4.35)}$$

Equations 4.28 and 4.29 are again used to arrive at the final form of the κ component balance. Substitution of the above two variables yields:

$$\frac{d\kappa}{d\tau} = \frac{1}{1+r}(\kappa_D - \kappa) - n(\tau) \qquad \textbf{(4.36)}$$

A closer inspection of Equation 4.36 suggests that for an increasing number of stages, the value of κ will become increasingly negative. This has little implication for hampering the interpretation of the result as whether κ increases positively or negatively is in effect the same thing when only relative values are to be compared. For the purposes of a pleasing graphical representation, the plot will be of $|\kappa|$.

From Equation 4.29 it should be clear that n is a function of τ, and thus integration is not possible unless this relationship is included in the solution equations. The rate relationship is given by Equation 4.29, however, using Equation 4.24 and utilizing the defined dimensionless variable given in Equation 4.28, the following useful rate expression is obtained:

$$\frac{dn}{d\tau} = 1 - \frac{1}{1+r} \qquad \textbf{(4.37)}$$

For the same conditions as those for Equation 4.30 shown in Figure 4.5, the solution to Equations 4.36 and 4.37 may be found. The graphical output is shown in Figure 4.6 for the same range of reflux ratios as in Figure 4.5. Note that the absolute value of the cost variable is plotted. This is merely an inflection from the negative to the positive and has little bearing on the results as only relative values are to be considered.

The equivalent distillate cost is set to zero and a reverse cost is performed as the composition is integrated down the column section. The equivalent time/stage steps are taken. The variable introduced in Equation 4.32, n, need not be specified as it the link between Equations 4.36 and 4.37, and effectively cancels as it is specific to each integration step.

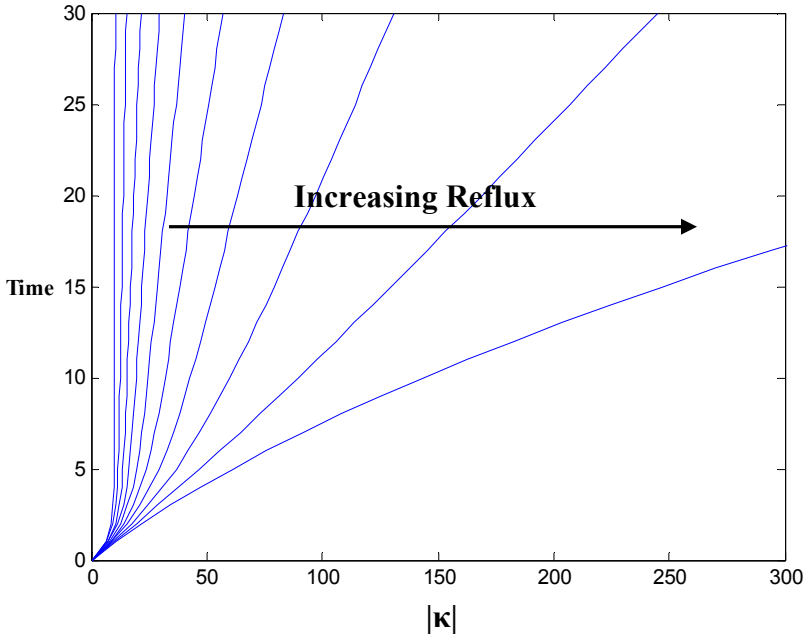

Figure 4.6: Change in costing function with respect to time/stages for a range of reflux ratios from 0.01 to 110.

The costing variable, κ, in Figure 4.6 serves to track the vapour composition in successive stages along the column profile. For this reason it is a function of composition. For the lower refluxes the column profiles pinch and thus additional stages have little effect on the cost (κ). For higher refluxes the composition profile is completed in less than the specified number of stages and thus the additional stages become increasingly costly.

In the construction of figures 4.5 and 4.6, an equal number of time steps and equal refluxes were specified for the solutions of equations 4.30, 4.36 and 4.37. Thus the

composition values for each time step and reflux correspond to a cost value for the same time step and reflux. The composition as a function of cost for the reflux range is represented in Figure 4.7. This is the equivalent of the feasible attainable region, but is constrained under the specified reflux range and number of stages.

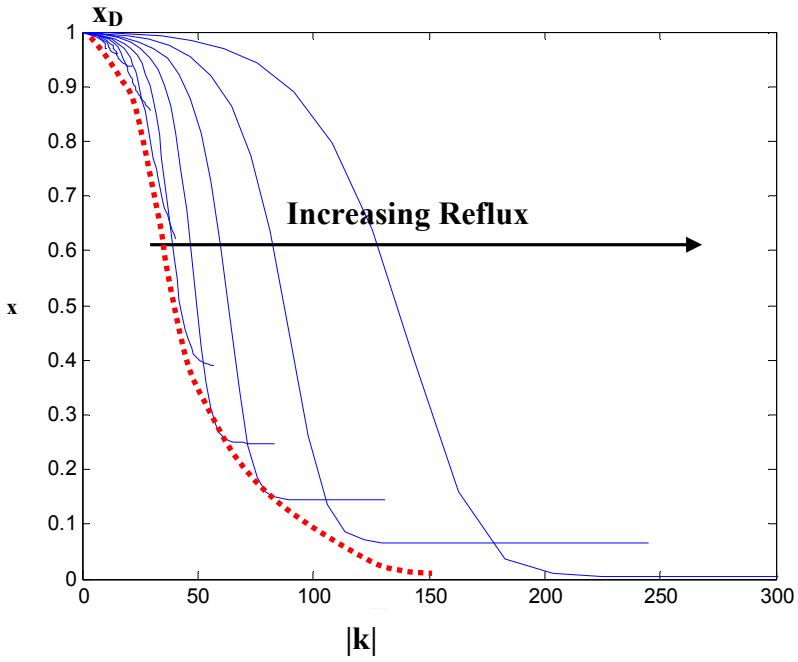

Figure 4.7: Column composition change with respect to component 1 showing increased cost with increase in reflux.

As shown in Figure 4.7, a high reflux provides a means to fully separate the two components along the length of the column section. This is however the most costly method. The other limit of the attainable region, given by the dashed line, is composed of adjacent column sections with successively increasing reflux ratios. The profiles are for the same number of stages and the turning points form the points along the lower dashed boundary. This lower boundary may be thought of in terms of a number of successive column sections. So where one column section starts to turn, the next could begin at a slightly higher reflux. The entire composition profile could then be realised with minimum cost associated with the formation of a vapour at each stage. The penalty for making extra vapour has not however, been taken into account.

A similar result was found by Kauchali et al. (1999, 2000) where the reflux was controlled by differentially condensing or vaporising of streams.

Introducing column sections may provide the minimum cost but it increases the column complexity. Remember that column sections are sections of stages in between points of addition or removal of material or heat to or from the column. A large number of column sections, implies that a strict composition control regime would have to be implemented. It would seem that the outer boundaries of the attainable region have some limitations in this case. There is one other piece of information however, that has not yet been considered. All state variables are required to be expressed as rates, thus each profile has an associated number of stages or time steps.

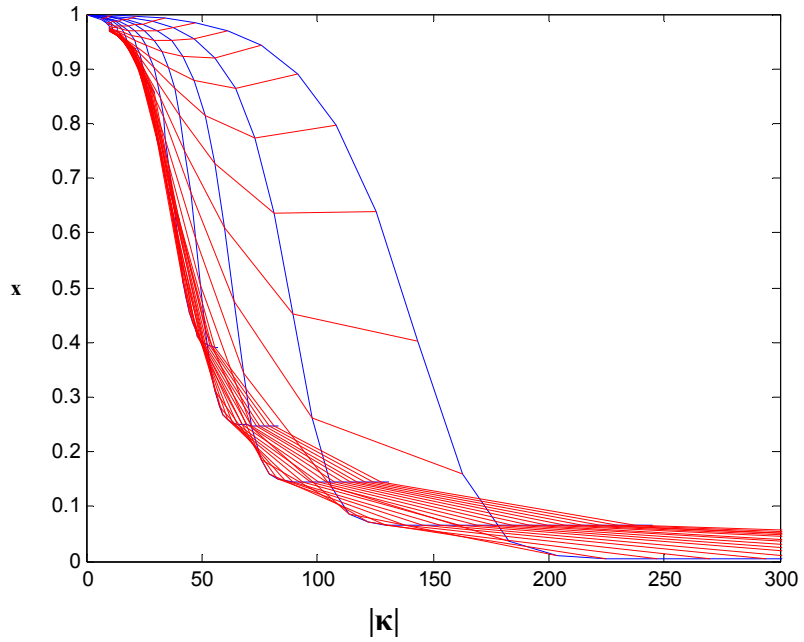

Figure 4.8: Column composition change with respect to component 1 showing increased cost with increase in reflux. Iso-stage points are linked to show convexities.

These time steps have been added to the profiles in Figure 4.7 to give Figure 4.8. The time steps allow reflux ratios to be compared according to cost and minimum number of stages. The constant time lines joining the time steps for each reflux ratio are

notably convex in the upper half of the region. The profiles given by the reflux ratios going through the outermost convexity are moving at the fastest rate. This convex hull of extreme points (constrained as they are) is referred to as a protrusion (Feinberg & Hildebrandt 1997). By selecting profiles running through the outermost points of the protrusion (for an equivalent number of equilibrium stages) one may minimise the cost and the number of stages for a series of column sections.

4.3.2 EXPANSION OF ATTAINABLE REGION USING DISTRIBUTED REFLUX

The resulting region in Case Study 1 is a feasible constrained attainable region. The extreme points of the trajectories are limited by the number of stages and their position to each other is influenced by reflux ratio. An increase in the number of stages for the column section is demonstrated in Figure 4.9 (bold lines: same stages). An increase in the number of stages is shown by the dashed line for each reflux. Once the composition profiles pinch, an increase in stages has no effect on composition.

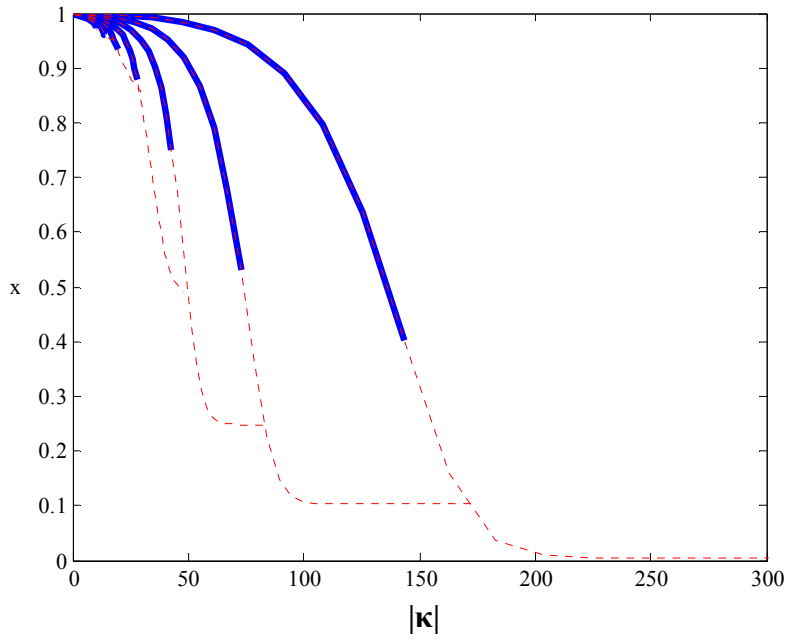

Figure 4.9: Effect of the increase in number of stages for different reflux ratios.

For the attainable regions in reactor networks, the trajectories to the extreme points have been shown to be plug flow trajectories (Feinberg & Hildebrandt 1997). The boundaries of the AR were traversed by using DSRs and CSTRs. A similar situation exists for distillation systems where the trajectories are column section profiles and the corresponding AR boundaries may be traversed by using differential or bulk mixing, analogous to DSRs or CSTRs.

The same configuration of the simple distillation column in Case Study 1 will be used to illustrate the expansion of the attainable region given by Figure 4.8 at a minimum cost. The lower dashed line in Figure 4.7 was said to be comprised of a large number of adjacent column sections where the composition of the feed to each section was controlled. An optimum number of stages for each section would ensure the correct starting point for the next column section just prior to the turning point. The expansion occurs along this boundary as this constitutes the lowest cost saving opportunities.

The region is expanded by differentially returning the reflux to the column. This is done by mixing the distillate (x_D) from the top column section with the liquid bottoms of the same column section. The result is a liquid feed to the next column section somewhere between the distillate and bottoms composition of the previous column section. The same mixing with the top distillate (x_D) is performed for successive column sections. The result is a series of rectifying column sections with differential mixing by split reflux addition. The column setup is illustrated in Figure 4.10 below.

It is assumed that the reflux ratio would be controlled by some form of differential condensing or vaporisation, so that only the compositions of the streams to successive column sections would be affected by the mixing.

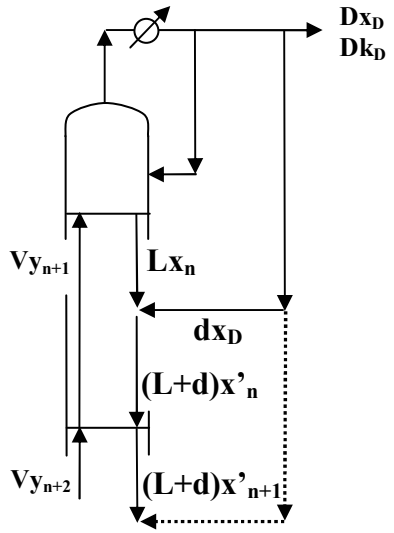

Figure 4.10: Rectifying section of simple column preceded by column sections formed by differential reflux return.

As before, the column sections are assumed to operate at steady state; to be adiabatic and the heats of vaporisation are assumed to be constant. Thus there is constant molar overflow for all the column sections, resulting in only mass transfer having been considered for the construction of the AR.

The construction of the expansion of the AR is done graphically. This may be done due to the assumption made in Equation 4.2, whereby the capacity variables obey the linear mixing rule. Thus mixing is represented by a straight line on a $|\kappa|$ vs. composition plot. The mathematical equations governing the overall mass balance DE and the overall κ balance DE are offered below. The full derivation is given in APPENDIX C. The overall component mass balance is given by Equation 4.38.

$$\frac{dx}{d\tau} = (x - y) + \left(\frac{1}{1+r}\right)(x_D - x) \qquad \textbf{(4.38)}$$

Where:

$$d\tau = \frac{\dot{V}}{(\dot{L} + \dot{d})} dn \tag{4.39}$$

The differential amount of reflux added to each successive column section is given by d and n is the number of stages for the particular column section. The overall component κ balance is given by equations 4.40 and 4.41.

$$\frac{d\kappa}{d\tau} = \left(\frac{1}{1+r} \right) (\kappa_D - \kappa) - n \tag{4.40}$$

$$\frac{dn}{d\tau} = \left(1 - \frac{1}{1+r} \right) \tag{4.41}$$

For the rectifying column section, prior to any differential reflux addition, the basic AR is constructed for the solutions to equations 4.38, 4.40 and 4.41 where the differential reflux addition term, d, in equation 4.39 is zero. The result is shown in Figure 4.11.

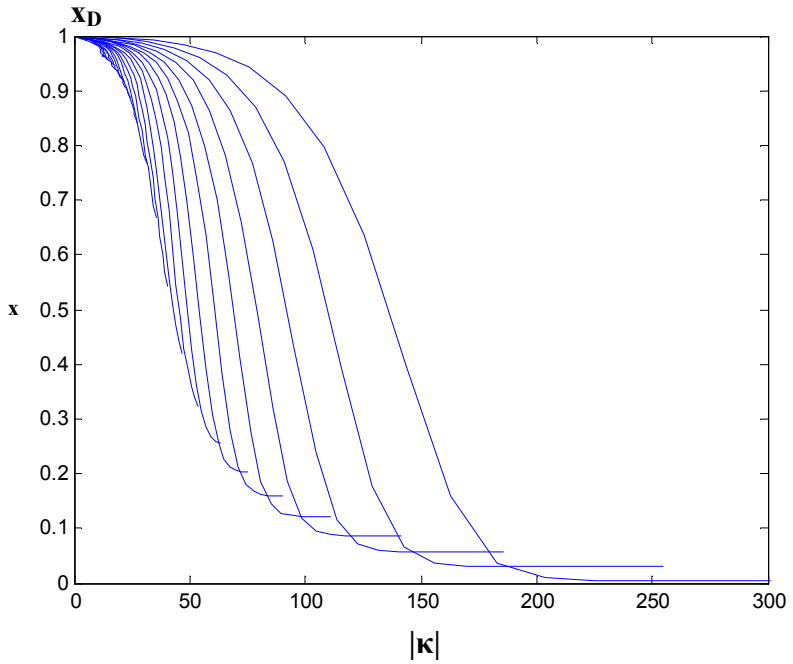

Figure 4.11: Column composition change with respect to component 1 showing increased cost with increase in reflux.

Figure 4.12 shows the gradual graphical expansion of the AR given in Figure 4.11. A profile along the inside boundary of the AR is selected. It should preferably just have reached its turning point, thus the number of stages are optimal.

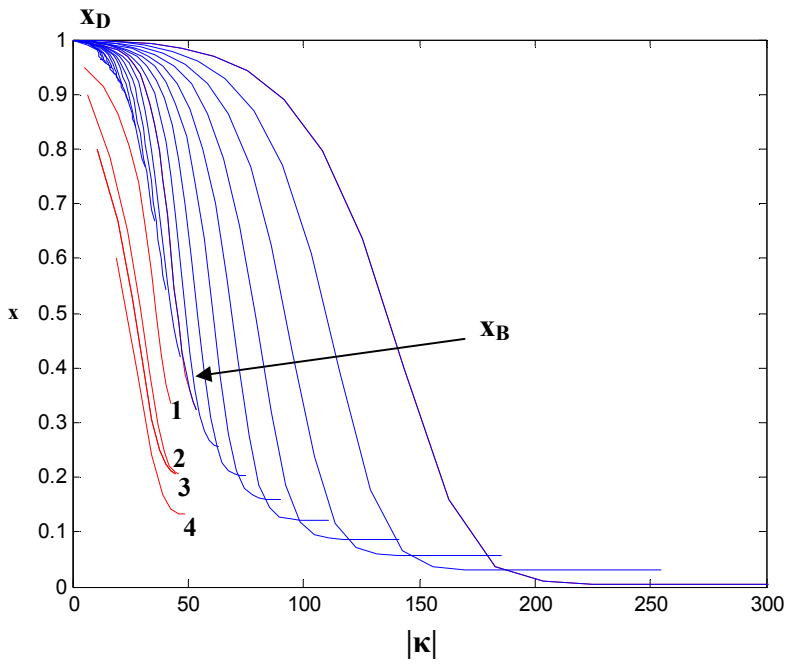

Figure 4.12: Expansion of AR using successive differential mixing with distillate.

In Figure 4.12, the end profile composition, x_B, is then mixed with the distillate of the first column section, x_D, along a mixing line joining the two points. The next column section then begins at the new mixing point and the profile terminates at point 1 for the same reflux and an optimum number of stages. The same process may be repeated for points 2, 3 and 4 etc. to complete the extended region where the reflux is constant for each successive column section. The expanded region is shown in Figure 4.13.

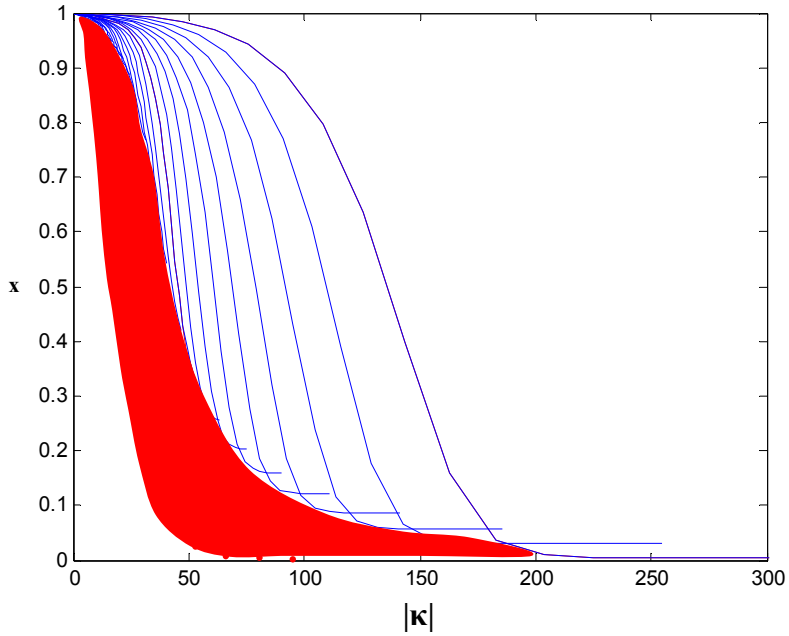

Figure 4.13: Expanded region of AR by use of differential mixing.

Thus by bulk mixing one may reach newly attainable points along the boundary of the expanded AR, analogous to a CSTR. For a large number of differentially mixed stages, one may incrementally move along an AR boundary as shown in Figure 4.12, this being analogous to a DSR. The overall result is a surface of achievable composition profiles with associated costs.

The point has been to demonstrate the universal behaviour of AR theory and its application in the construction of distillation systems. The procedure may be extended to a ternary system where a third component of intermediate relative volatility is introduced. An example is shown in Figure 4.14.

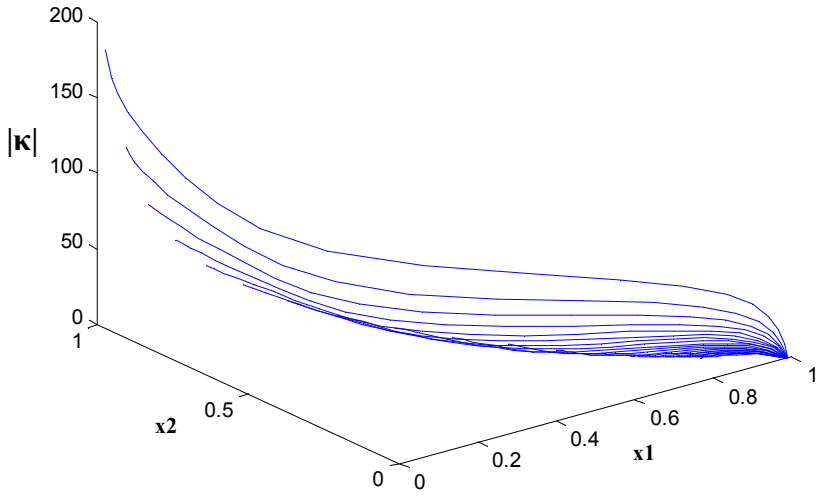

Figure 4.14: Construction of AR for ternary system showing equivalent number of stages for different refluxes.

4.4 CONCLUSIONS

A new method of evaluating decisions in distillation column synthesis has been introduced. A capacity variable arises out of a unique component balance based on existing definitions of the capacity variable. The variable provides a cumulative measure of the costs associated with equilibrium separation processes. The composition and cost vector for a simple binary distillation system are used to construct a constrained feasible region. The tool is not limited to binary mixtures and may be applied to higher order systems.

The boundary points of the region are composition trajectories for column sections and are specific to a reflux ratio policy and a set number of stages. Addition of mixing as a fundamental process expands the AR and results in a convex boundary. The boundaries of the AR may be traversed by simple combinations of the fundamental process units as is the case in previous work in reactor networks.

The capacity variable and composition change along a column section are functions of a dimensionless time step equivalent to an equilibrium stage in the column. Convexities within the AR allow the selection of optimal composition profiles to minimize cost and number of stages.

Previous work has concentrated on feasibility or optimization using AR techniques. Combination of the costing measure and AR theory provides a comparative optimization technique for all possible alternatives within a candidate feasible attainable region. Thus simultaneous evaluation of multiple feasible separation schemes is possible via a common costing factor.

REFERENCES

CHAPTER 2

Castillo, F.J.L., Thong, D.Y.-C. and Towler, G.P. (1988). *Homogeneous Azeotropic Distillation. 1. Design Procedure for Single-Feed Columns at Non-Total Reflux*. Industrial Engineering Chemistry Research **31**, 2345.

Doherty, M.F., Perkins, J.D., (1978). *On The dynamics of Distillation Processes. I. The Simple Distillation of Multi-Component Non-Reacting, Homogeneous Liquid Mixtures*. Chemical Engineering Science **33**, 281.

Fenske, M.R., (1932). Industrial Engineering Chemistry **24**, 482.

Franklin, N.L., (1986). "*Counterflow Cascades: Part 1*", Chemical Engineering Research Design Vol. **64**, 56 – 64.

Hauan, S., Ciric, A., Westerberg, A.W. and Lien, K.M., (1998). *Difference Points in Extractive and Reactive Cascades I- Basic Properties and Analysis*. Submitted to Chemical Engineering Science.

Hausen, H., (1952). *Rektifikation Idealer Dreistoff-Gemische*. Z. Angew. Phys. **4**, 41.

Hoffmann, E.J., (1964). "*Azeotropic and Extractive Distillation*" Wiley (Interscience), New York.

Holland, S.T., Tapp, M., Hildebrandt, D., Glasser, D. and Hausberger, B., (2004). *Novel Separation System Design Using "Moving Triangles"*. Computers and Chemical Engineering **29** (1), 181 – 189.

Lee., J.W. & Westerberg., A.W., (2000). *Visualisation of Stage Calculations in Ternary Reacting Mixtures.* Computers and Chemical Engineering **24** (2), 639 – 644.

Ostwald. W., (1902). *Lehrbuch Der Algemeinen Chemie. Verwandtschaftslehre*. Verlag von Wilhelm Engelmann: Leipzig, Germany, part1.

Rische, E.A., (1955). *Rektifikation Idealer DreistoffGemische Unter Der Voraussetzung, Daß Der Widerstand Des Stoffaustausches Allein Auf Der Flussigkeitsseite Liegt.* Z. Angew. Phys. **7**, 90.

Serafimov, L.A., (1968). *Theoretical Principles of Distillation Sequences Design and Synthesis for Non-Ideal Multi-component Mixtures*. Ph.D. Thesis, Lomonosov Institute of Fine Chemical Technology, Moscow.

Shreinemakers, F.A.H., (1902). *Einige Bemerkungen Ueber Dampfdruecke Ternaerer Gemische*. Z. Phys. Chem. **43**, 671.

Tapp, M., Holland, S.T., Hildebrandt, D., and Glasser, D., (2003). *Column Profile Maps Part B: Singular Points and Phase Diagram Behaviour for Ideal and Non-Ideal Systems*. Industrial Engineering Chemistry Research, submitted for publication.

Tapp, M., Holland, S.T., Hildebrandt, D., Glasser, D., (2004). "*Column Profile Maps Part A: Derivation and Interpretation of Column Profile Maps "*. Industrial Engineering Chemistry Research **43** (2), 364 – 374.

Van Dongen, d.B., Doherty, M.F., (1985). *Design and Synthesis of Homogeneous Azeotropic Distillations. 1. Problem Formulation for a Single Column*. Industrial Engineering Chemical Fundamentals **24**, 454.

Yeomanns, H., Grossmann, I.E., (1998). "*A Disjunctive Programming Method for the Integration of Heat Integrated Distillation Sequences*." A.I.Ch.E Annual Meeting, Miami.

CHAPTER 3

Bausa, J., von Watsdorf, R. and Marquardt, W., (1998). *Minimum Energy Demand for Non-Ideal Multi-Component Distillation: I. Simple Columns*. A.I.Ch.E. Journal **44** (10), 2181 – 2198.

Doherty, M.F., Perkins, J.D., (1978). *On The dynamics of Distillation Processes. I. The Simple Distillation of Multi-Component Non-Reacting, Homogeneous Liquid Mixtures*. Chemical Engineering Science **33**, 281.

Doherty, M.F., Perkins, J.D., (1979). *On The dynamics of Distillation Processes. III. The Topological Structure of Ternary Residue Curve Maps*. Chemical Engineering Science **34**, 1401.

Feng, G., Fan, L.T. and Freidler, F., (2000). *Synthesizing Alternative Sequences via a P-graph Based Approach in Azeotropic Distillation Systems*. Waste Management **20**, 639-643.

Feng, G., Fan, L.T., Seib, P.A., Bertok, B., Kalotai, L. and Freidler, F., (2003). *Graph-theoretic Method for the Algorithmic Synthesis of Azeotropic-Distillation Systems*. Industrial Engineering Chemistry Research **42**, 3602-3611.

Freidler, F., Tarjan, K., Huang, Y.W. and Fan, L.T., (1992). *Graph-theoretic Approach to Process Synthesis Axioms and Theorems*. Chemical Engineering Science **47** (8), 1973-1988.

Freidler, F., Varga, J.B., and Fan, L.T., (1995). *Decision Mapping: A Tool for Consistent and Complete Decisions in Process Synthesis*. Chemical Engineering Science **50** (11), 1755-1768.

Hausen, H., (1952). *Rektifikation Idealer Dreistoff-Gemische*. Z. Angew. Phys. **4**, 41.

Henley, E.J. and Williams, R.A., (1973). *Graph Theory In Modern Engineering*. Academic Press, New York.

Julka, V. and Doherty, M.F., (1993). *Geometric Non-linear analysis of Multi-Component Non-Ideal Distillation: A Simple Computer-Aided Design Procedure*. Chemical Engineering Science **48**, 1367 – 1391.

Kiva, V.N., Hilmen, E.K. and Skogestad, S., 2003. *Azeotropic Phase Equilibrium Diagrams: A Survey*. Chemical Engineering Science **58**, 1903 – 1953.

Knight, J.R., and Doherty, M.F., (1990). *Systematic Approaches to the Synthesis of Separation Schemes for Azeotropic Mixtures*. Foundations of Computer-Aided Process Design **12**, 417 – 433.

Ostwald. W., (1902). *Lehrbuch Der Algemeinen Chemie. Verwandtschaftslehre*. Verlag von Wilhelm Engelmann: Leipzig, Germany, part1.

Peterson, E.J., Partin, L.R., (1997). *Temperature Sequences for Categorizing All Ternary Distillation Boundary Maps*. Industrial Engineering Chemistry Research **36**, 1799-1811.

Petlyuk, F.B., Kievski, V.Ya. and Serafimov, L.A., (1975a). *Thermodynamic and Topologic Analysis of the Phase Diagram of Polyazeotropic mixtures. I. Definition of Distillation Regions Using a Computer [Computer Aided determination of azeotropic distillation regions]*. Russian Journal of Physical Chemistry, **69** (12), 3105 – 3108.

Petlyuk, F.B., Kievski, V.Ya. and Serafimov, L.A., (1977a). *Thermodynamic Topological Analysis of VLE Diagrams for Multi-Component Mixtures. III. Algorithm of Structure Graph Drawing for Four Component Mixtures.* Russian Journal of Physical Chemistry, **71** (2), 315 – 318.

Petlyuk, F.B., Kievski, V.Ya. and Serafimov, L.A., (1977b). *A Combined Thermodynamic and Topological Analysis of Phase Equilibrium Diagrams for Polyazeotropic systems – V. The Use of the phase Equilibrium Model in Combined Thermodynamic and Topological Analysis.* Russian Journal of Physical Chemistry, **51**, 338 – 340.

Petlyuk, F.B., Kievski, V.Ya. and Serafimov, L.A., (1977c). *Method for the Isolation of the Regions of Rectification of Polyazeotropic Mixtures Using an Electronic Computer [Computer Aided determination of azeotropic distillation regions in Multi-Component Mixtures]*. Theoretical Foundations of Chemical Engineering, **11** (1), 3 – 10.

Petlyuk, F.B., Kievski, V.Ya. and Serafimov, L.A., (1978). *Thermodynamic Topological Analysis of VLE Diagrams for Multi-Component Mixtures. IV. Use of the Structure Matrix for Analysis of feasible separations of the wood Pyrolysis Product.* Russian Journal of Physical Chemistry, **72** (5), 1145 – 1148.

Rev, E., (1994). *Optimal Exploration of Residue Curve Map Topologies in Higher Dimensions.* Hungarian Journal of Industrial Chemistry **22**, 41-46.

Rische, E.A., (1955). *Rektifikation Idealer DreistoffGemische Unter Der Voraussetzung, Daß Der Widerstand Des Stoffaustausches Allein Auf Der Flussigkeitsseite Liegt.* Z. Angew. Phys. **7**, 90.

Rooks, R.E., Julka, V., Doherty, M.F. and Malone, M.F., (1998). *Structure of Distillation Regions for Multi-Component Azeotropic Mixtures*. A.I.Ch.E. Journal, **44** (6), 1382 – 1391.

Safrit, B.T. and Westerberg, A.W., (1997). *Algorithm for Generating the Distillation Regions for Azeotropic Multi-component mixtures*. Industrial and Engineering Chemistry Research **36**, 1827 – 1840.

Serafimov, L.A., (1968). *Theoretical Principles of Distillation Sequences Design and Synthesis for Non-Ideal Multi-component Mixtures*. Ph.D. Thesis, Lomonosov Institute of Fine Chemical Technology, Moscow.

Shreinemakers, F.A.H., (1902). *Einige Bemerkungen Ueber Dampfdruecke Ternaerer Gemische*. Z. Phys. Chem. **43**, 671.

Thong, D.Y.-C., and Jobson, M., (2001a). *Multi-Component Homogeneous Azeotropic Distillation 1. Assessing Product Feasibility*. Chemical Engineering Science **56**, 4369-4391.

Thong, D.Y.-C., and Jobson, M., (2001b). *Multi-Component Homogeneous Azeotropic Distillation 2. Column Design*. Chemical Engineering Science **56**, 4393-4416.

Thong, D.Y.-C., and Jobson, M., (2001c). *Multi-Component Homogeneous Azeotropic Distillation 3. Column Sequence Synthesis*. Chemical Engineering Science **56**, 4417-4432.

Wasylkiewicz, S.K., Kobylka, L.C. and Castillo, F.J.L., (2000). *Optimal Design of Complex Azeotropic Distillation Systems*. Chemical Engineering Journal Research **79**, 219-227.

Zharov, V.T., (1967). *Free Evaporation of Homogeneous Multi-Component Solutions*. Russ. J. Phys. Chem. **41** (11), 1539.

Zharov, V.T., (1968). *Phase Transformations (Distillation Lines) and Rectification of Multi-Component Solutions*. Russ. J. Appl. Chem. **41** (12), 2530.

CHAPTER 4

Doherty, M.F., Perkins, J.D., (1978). *On the Dynamics of Distillation Processes 1-3.* Chemical Engineering Science **33.**

Feinberg, M., Hildebrandt, D., (1997). *Optimal Reactor Design from a Geometric Viewpoint – I. Universal Properties of the Attainable Region*. Chemical Engineering Science **52 (10)**, 1637-1665.

Feinberg, M., (1999). *Recent Results in Optimal Reactor Synthesis via Attainable Region Theory*. Chemical Engineering Science **54**, 2535-2543.

Gadewar, S.B., Malone, M.F. and Doherty, M.F., (2002). *Feasible Region For A Countercurrent Cascade Of Vapour-Liquid CSTRs.* American Institute of Chemical Engineers Journal. **48 (4)**, 800-814.

Godorr, S.A., Hildebrandt, D. and Glasser, D., (1994). *The Attainable Region for Systems with Mixing and Multiple-Rate Processes; Finding Optimal Reactor Structures*. Chemical Engineering **54 (21)**, 175-186.

Glasser, D. & Hildebrandt, D., (1997). *Reactor and Process Synthesis*. Computers and Chemical Engineering, **21**, S775 – S783.

Hildebrandt, D., & Bieglar, L.T., (1995). Synthesis of *Chemical Reactor Networks*. American Institute of Chemical Engineers Symposium Series, **305**, 52 – 67.

Horn, F.J.M., (1964). Attainable and Non-Attainable Regions in Chemical Reaction Technique. In Chemical Reaction Engineering (Proceedings of the 3rd European Symposium). Pergamon Press, London, U.K.

Jobson, M., Hildebrandt, D. and Glasser, D., (1996). *Variables Indicating the Cost of Vapour-Liquid Equilibrium Separation Processes*. Chemical Engineering Science **51 (21)**, 4749-4757.

Kauchali, S., McGregor, C. and Hildebrandt, D., (1999). *The Attainable Region for Simple Binary Distillation.* Presented at the annual American Institute of Chemical Engineers Meeting. Dallas, TX, October 31 – November 5.

Kauchali, S., McGregor, C. and Hildebrandt, D., (2000). *Binary Distillation Revisited Using The Attainable Region Theory.* Computers and Chemical Engineering **24**, 231-237.

McGregor, C., (1998). *The Attainable Region Analysis for Systems with Reaction and Mass Transfer. Ph*.D. Thesis. University of the Witwatersrand, Johannesburg (Chapter 9).

McGregor, C., Glasser, D. and Hildebrandt, D., (1999). *The Attainable Region and Pontryagin's Maximum Principle*. Industrial Engineering Chemistry Research **38**, 652-659.

APPENDIX A: EXPERIMENTAL DATA AND DATA ANALYSIS

COMPOSITION CALCULATIONS

Composition samples are taken during the experiments at the sample ports shown in Figure A.1 below. The samples are stored in 1.5ml sample vials for GC analysis. The calibration procedure of the GC is outlined in APPENDIX B.

The pure components in the samples are represented as peaks in the GC output. The curves of the peaks are integrated to give areas. The areas of many calibration mixtures are used in the GC calibration (see APPENDIX B) to calculate response factors which allow the conversion of the peak areas to mole fractions.

The response factors are used to calculate the mole fractions in a sample from the GC pure component peak areas. The relationship is shown in equation A.1 for a three component system:

$$x_1 = \frac{k_1 A_1}{k_1 A_1 + k_2 A_2 + k_3 A_3} \qquad \textbf{(A.1)}$$

K is the response factor of the particular component. *A* is the peak area reported by the GC and *x* is the calculated mole fraction for the particular component. The component mole fractions were calculated using equation A.1 and the response factors calculated in APPENDIX B.

REFLUX AND DELTA POINTS

The entire experiment is timed and volumes of materials are recorded before and after experimentation at a temperature of 30°C. Using the calculated molar fractions, the molar flow rate may be found from the volumetric flow rates.

The molar flow rate of the top and bottom liquid and vapour streams is then used to calculate the reflux ratio via equation A.2.

$$R_{\Delta(T,B)} = \frac{\dot{L}_{(T,B)}}{\dot{V}_{(T,B)} - \dot{L}_{(T,B)}} \qquad \textbf{(A.2)}$$

Using the calculated molar flows for the top and bottom liquid and vapour streams and their calculated compositions, the delta composition difference point may be calculated with equation A.3.

$$x_{\Delta(T,B)} = \left(\frac{\dot{V}_{(T,B)} y_{(T,B)} - \dot{L}_{(T,B)} x_{(T,B)}}{\dot{V}_{(T,B)} - \dot{L}_{(T,B)}} \right) \qquad \textbf{(A.3)}$$

The calculated reflux ratio and delta points are then used to construct the theoretical column profile map unique to the specified reflux ratio and fixed delta point.

A qualitative schematic of the apparatus function areas and sample ports is shown below in Figure A.1. The experimental sample GC area outputs and corresponding molar compositions; and the reflux ratios and delta points for each of the nine experiments are tabulated below in tables A.1 to A.18.

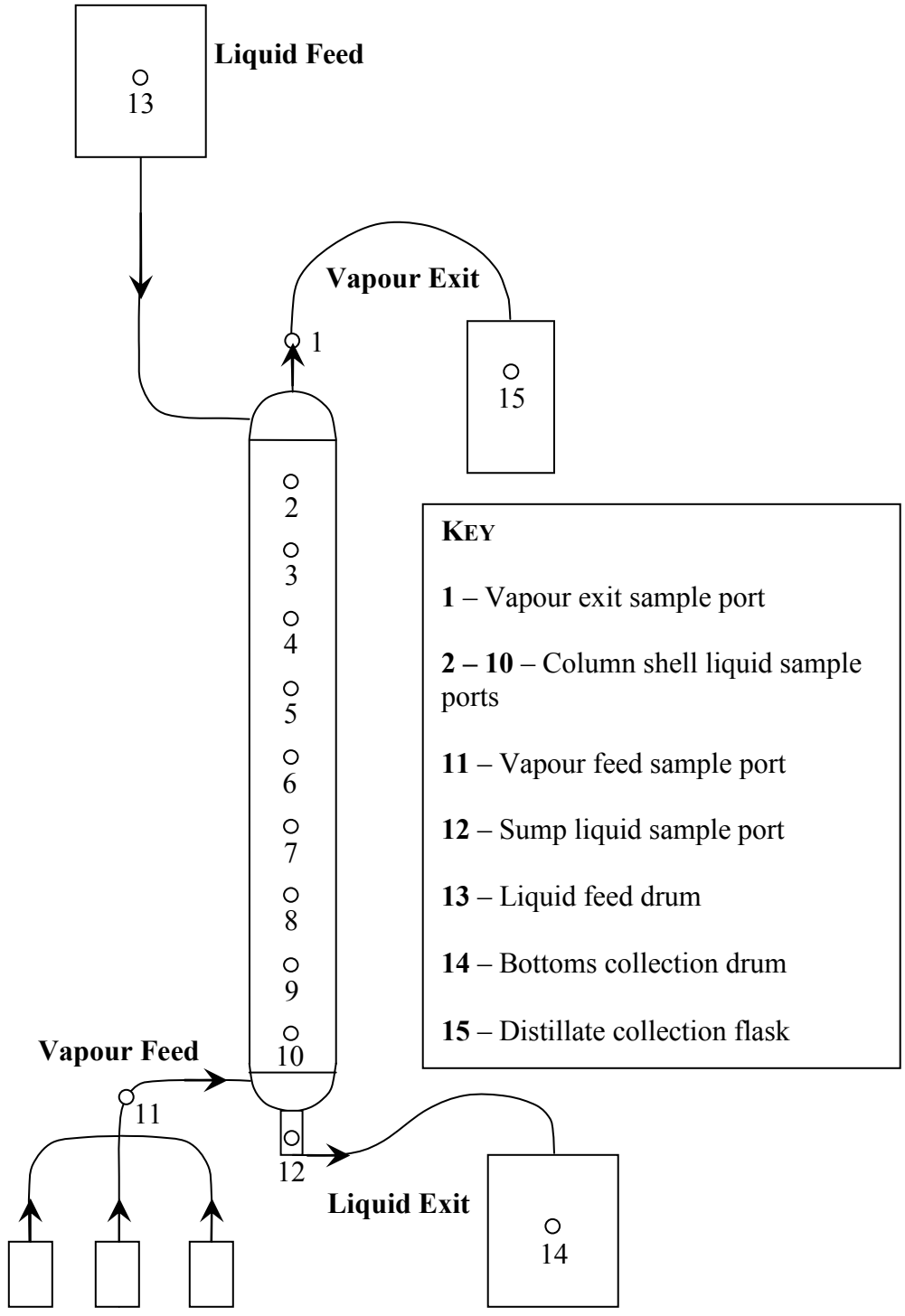

Figure A.1: Qualitative schematic of column apparatus showing various sampling ports and column function areas.

EXPERIMENT 1

	GC Areas			Mol Frac		
	A	M	E	A	M	E
1	3102.56	953.73	78.16	0.6667	0.3128	0.0205
1	3090.25	934.18	81.19	0.6696	0.3089	0.0215
2	3074.57	1171.64	192.36	0.6031	0.3508	0.0461
2	2866.80	1073.96	179.69	0.6067	0.3468	0.0465
3	3368.17	1000.58	79.69	0.6746	0.3059	0.0195
3	3504.46	1012.76	81.40	0.6805	0.3001	0.0193
4	2988.43	918.85	91.79	0.6637	0.3114	0.0249
4	3591.77	1119.37	107.30	0.6613	0.3145	0.0242
5	3180.71	1044.42	148.14	0.6418	0.3216	0.0366
5	3622.67	1138.79		0.6758	0.3242	0.0000
6	3391.68	1019.49	96.17	0.6696	0.3072	0.0232
6	3204.15	958.12	90.88	0.6707	0.3061	0.0233
7	3126.21	1099.26	180.91	0.6221	0.3339	0.0440
7	3142.66	1018.81	179.43	0.6392	0.3162	0.0446
8	2936.16	948.45	150.61	0.6428	0.3169	0.0403
8	3103.89	996.07	136.56	0.6479	0.3173	0.0349
9	3481.25	1040.09	125.91	0.6666	0.3039	0.0295
9	3426.79	1030.50	122.95	0.6654	0.3054	0.0292
10	1753.74	636.27	874.98	0.4622	0.2559	0.2820
10	2339.89	798.65	1113.26	0.4756	0.2477	0.2767
11	1555.01	55.59	3495.75	0.2629	0.0143	0.7227
11	1539.41	51.87	3467.14	0.2628	0.0135	0.7237
12	3056.03	1072.62	634.94	0.5588	0.2993	0.1420
12	2603.87	914.44	531.60	0.5600	0.3002	0.1398
13	3976.37	1383.83		0.6531	0.3469	0.0000
13	2809.19	1126.01	192.83	0.5897	0.3608	0.0495
13	2993.58	1153.18	197.69	0.5993	0.3523	0.0484
14	2579.85	926.44	609.90	0.5443	0.2983	0.1574
14	2997.60	1060.43	702.95	0.5475	0.2956	0.1570
15	3035.02	834.97	242.11	0.6590	0.2767	0.0643
15	3330.10	911.01	280.78	0.6576	0.2746	0.0678

Table A.1: GC output areas and corresponding calculated molar fractions for Experiment 1.

	A	M	E	ml/min	mol/min
Liq Top (13)	0.5993	0.3523	0.0484	644.615	9.416
Vap Top (1)	0.6696	0.3089	0.0215	59.203	0.845
Liq Bottom (12)	0.5600	0.3002	0.1398	606.270	9.164
Vap Bottom (11)	0.2628	0.0135	0.7237	44.858	0.885

L/V Top	11.145
Reflux Top	-1.099
L/V Bottom	10.359
Reflux Bottom	-1.107

	A	M	E
x_{Δ} Top	0.5924	0.3566	0.0510
x_{Δ} Bottom	0.5918	0.3308	0.0774

Table A.2: Experiment 1 data for calculation of top and bottom reflux ratios and delta points.

EXPERIMENT 2

	GC Areas			Mol Frac		
	A	**M**	**E**	**A**	**M**	**E**
1	3289.27	921.00	325.09	0.6459	0.2760	0.0781
1	3264.80	918.88	323.61	0.6449	0.2770	0.0782
2	2837.24	864.84	416.39	0.6080	0.2829	0.1091
2	2616.39	797.84	379.63	0.6087	0.2833	0.1080
3	3533.53	791.85		0.7452	0.2548	0.0000
3	3059.21	765.48	361.35	0.6552	0.2502	0.0946
4	2295.95	716.25	536.34	0.5676	0.2702	0.1621
4	2568.34	796.30	598.32	0.5688	0.2691	0.1620
5	3205.76	807.57	940.74	0.5736	0.2205	0.2058
5	2944.79	730.53	853.85	0.5770	0.2184	0.2046
6	2706.33	629.04	545.60	0.6245	0.2215	0.1540
6	2821.95	666.31	578.13	0.6208	0.2237	0.1555
7	2920.66	716.21	897.75	0.5714	0.2138	0.2148
7	2823.74	706.96	889.72	0.5658	0.2162	0.2180
8	2508.15	584.78	1015.02	0.5403	0.1923	0.2674
8	2375.29	580.09	1013.61	0.5278	0.1967	0.2754
9	2978.65	778.24	1327.16	0.5145	0.2052	0.2803
9	2178.16	575.67	985.01	0.5112	0.2062	0.2827
10	695.92	425.89	1928.58	0.1879	0.1755	0.6367
10	780.47	311.41	1816.53	0.2245	0.1367	0.6388
11	1240.49	45.71	2643.75	0.2731	0.0154	0.7116
11	1771.27	64.70	3885.02	0.2675	0.0149	0.7175
12	1495.78	490.52	1613.68	0.3547	0.1775	0.4679
12	1492.58	495.06	1603.96	0.3546	0.1795	0.4659
13	2615.26	944.54	438.26	0.5694	0.3139	0.1167
13	3407.44	1235.60	557.36	0.5703	0.3156	0.1141
14	1585.69	512.33	2703.06	0.2795	0.1378	0.5826
14	1478.46	479.67	2543.07	0.2779	0.1376	0.5845
15	2347.12	595.27	538.16	0.5997	0.2321	0.1681
15	2792.26	720.90	636.85	0.5978	0.2355	0.1667

Table A.3: GC output areas and corresponding calculated molar fractions for Experiment 2.

	A	M	E	ml/min	mol/min
Liq Top (13)	0.5703	0.3156	0.1141	197.319	2.954
Vap Top (1)	0.6459	0.2760	0.0781	151.515	2.207
Liq Bottom (12)	0.2779	0.1376	0.5845	139.420	2.606
Vap Bottom (11)	0.2675	0.0149	0.7175	94.848	1.863

L/V Top	1.339
Reflux Top	-3.953
L/V Bottom	1.398
Reflux Bottom	-3.510

	A	M	E
x_Δ Top	0.3471	0.4325	0.2204
x_Δ Bottom	0.3039	0.4456	0.2505

Table A.4: Experiment 2 data for calculation of top and bottom reflux ratios and delta points.

EXPERIMENT 3

	GC Areas			Mol Frac		
	A	M	E	A	M	E
1	3171.78	812.85	441.16	0.6405	0.2505	0.1089
1	3418.64	859.65	489.00	0.6416	0.2462	0.1122
2	2548.94	893.17	773.09	0.5248	0.2806	0.1946
2	2936.84	1052.81	891.36	0.5213	0.2852	0.1935
3	2521.84	751.10	454.98	0.5970	0.2713	0.1317
3	2214.52	673.15	406.35	0.5923	0.2748	0.1329
4	3102.47	971.57	588.86	0.5848	0.2795	0.1357
4	2797.17	876.52	538.58	0.5835	0.2791	0.1374
5	2549.31	980.87	1024.92	0.4810	0.2825	0.2365
5	2309.26	885.74	928.07	0.4815	0.2819	0.2366
6	2771.76	1716.19	981.75	0.4205	0.3974	0.1821
6	2276.73	1450.26	830.40	0.4135	0.4020	0.1844
7	2257.64	1401.94	935.42	0.4074	0.3861	0.2064
7	2270.16	1411.68	940.85	0.4072	0.3864	0.2064
8	2318.45	2086.77	1301.76	0.3268	0.4489	0.2244
8	1941.59	1770.44	1113.17	0.3233	0.4500	0.2267
9	1877.21	1807.83	1052.50	0.3169	0.4658	0.2173
9	1908.80	1833.90	1068.51	0.3174	0.4654	0.2172
10	1097.32	2662.26	1881.42	0.1471	0.5446	0.3084
10	1060.84	2598.75	1836.72	0.1459	0.5453	0.3088
11	239.27	7651.44	4109.79	0.0141	0.6892	0.2966
12	967.47	2609.86	1907.19	0.1328	0.5469	0.3202
12	904.32	2434.14	1795.07	0.1327	0.5452	0.3221
13	2236.07	830.71	657.34	0.5191	0.2943	0.1866
13	2287.37	815.65	652.89	0.5282	0.2874	0.1844
14	1203.19	1882.63	1429.24	0.2066	0.4933	0.3001
14	906.58	1450.47	1104.82	0.2028	0.4951	0.3022
15	2840.79	1144.05	529.61	0.5427	0.3336	0.1237
15	2320.33	909.06	464.06	0.5427	0.3245	0.1327

Table A.5: GC output areas and corresponding calculated molar fractions for Experiment 3.

	A	M	E	ml/min	mol/min
Liq Top (13)	0.5282	0.2874	0.1844	200.963	3.100
Vap Top (1)	0.6416	0.2462	0.1122	146.667	2.158
Liq Bottom (12)	0.1327	0.5452	0.3221	141.097	2.519
Vap Bottom (11)	0.0141	0.6892	0.2966	75.200	1.378

L/V Top	1.436
Reflux Top	-3.292
L/V Bottom	1.829
Reflux Bottom	-2.207

	A	M	E
x_{Δ} Top	0.2684	0.3819	0.3497
x_{Δ} Bottom	0.2758	0.3713	0.3529

Table A.6: Experiment 3 data for calculation of top and bottom reflux ratios and delta points.

EXPERIMENT 4

	GC Areas			Mol Frac		
	A	**M**	**E**	**A**	**M**	**E**
1	1990.65	770.90	329.06	0.5577	0.3296	0.1127
1	2309.25	966.44	412.53	0.5385	0.3439	0.1176
2	2510.47	1592.24	1025.93	0.4052	0.3923	0.2025
2	2406.61	1556.71	1002.96	0.4005	0.3954	0.2041
3	2424.37	1106.52	431.84	0.5224	0.3639	0.1138
3	2700.78	1264.80	465.73	0.5193	0.3712	0.1095
4	2748.88	1508.66	789.90	0.4568	0.3826	0.1605
4	2389.54	1311.52	694.15	0.4560	0.3820	0.1620
5	2222.27	1373.43	746.48	0.4248	0.4007	0.1745
5	1972.66	1246.71	670.98	0.4201	0.4052	0.1747
6	2861.77	1304.15	721.13	0.4991	0.3471	0.1538
6	2589.12	1189.13	661.71	0.4967	0.3481	0.1552
7	2490.79	1345.86	866.87	0.4444	0.3665	0.1891
7	2351.29	1274.89	824.05	0.4433	0.3668	0.1900
8	2418.50	1291.99	842.31	0.4462	0.3638	0.1900
8	1971.62	1066.36	715.11	0.4407	0.3638	0.1955
9	2668.55	1346.10	773.30	0.4708	0.3624	0.1668
9	2258.41	1123.09	665.03	0.4719	0.3582	0.1699
10	1728.29	2308.76	646.86	0.2860	0.5831	0.1309
11	2151.03	2219.14	20.61	0.3867	0.6088	0.0045
11	1851.08	1954.20		0.3830	0.6170	0.0000
12	2497.92	1535.28	870.99	0.4229	0.3967	0.1803
12	2247.58	1348.95	774.49	0.4278	0.3919	0.1803
13	2622.85	1239.14	955.11	0.4616	0.3328	0.2055
13	2930.57	1390.14	1074.69	0.4603	0.3332	0.2064
14	1652.35	1425.23	566.29	0.3656	0.4812	0.1532
14	1535.82	1307.42	534.44	0.3670	0.4768	0.1562
15	2947.46	1133.86	418.70	0.5679	0.3334	0.0987
15	3055.20	1154.45	456.27	0.5684	0.3278	0.1038

Table A.7: GC output areas and corresponding calculated molar fractions for Experiment 4.

	A	M	E	ml/min	mol/min
Liq Top (13)	0.4603	0.3332	0.2064	218.333	3.447
Vap Top (1)	0.5385	0.3439	0.1176	68.485	1.034
Liq Bottom (12)	0.4278	0.3919	0.1803	198.333	3.133
Vap Bottom (11)	0.3830	0.6170	0.0000	56.212	0.853

L/V Top	3.333
Reflux Top	-1.429
L/V Bottom	3.673
Reflux Bottom	-1.374

	A	M	E
x_Δ Top	0.4268	0.3287	0.2445
x_Δ Bottom	0.4446	0.3076	0.2477

Table A.8: Experiment 4 data for calculation of top and bottom reflux ratios and delta points.

EXPERIMENT 5

	GC Areas			Mol Frac		
	A	M	E	A	M	E
1	2389.11	720.62	295.58	0.6205	0.2856	0.0939
1	2445.06	737.99	302.71	0.6203	0.2857	0.0939
2	2698.21	1289.88	908.57	0.4670	0.3407	0.1923
2	2739.39	1293.77	912.76	0.4699	0.3387	0.1914
3	2361.81	845.63	392.61	0.5715	0.3123	0.1162
3	2081.23	746.72	346.84	0.5710	0.3127	0.1164
4	2988.83	1371.23	445.50	0.5312	0.3719	0.0968
4	2881.81	1390.27	406.26	0.5239	0.3857	0.0903
5	1735.12	1285.12	583.41	0.3935	0.4448	0.1618
5	1483.86	1216.78	520.49	0.3731	0.4669	0.1600
6	2132.32	2458.59	983.61	0.3009	0.5294	0.1697
6	1795.11	2099.11	813.64	0.2995	0.5345	0.1660
7	1694.84	2287.00	784.82	0.2758	0.5680	0.1562
7	1161.85	1579.23	575.09	0.2718	0.5637	0.1645
8	1550.11	3004.34	752.46	0.2197	0.6499	0.1304
8	1540.21	2900.16	744.63	0.2240	0.6436	0.1324
9	1703.22	2839.96	813.66	0.2422	0.6163	0.1415
9	1553.15	2614.67	744.09	0.2407	0.6183	0.1410
10	1116.10	3613.19	928.15	0.1437	0.7101	0.1462
10	1025.06	3311.29	851.49	0.1440	0.7098	0.1462
11	97.81	5646.18	16.75	0.0112	0.9865	0.0023
11		4730.16		0.0000	1.0000	0.0000
12	1039.91	3224.14	819.73	0.1494	0.7067	0.1440
12	1190.78	3690.95	946.98	0.1492	0.7057	0.1451
13	1752.85	780.55	544.29	0.4856	0.3300	0.1844
13	1900.51	875.62	614.87	0.4765	0.3350	0.1885
14	852.50	2229.79	595.25	0.1711	0.6829	0.1461
14	936.60	2222.59	567.44	0.1865	0.6754	0.1382
15	2958.73	1430.65	429.11	0.5221	0.3853	0.0926
15	2837.28	1344.24	406.58	0.5268	0.3809	0.0923

Table A.9: GC output areas and corresponding calculated molar fractions for Experiment 5.

	A	M	E	ml/min	mol/min
Liq Top (13)	0.4765	0.3350	0.1885	87.656	1.371
Vap Top (1)	0.6203	0.2857	0.0939	47.792	0.703
Liq Bottom (12)	0.1492	0.7057	0.1451	73.499	1.235
Vap Bottom (11)	0.0000	1.0000	0.0000	37.472	0.627

L/V Top	1.950
Reflux Top	-2.053
L/V Bottom	1.971
Reflux Bottom	-2.030

	A	M	E
x_{Δ} Top	0.3250	0.3869	0.2881
x_{Δ} Bottom	0.3029	0.4026	0.2945

Table A.10: Experiment 5 data for calculation of top and bottom reflux ratios and delta points.

EXPERIMENT 6

	GC Areas			Mol Frac		
	A	**M**	**E**	**A**	**M**	**E**
1	2556.58	664.30	255.23	0.6585	0.2611	0.0804
1	2380.10	619.41	239.08	0.6579	0.2613	0.0808
2	3258.55	1234.63	660.62	0.5476	0.3166	0.1358
2	2751.81	1043.09	568.56	0.5461	0.3159	0.1380
3	2572.37	728.81	338.25	0.6277	0.2714	0.1009
3	2272.33	650.89	302.43	0.6250	0.2732	0.1017
4	2761.81	722.79	262.48	0.6598	0.2635	0.0767
4	2703.05	712.48	260.13	0.6579	0.2647	0.0774
5	3048.30	955.80	539.13	0.5900	0.2823	0.1276
5	2757.75	879.48	481.86	0.5881	0.2862	0.1257
6	2470.60	806.27	469.88	0.5778	0.2878	0.1344
6	2028.22	653.85	375.73	0.5819	0.2863	0.1318
7	3501.72	1120.43	625.61	0.5859	0.2861	0.1280
7	2698.07	871.72	485.55	0.5837	0.2878	0.1285
8	1870.95	648.92	377.39	0.5631	0.2980	0.1389
8	2348.87	812.73	472.41	0.5637	0.2977	0.1386
9	3486.71	1056.45	517.45	0.6083	0.2813	0.1104
9	3472.80	1037.38	514.16	0.6109	0.2785	0.1106
10	2398.78	697.11	295.92	0.6272	0.2782	0.0946
10	2543.24	736.41	310.53	0.6285	0.2777	0.0938
11	3556.49	719.06	18.68	0.7605	0.2346	0.0049
11	3890.75	812.12		0.7584	0.2416	0.0000
12	2247.18	679.99	286.80	0.6181	0.2854	0.0965
12	2116.86	633.78	267.01	0.6207	0.2836	0.0957
13	3353.02	1105.65	701.17	0.5685	0.2861	0.1454
13	3346.18	1111.44	704.46	0.5668	0.2873	0.1459
14	2442.07	764.24	308.85	0.6127	0.2926	0.0947
14	2092.02	655.60	265.29	0.6122	0.2928	0.0949
15	3415.35	889.64	340.05	0.6582	0.2617	0.0801
15	3411.60	904.75	346.08	0.6541	0.2647	0.0811

Table A.11: GC output areas and corresponding calculated molar fractions for Experiment 6.

	A	M	E	ml/min	mol/min
Liq Top (13)	0.5668	0.2873	0.1459	145.441	2.198
Vap Top (1)	0.6579	0.2613	0.0808	86.385	1.256
Liq Bottom (12)	0.6207	0.2836	0.0957	135.941	2.001
Vap Bottom (11)	0.7584	0.2416	0.0000	84.013	1.169

L/V Top	1.751
Reflux Top	-2.332
L/V Bottom	1.712
Reflux Bottom	-2.404

	A	M	E
x_Δ Top	0.4455	0.3219	0.2326
x_Δ Bottom	0.4273	0.3426	0.2301

Table A.12: Experiment 6 data for calculation of top and bottom reflux ratios and delta points.

EXPERIMENT 7

	GC Areas			Mol Frac		
	A	**M**	**E**	**A**	**M**	**E**
1	2709.16	699.88	259.18	0.6617	0.2609	0.0774
1	2694.73	692.95	257.65	0.6625	0.2600	0.0775
2	2880.50	957.65	569.15	0.5718	0.2901	0.1381
2	3211.65	1039.73	628.31	0.5769	0.2850	0.1380
3	2572.37	728.81	338.25	0.6277	0.2714	0.1009
3	2272.33	650.89	302.43	0.6250	0.2732	0.1017
4	3778.54	976.61	346.91	0.6637	0.2618	0.0745
4	3897.92	927.08		0.7337	0.2663	0.0000
5	3139.36	1030.43	570.10	0.5804	0.2907	0.1289
5	2041.87	657.76	360.03	0.5857	0.2880	0.1263
6	3093.33	1070.09	643.44	0.5611	0.2962	0.1427
6	3191.18	1124.93	674.85	0.5566	0.2994	0.1439
7	2942.49	935.30	502.85	0.5903	0.2864	0.1234
7	2715.37	873.52	442.16	0.5917	0.2905	0.1178
8	3442.25	1109.76	554.03	0.5921	0.2913	0.1165
8	3613.46	1199.99	597.52	0.5851	0.2966	0.1183
9	2945.46	957.80	431.10	0.5969	0.2962	0.1068
9	2499.97	805.88	368.48	0.5980	0.2942	0.1078
10	3449.97	1198.03	498.64	0.5859	0.3105	0.1036
10	3140.28	1086.39	456.30	0.5863	0.3095	0.1042
11	2578.96	624.77		0.7301	0.2699	0.0000
11	3207.88	776.92		0.7301	0.2699	0.0000
12	2527.04	1016.28	433.72	0.5484	0.3366	0.1151
12	2537.73	966.12	430.14	0.5592	0.3249	0.1159
13	3353.02	1105.65	701.17	0.5685	0.2861	0.1454
13	3346.18	1111.44	704.46	0.5668	0.2873	0.1459
14	2442.07	764.24	308.85	0.6127	0.2926	0.0947
14	2092.02	655.60	265.29	0.6122	0.2928	0.0949
15	3676.36	970.34	384.57	0.6533	0.2631	0.0836
15	3349.87	905.86	342.26	0.6504	0.2684	0.0813

Table A.13: GC output areas and corresponding calculated molar fractions for Experiment 7.

	A	M	E	ml/min	mol/min
Liq Top (13)	0.5668	0.2873	0.1459	164.833	2.492
Vap Top (1)	0.6579	0.2613	0.0808	86.385	1.256
Liq Bottom (12)	0.6207	0.2836	0.0957	154.067	2.268
Vap Bottom (11)	0.7584	0.2416	0.0000	84.013	1.169

L/V Top	1.984
Reflux Top	-2.016
L/V Bottom	1.941
Reflux Bottom	-2.063

	A	M	E
x_{Δ} Top	0.4742	0.3137	0.2120
x_{Δ} Bottom	0.4742	0.3283	0.1975

Table A.14: Experiment 7 data for calculation of top and bottom reflux ratios and delta points.

EXPERIMENT 8

	GC Areas			Mol Frac		
	A	M	E	A	M	E
1	2558.71	651.80	214.97	0.6705	0.2607	0.0689
1	2552.45	647.71	214.01	0.6712	0.2600	0.0688
2	3276.93	1111.32	616.37	0.5722	0.2962	0.1316
2	3481.67	1160.97	650.98	0.5755	0.2929	0.1316
3	2946.02	742.85	278.65	0.6665	0.2565	0.0771
3	2357.68	600.67	226.41	0.6639	0.2581	0.0780
4	3117.35	818.54	362.78	0.6481	0.2597	0.0922
4	3583.30	910.10	400.73	0.6560	0.2543	0.0897
5	2493.32	704.41	367.69	0.6205	0.2676	0.1119
5	2342.95	669.08	350.35	0.6178	0.2692	0.1130
6	3717.32	911.62	523.09	0.6467	0.2420	0.1113
6	3602.41	867.53	503.98	0.6499	0.2389	0.1112
7	3018.54	639.92	413.03	0.6708	0.2170	0.1122
7	2710.71	573.23	369.70	0.6714	0.2167	0.1120
8	3680.12	685.12	411.44	0.7038	0.2000	0.0962
8	3409.48	613.30	369.48	0.7107	0.1951	0.0942
9	2941.54	524.28	307.16	0.7144	0.1943	0.0912
9	2420.76	437.55	256.10	0.7116	0.1963	0.0921
10	3864.71	602.28	444.13	0.7255	0.1725	0.1019
10	3861.44	609.75	451.48	0.7226	0.1741	0.1033
11	3271.99			1.0000	0.0000	0.0000
11	3140.37			1.0000	0.0000	0.0000
12	3621.40	521.16	387.74	0.7404	0.1626	0.0969
12	3711.01	536.42	398.11	0.7398	0.1632	0.0970
13	3313.10	1114.74	626.09	0.5732	0.2943	0.1325
13	3253.01	1062.95	598.32	0.5802	0.2893	0.1305
14	3106.22	341.91	269.28	0.7849	0.1319	0.0832
14	2815.44	303.05	237.99	0.7889	0.1296	0.0815
15	4134.47	877.86	325.08	0.7041	0.2282	0.0677
15	3518.45	775.60	269.58	0.6992	0.2352	0.0655

Table A.15: GC output areas and corresponding calculated molar fractions for Experiment 8.

	A	M	E	ml/min	mol/min
Liq Top (13)	0.5802	0.2893	0.1305	163.065	2.447
Vap Top (1)	0.6712	0.2600	0.0688	80.482	1.162
Liq Bottom (12)	0.7398	0.1632	0.0970	173.452	2.485
Vap Bottom (11)	1.0000	0.0000	0.0000	92.771	1.225

L/V Top	2.105
Reflux Top	-1.905
L/V Bottom	2.028
Reflux Bottom	-1.972

	A	M	E
x_{Δ} Top	0.4978	0.3159	0.1863
x_{Δ} Bottom	0.4867	0.3219	0.1914

Table A.16: Experiment 8 data for calculation of top and bottom reflux ratios and delta points.

EXPERIMENT 9

	GC Areas			Mol Frac		
	A	M	E	A	M	E
1	2558.71	651.80	214.97	0.6705	0.2607	0.0689
1	2552.45	647.71	214.01	0.6712	0.2600	0.0688
2	2720.40	801.95	434.87	0.6078	0.2734	0.1188
2	2625.70	773.28	406.43	0.6102	0.2743	0.1155
3	3468.17	766.12	287.51	0.6952	0.2344	0.0705
3	2941.77	658.91	252.27	0.6912	0.2363	0.0725
4	3453.17	789.97	370.74	0.6755	0.2358	0.0887
4	2711.47	618.41	292.10	0.6758	0.2352	0.0890
5	4003.36	785.38		0.7696	0.2304	0.0000
5	3594.85	806.09	452.70	0.6684	0.2287	0.1029
6	3118.53	765.92	482.71	0.6393	0.2396	0.1210
6	5959.25	1490.17	933.38	0.6357	0.2426	0.1217
7	4191.80	711.63	392.13	0.7281	0.1886	0.0833
7	3701.79	607.55	336.02	0.7345	0.1840	0.0815
8	3503.96	473.66	315.34	0.7597	0.1567	0.0836
8	2457.22	339.32	226.83	0.7555	0.1592	0.0853
9	4308.02	580.50	385.46	0.7604	0.1564	0.0832
9	3434.76	459.19	310.86	0.7606	0.1552	0.0842
10	3232.66	312.89	275.76	0.7987	0.1180	0.0833
10	3454.11	329.43	295.23	0.8000	0.1164	0.0836
11	3271.99			1.0000	0.0000	0.0000
11	3140.37			1.0000	0.0000	0.0000
12	3571.14	367.99	277.91	0.7985	0.1256	0.0760
12	3636.71	354.87	289.93	0.8023	0.1195	0.0782
13	3313.10	1114.74	626.09	0.5732	0.2943	0.1325
13	3253.01	1062.95	598.32	0.5802	0.2893	0.1305
14	3106.22	341.91	269.28	0.7849	0.1319	0.0832
14	2815.44	303.05	237.99	0.7889	0.1296	0.0815
15	3665.29	893.93	326.88	0.6751	0.2513	0.0736
15	3182.38	805.46	275.94	0.6701	0.2588	0.0710

Table A.17: GC output areas and corresponding calculated molar fractions for Experiment 9.

	A	M	E	ml/min	mol/min
Liq Top (13)	0.5802	0.2893	0.1305	137.838	2.068
Vap Top (1)	0.6712	0.2600	0.0688	80.482	1.162
Liq Bottom (12)	0.8023	0.1195	0.0782	139.919	1.967
Vap Bottom (11)	1.0000	0.0000	0.0000	92.771	1.225

L/V Top	1.779
Reflux Top	-2.284
L/V Bottom	1.605
Reflux Bottom	-2.652

	A	M	E
xΔ Top	0.4633	0.3270	0.2097
xΔ Bottom	0.4758	0.3168	0.2074

Table A.18: Experiment 9 data for calculation of top and bottom reflux ratios and delta points.

APPENDIX B: GC CONFIGURATION AND CALIBRATION

AGILENT 6820 GC CONFIGURATION

Gas flows:

- Gas type: Hydrogen

For Hydrogen, an optimal column gas velocity of between 50 – 60 cm/s is recommended. For column diameter of 450μm, flowrates are:

  - 50 cm/s: 4.77 ml/min
  - 60 cm/s: 5.72 ml/min

- Column Flow: 5.6 ml/min
- Auxiliary Flow: 3.6 ml/min

Reference Gas Flow = 3*(Column + Auxiliary)

- Reference Flow: 27.3 ml/min
- Split Vent Flow: 278 ml/min
- Split: 50:1 (Split Vent Flow/Column Flow)

Column:

- Type: Capillary column DB-5
- Length: 30m
- Nominal Diameter: 450μm
- Temperature Setting: Isothermal 60°C
- Run Time: 1.2min

Front inlet:

- Temperature 250°C
- Mode: split

Front Detector:

- Temperature 250°C
- Data Acquisition Rate: 10Hz

GC CALIBRATION

The following is the procedure used for the calculation of the response factors of acetone, methanol and ethanol for the current GC configuration.

The following are mole fractions for acetone (A), methanol (M) and ethanol (E) of calibration mixtures calculated from mixtures prepared on a scale.

$$x_A := \begin{bmatrix} 0.080614707 \\ 0.441302154 \\ 0.876772421 \\ 0 \\ 0 \\ 0 \\ 0.058399136 \\ 0.356181582 \\ 0.830828557 \\ 0.078321794 \\ 0.068006505 \\ 0.059907909 \\ 0.722589696 \\ 0.151158354 \\ 0.130105652 \\ 0.495118455 \\ 0.22230343 \\ 0.214721556 \\ 0.301094289 \end{bmatrix} \quad x_M := \begin{bmatrix} 0 \\ 0 \\ 0 \\ 0.13895947 \\ 0.588869672 \\ 0.928307956 \\ 0.941600864 \\ 0.643818418 \\ 0.169171443 \\ 0.139859292 \\ 0.549278483 \\ 0.86494089 \\ 0.162741297 \\ 0.284947031 \\ 0.706439667 \\ 0.296917081 \\ 0.406440612 \\ 0.515114086 \\ 0.408236909 \end{bmatrix} \quad x_E := \begin{bmatrix} 0.919385293 \\ 0.558697846 \\ 0.123227579 \\ 0.86104053 \\ 0.411130328 \\ 0.071692044 \\ 0 \\ 0 \\ 0 \\ 0.781818913 \\ 0.382715011 \\ 0.075151201 \\ 0.114669008 \\ 0.563894616 \\ 0.163454682 \\ 0.207964464 \\ 0.371255958 \\ 0.270164358 \\ 0.290668803 \end{bmatrix}$$

The calibration mixtures were then analysed in the GC and the reported peak areas for the three pure components corresponding to the calibration mixtures were recorded. The areas are shown below.

$$AA := \begin{bmatrix} 255.18343 \\ 1143.46769 \\ 929.99596 \\ 0 \\ 0 \\ 0 \\ 193.4249 \\ 2012.79255 \\ 2867.70796 \\ 492.87456 \\ 375.75848 \\ 464.01605 \\ 3181.39439 \\ 883.7325368 \\ 1011.397589 \\ 2274.676338 \\ 1448.057565 \\ 1074.246144 \\ 1715.71242 \end{bmatrix} \quad AM := \begin{bmatrix} 0 \\ 0 \\ 0 \\ 434.8242 \\ 1737.58666 \\ 937.75842 \\ 2101.92588 \\ 2398.98112 \\ 380.13208 \\ 586.36931 \\ 2015.16151 \\ 4419.05461 \\ 466.73901 \\ 1096.275506 \\ 3684.711931 \\ 909.4904754 \\ 1747.584608 \\ 1704.387053 \\ 1521.174275 \end{bmatrix} \quad AE := \begin{bmatrix} 2742.17637 \\ 1152.89494 \\ 100.32854 \\ 3449.20831 \\ 1521.28648 \\ 90.27864 \\ 0 \\ 0 \\ 0 \\ 4191.23755 \\ 1769.25488 \\ 472.28694 \\ 401.96662 \\ 2719.562438 \\ 1056.96561 \\ 795.8716827 \\ 1989.709299 \\ 1110.03638 \\ 1350.043696 \end{bmatrix}$$

Then a matrix is created to assign an integer reference to the 19 mixtures.

$$n := 0 .. 18$$

The response factor calculation requires an initial guess value for each factor.

$$kE := 0.400531$$

$$kM := 0.32092$$

$$kA := 0.262448$$

The predicted mole fractions of the three components are linked via the following three relationships.

$$xMp_n := \frac{kM \cdot AM_n}{kM \cdot AM_n + kE \cdot AE_n + kA \cdot AA_n}$$

$$xEp_n := \frac{kE \cdot AE_n}{kM \cdot AM_n + kE \cdot AE_n + kA \cdot AA_n}$$

$$xAp_n := \frac{kA \cdot AA_n}{kM \cdot AM_n + kE \cdot AE_n + kA \cdot AA_n}$$

Where k is the response factor, A is the GC peak area and x is the predicted mole fraction.

An error term is defined as the sum of the square difference between the known and the predicted mole fractions from the guess values of the response factors.

$$\begin{aligned} Error(kM, kE, kA) := & \sum_{n=0}^{18} \left[xM_n - \left(\frac{kM \cdot AM_n}{kM \cdot AM_n + kE \cdot AE_n + kA \cdot AA_n} \right) \right]^2 \dots \\ & + \sum_{n=0}^{18} \left[xE_n - \left(\frac{kE \cdot AE_n}{kM \cdot AM_n + kE \cdot AE_n + kA \cdot AA_n} \right) \right]^2 \dots \\ & + \sum_{n=0}^{18} \left[xA_n - \left(\frac{kA \cdot AA_n}{kM \cdot AM_n + kE \cdot AE_n + kA \cdot AA_n} \right) \right]^2 \end{aligned}$$

The partial derivatives of the error functions for each component are then equated to zero and a minimizing function is used to minimise the error by finding the correct combination of response factors.

given

$$\text{Error}(kM, kE, kA) = 0$$

$$\frac{d}{dkM}\text{Error}(kM, kE, kA) = 0 \qquad \frac{d}{dkA}\text{Error}(kM, kE, kA) = 0 \qquad \frac{d}{dkE}\text{Error}(kM, kE, kA) = 0$$

$$\begin{bmatrix} kM \\ kE \\ kA \end{bmatrix} := \text{minerr}(kM, kE, kA)$$

$$\begin{bmatrix} kM \\ kE \\ kA \end{bmatrix} = \begin{bmatrix} 0.407476 \\ 0.326485 \\ 0.266999 \end{bmatrix}$$

$$\text{Error}(kM, kE, kA) = 5.25081 \cdot 10^{-4}$$

The predicted mole fractions may then be recalculated with the true response factor values.

$$xMp_n := \frac{kM \cdot AM_n}{kM \cdot AM_n + kE \cdot AE_n + kA \cdot AA_n}$$

$$xAp_n := \frac{kA \cdot AA_n}{kM \cdot AM_n + kE \cdot AE_n + kA \cdot AA_n}$$

$$xEp_n := \frac{kE \cdot AE_n}{kM \cdot AM_n + kE \cdot AE_n + kA \cdot AA_n}$$

The predicted molar fractions are then plotted against the known molar fractions from the calibration mixtures to yield the calibration curves for the three components shown in figures B.1 to B.3 below.

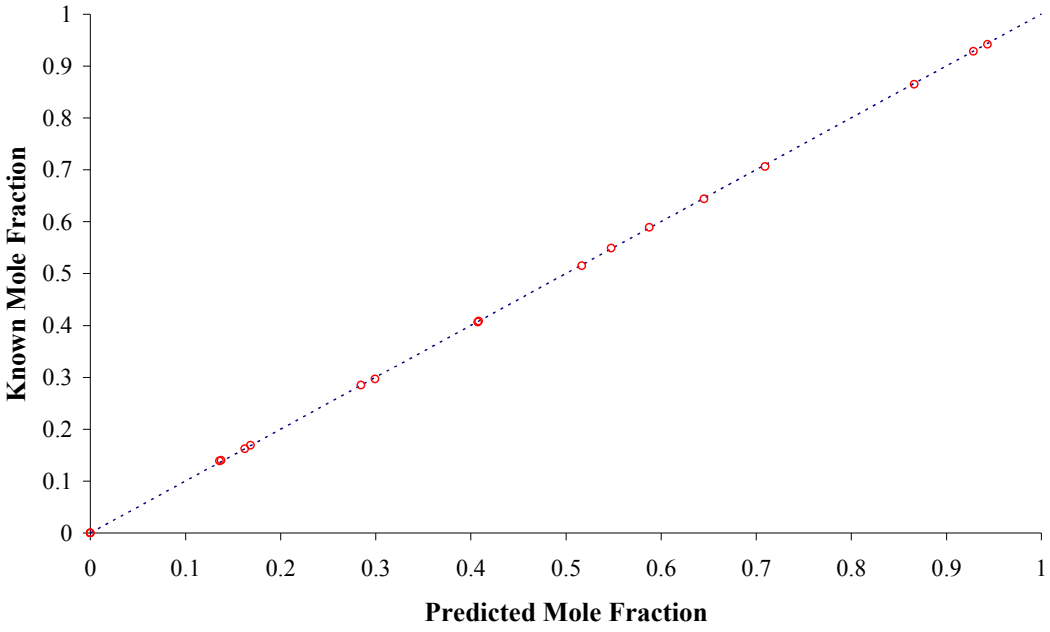

Figure B.1: Methanol Calibration Curve

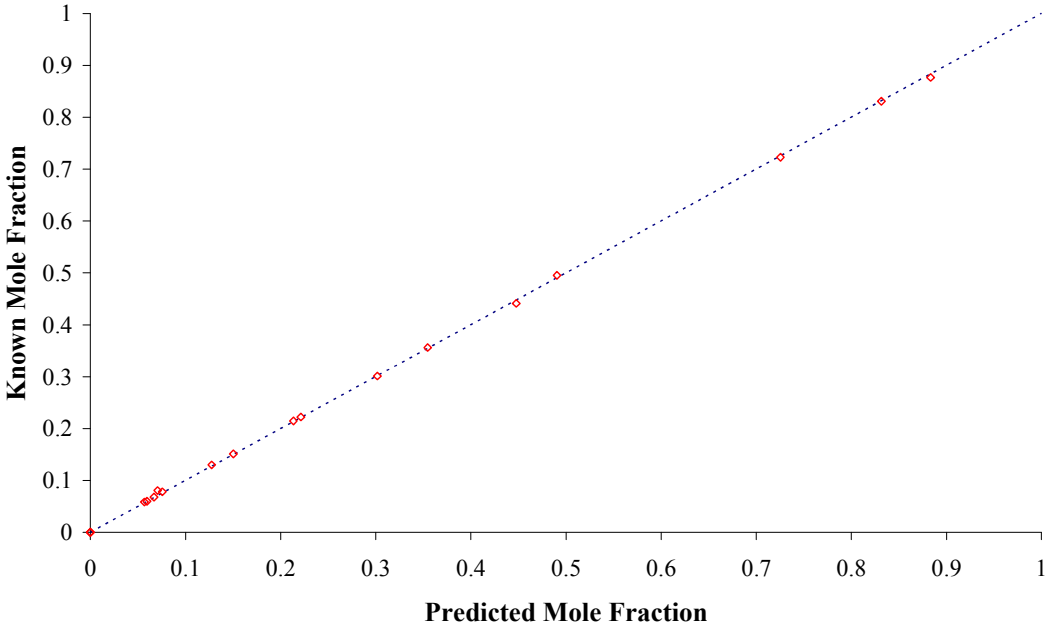

Figure B.2: Acetone Calibration Curve

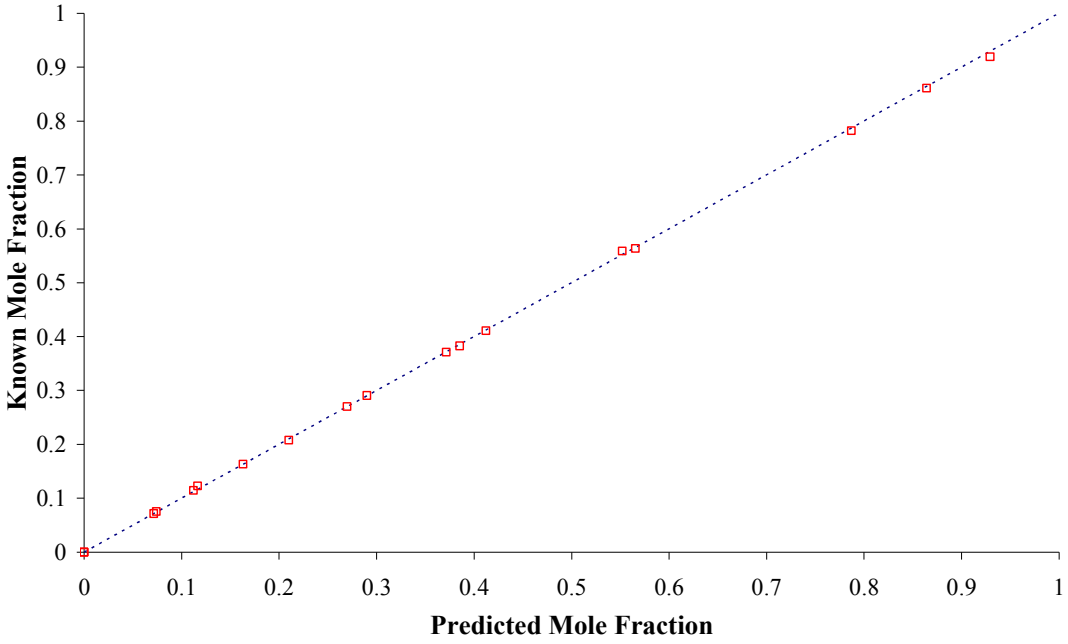

Figure B.3: Ethanol Calibration Curve

APPENDIX C: DISTRIBUTED REFLUX COLUMN DERIVATION

A distillation column is considered where the reflux is returned differentially to successive column sections. The column setup is illustrated in Figure C.1 below.

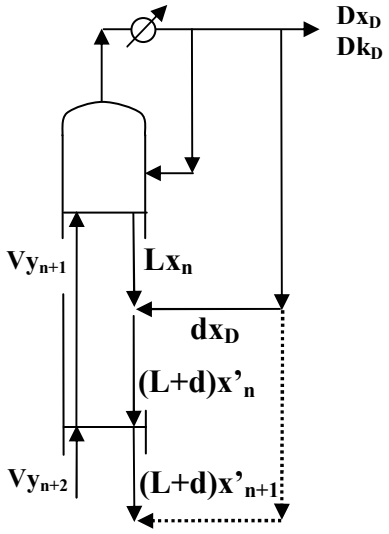

Figure C.1: Rectifying section of simple column preceded by column sections formed by differential reflux return.

The column sections are assumed to operate at steady state; to be adiabatic and the heats of vaporisation are assumed to be constant. Thus there is constant molar overflow for all the column sections, resulting in only mass transfer being considered.

The mass balance and component mass balance for the system are given by equations C1 and C2 respectively.

$$\dot{V} = \dot{D} + \left(\dot{L} + \dot{\mathrm{d}}\right) \qquad \textbf{(C.4)}$$

$$\dot{V}y_{n+2} = (\dot{L} + \dot{d})x'_{n+1} + \dot{D}x_D \qquad \textbf{(C.5)}$$

An algebraic trick is employed so that limits may be applied and the balance is put into differential form (Doherty and Perkins, 1978) to obtain the overall mass balance DE for the system, given by Equation A.4.

$$\dot{V}y_{n+2} + (\dot{L} + \dot{d})x'_{n+2} = (\dot{L} + \dot{d})x'_{n+1} + \dot{D}x_D + (\dot{L} + \dot{d})x'_{n+2} \quad \textbf{(C.6)}$$

The dashed liquid composition is to denote the change in composition of the liquid after the addition of the reflux for successive stages.

$$(\dot{L} + \dot{d})\frac{dx}{dn} = \dot{V}(x - y) + \dot{D}(x_D - x) \quad \textbf{(C.7)}$$

This may be further simplified using equations C.6 and C.7:

$$\frac{dx}{d\tau} = (x - y) + \left(\frac{1}{1 + r}\right)(x_D - x) \quad \textbf{(C.8)}$$

Where:

$$d\tau = \frac{\dot{V}}{(\dot{L} + \dot{d})}dn \quad \textbf{(C.9)}$$

$$r = \frac{\dot{L}}{\dot{D}} \quad \textbf{C.10)}$$

The same procedure is now followed to obtain the κ balance. As discussed in section 3.2.1, the κ balance for an equilibrium separation step is shown to be:

$$\Sigma FiKi \;\; Streams \;\; entering \;\; flash + Vapour \;\; produced \;\; in \;\; flash$$
$$= \Sigma FiKi \;\; Streams \;\; leaving \;\; flash$$

The general balance equation is then applied to Figure C.1. The differential amount of reflux added to each successive column section is given by *d* and *n* is the number of stages for the particular column section.

The component κ balance is given by equation C.8. The additional term added to each side is in preparation for the differential form of the balance.

$$\dot{V}\kappa_{n+2} + \dot{V} * n + (\dot{L} + \dot{d})\kappa'_{n+2} = (\dot{L} + \dot{d})\kappa'_{n+1} + \dot{D}\kappa_D + (\dot{L} + \dot{d})\kappa'_{n+2} \qquad \textbf{(C. 11)}$$

The component balance is then represented in differential form (Doherty and Perkins, 1978).

$$(\dot{L} + \dot{d})\frac{d\kappa}{dn} = \frac{\dot{D}}{\dot{V}}(\kappa_D - \kappa) - n \qquad \textbf{(C.12)}$$

Using equations C.6 and C.7, the following is obtained:

$$\frac{d\kappa}{d\tau} = \left(\frac{1}{1+r}\right)(\kappa_D - \kappa) - n \qquad \textbf{(C.13)}$$

Substituting equation C.7 into C.6 links the number of stages and the reflux ratio.

$$\frac{dn}{d\tau} = (1 - \frac{1}{1+r} + \frac{\dot{d}}{\dot{V}}) \qquad \textbf{(C.14)}$$

Equations C.5, C.10 and C.11 may now be used to solve the system and link successive composition changes to the costing function.